Evaluation and Control of Pirssonite Scale Formation in Green Liquor Systems of the Kraft Process

by

Tasnuva Zakir

A thesis submitted in conformity with the requirements
for the degree of Masters of Applied Science

Graduate Department of Chemical Engineering and Applied Chemistry
University of Toronto

Evaluation and Control of Pirssonite Scale Formation in Green Liquor Systems of the Kraft Process

Tasnuva Zakir

Masters of Applied Science

Graduate Department of Chemical Engineering and Applied Chemistry
University of Toronto

2011

Abstract

Scaling in green liquor handling systems is a persistent problem in many kraft mills. Scaling is commonly believed to be the result of pirssonite ($Na_2Ca(CO_3)_2 \cdot 2H_2O$) deposition. In this work, scale characterization was performed by analyzing 12 scale samples obtained from 10 kraft mills. Only 4 samples were identified as pirssonite while the remaining consisted of $CaCO_3$. The predominant presence of $CaCO_3$ in the scale samples was found to be the result of selective dissolution of Na_2CO_3 from pirssonite scale, leaving $CaCO_3$ behind. Experimental studies were also conducted to study pirssonite solubility under green liquor conditions. Results obtained from these studies were used to create and validate a database for pirssonite in the OLI Systems® software to predict its formation. This database was used to generate a family of pirssonite solubility curves that can be used by the kraft mills as operational guidelines to prevent pirssonite precipitation.

Acknowledgments

I wish to express my sincere gratitude to my supervisors, *Professor Honghi Tran* and *Professor Vladimiros G. Papangelakis* for their excellent guidance and advice throughout the course of this work. Their supervision, motivation, enthusiasm and encouragement have been a major contributing factor in the successful completion of this project.

Many thanks are due to my Reading Committee members, *Professor Donald Kirk* and *Professor Edgar Acosta* for their constructive feedback and comments.

I am indebted to *Sue Mao* for her valuable advice and suggestions for this project. *Ghazal Azimi* is greatly acknowledged for the help provided with the OLI software. Special thanks are due to *Daniel, Anton, Liming* and *Monica* for their friendship and support over the last two years. I am also thankful to *Dr. Georgiana Moldoveanu* for proof-reading this thesis.

This work was conducted as part of the research program on "*Increasing Energy and Chemical Recovery Efficiency in the Kraft Process*", jointly supported by the *Natural Sciences and Engineering Research Council of Canada (NSERC)* and a consortium of the following companies: *Andritz, Babcock & Wilcox, Boise, Carter Holt Harvey, Celulose Nipo-Brasileira, Clyde-Bergemann, DMI Peace River Pulp, Fibria, International Paper, Irving Pulp & Paper, Metso Power, MeadWestvaco, StoraEnso Research and Tembec*. I would also like to thank and acknowledge *Ontario Graduate Scholarship in Science and Technology (OGSST)* for the financial support provided for this project.

I wish to pay very special thanks to my parents who are always there for me with their unconditional love and support. I wouldn't be the person I am today without their guidance and upbringing.

Last but certainly not the least; I would like to thank my best friend, my fiancé, *Enamul*, for his endless love, inspiration and motivation which have been the basis of achieving my goals over the past eight years. Without his continuous encouragement and unfailing support, I could not have accomplished this work. This thesis is dedicated to him.

Table of Contents

List of Tables

List of Figures

Chapter 1

1 Introduction

1.1 Kraft Process

The kraft process, also referred to as the sulfate process, is the dominant pulping process in the paper making industry. This process was invented by Carl F. Dahl in 1879 and was implemented in 1884 [1]. Today, the global production of kraft pulp is about 130 million tons/year, accounting for two-thirds of the world's virgin pulp production and for more than 90% of the chemical pulp. The reasons behind the dominance of the kraft process over other pulping process are the high strength of kraft pulp, the versatility of the process to handle almost all species of softwood and hardwood, and the favorable economics due to high chemical recovery efficiency (about 97%) [2].

In the kraft process, wood chips are cooked in a pressurized vessel called a digester at a high temperature (170^{o}C) and pressure (100 psig). The cooking liquor, also known as the white liquor, is made of aqueous sodium hydroxide (NaOH) and sodium sulphide (Na_2S). This digestion process dissolves lignin in white liquor and separates the fiber as shown in Figure 1-1. The resulting liquid generated from this process contains water, lignin fragments, and residual inorganic chemicals, which is called black liquor.

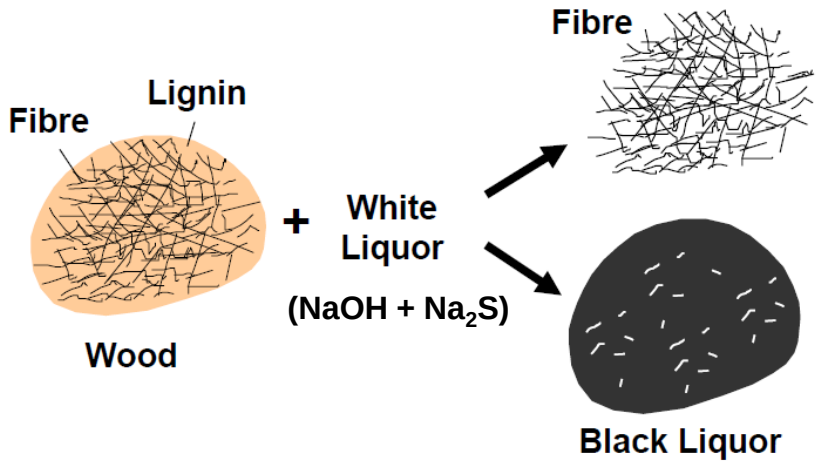

Figure 1-1: *Kraft pulping process [2]*

In the kraft chemical recovery cycle, black liquor must be concentrated in the multiple effect evaporators before being fed to the recovery boiler. In the recovery boiler, the concentrated black liquor is burnt to recover the chemicals needed for the digester. Steam and power are also generated in this process. The inorganic chemicals are converted into sodium carbonate (Na_2CO_3) and sodium sulfide (Na_2S), which exit the recovery boiler as molten smelt at about 850^{o}C. Molten smelt is further processed in the recausticizing process to generate white liquor.

1.2 Recausticizing Process

White liquor is produced in the recausticizing process from smelt generated in the recovery boiler. Quick lime (CaO) is slaked in smelt solution (green liquor) to produce white liquor and lime mud ($CaCO_3$). Lime mud is separated and washed to reduce its chemical content before being fed to the lime kiln. In the lime kiln, lime mud is calcined to quick lime for reuse. Lime mud washing water, known as weak wash, is recycled back to the dissolving tank to dissolve smelt in order to produce green liquor [3]. The following figure shows a schematic of the causticizing plant.

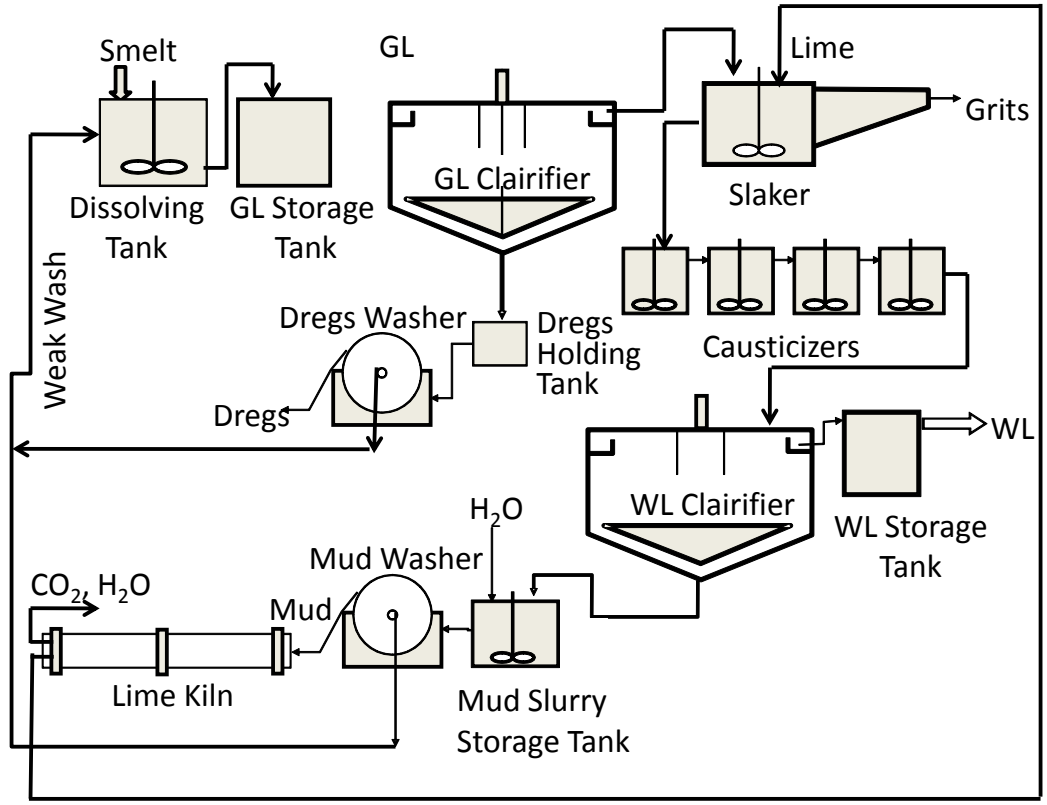

Figure 1-2: *Schematic of the causticizing plant process*

In the causticizing plant, two chemical reactions take place: slaking and causticizing. Quick lime (CaO) is slaked with water from green liquor solution to produce hydrated or slaked lime ($Ca(OH)_2$), which then reacts with Na_2CO_3 to produce NaOH.

Slaking $$CaO(s) + H_2O(aq) = Ca(OH)_2(s) \quad (1\text{-}1)$$

Causticizing $$Na_2CO_3(aq) + Ca(OH)_2(s) \leftrightarrow 2NaOH(aq) + CaCO_3(s) \quad (1\text{-}2)$$

The smelt dissolving tank is the first equipment in the recausticizing plant. Molten smelt discharged from the recovery boiler spouts is dissolved here using weak wash solution to make raw green liquor. Green liquor storage tanks are the next process equipment, which are designed to stabilize the temperature and the density of green liquor. The usual retention time for the storage tanks is about two to four hours. Raw green liquor usually contains particles called dregs. Typical green liquor contains about 800-1200 ppm of dregs but can surge as high as up to 4000 ppm due to improper operation of the recovery boiler [4]. The composition of dregs includes carbon and various amounts of iron, calcium, silica, alumina, magnesium, and some sulfides. These dregs are filtered in sedimentation type clarifiers where the dreg particles settle to the bottom and are collected in a dreg holding tank. In most mills two piping arrangements are used between the dissolving tank and the clarifier. One pipe is used as green liquor line carrying green liquor from the dissolving tank to the clarifier while the other is used to carry weak wash back to the dissolving tank. These two lines are regularly switched to minimize build ups in the green liquor line. Clarified green liquor from the top of the clarifier is then fed to the lime slaker followed by the causticizers. Quick lime (CaO) is introduced in the slaker to initiate the slaking and the causticizing reactions. The slaking reaction is exothermic and proceeds very fast to convert CaO into $Ca(OH)_2$, which then reacts very quickly with Na_2CO_3 in green liquor to produce NaOH and $CaCO_3$ in accordance with the causticizing reaction. It is critical to control the temperature of the incoming green liquor to the slaker to prevent any kind of boil over as a result of the slaking reaction. Most mills use a green liquor heater/cooler to maintain the slaker temperature below boiling point (100-104^o C) [3]. A series of agitated tanks (causticizers) are used after the slaker to maximize the causticizing efficiency by allocating enough residence time for the reaction to reach its maximum conversion. Since the causticizing reaction is a reversible equilibrium reaction, it will never reach full conversion. The slurry coming out of the causticizers is called white liquor, which is separated from lime mud in a sedimentation filter or

in a pressure filter known as the white liquor clarifier. Lime mud collected from the white liquor clarifier is washed, dewatered and sent to the lime kiln to produce fresh lime. Lime mud wash liquor (weak wash) is recycled back to the smelt dissolving tank and clarified white liquor is transported to the digester.

1.3 Green Liquor Scale

Green liquor scale is a major problem in most kraft mills. It is believed to be mainly composed of pirssonite, a double salt of sodium and calcium carbonates with the chemical formula $Na_2CO_3 \cdot CaCO_3 \cdot 2H_2O$ or $Na_2Ca(CO_3)_2 \cdot 2H_2O$ [5-7]. It often forms on the dissolving tank walls, floor, agitator shaft and blades, on the internal walls of pipelines and pumps, and to a lesser extent, in the storage tanks and clarifiers. An example of scaling in a pipeline is shown Figure 1-3. The scale, hard and stratified with black and gray layers, clogged about 85% of the cross-section opening of the pipe.

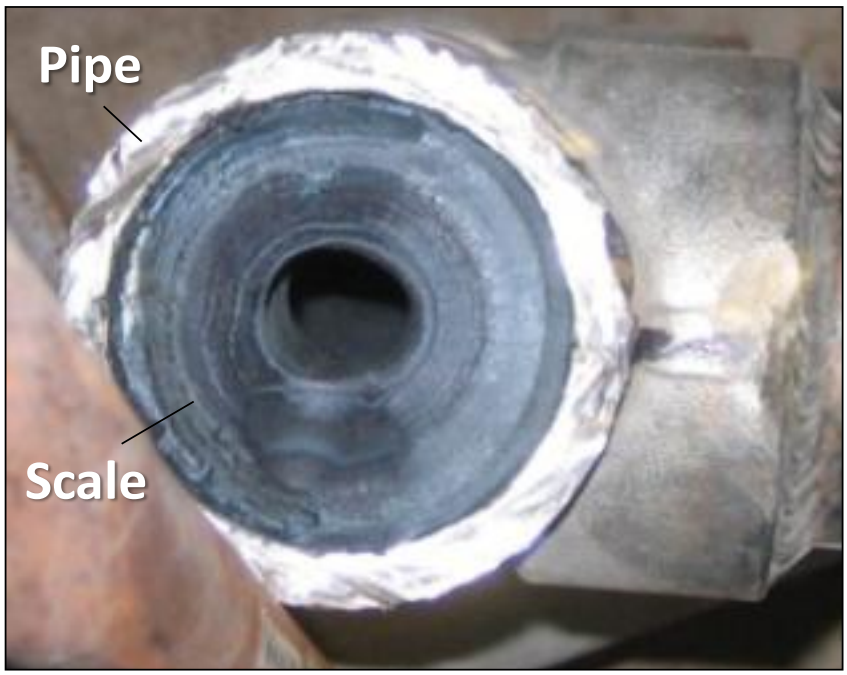

Figure 1-3: *Hard scale formed in a green liquor pipeline*

Scaling hinders mixing in the dissolving tank, restricts the liquor flow through pipelines and pumps, and in severe cases leads to unscheduled shutdowns for deposit removal. Scaling experience varies from mill to mill. Frederick et al. [6] discussed green liquor scale problems at the Weyerhaeuser Springfield mill where 6” (15 cm) valve openings in the raw green liquor

pipelines were reduced to only 1” (2.5 cm). Kosonen and Salmenoja [5] reported that at a mill in Imatra, Finland, the scale grew on the dissolving tank impeller blades so massively that the agitator motors exceeded the amperage limits and had to be stopped for scale removal in less than 3 months. This inevitably led to unscheduled shutdowns of the recovery boiler, resulting in substantial production losses.

1.4 Objectives

The overall aim of this work is to investigate green liquor scale in order to understand the mechanism and conditions that lead to its formation. Examining the solubility behavior of pirssonite in green liquor solution is of great interest, as pirssonite is believed to be the major component of green liquor scale. The ultimate goal of this work is to identify and confirm the potential of pirssonite scaling in green liquor systems with an aim to provide operational guidelines that may reduce its formation.

The specific objectives are:

1. To characterize green liquor scale by collecting and analyzing scale samples from various kraft mills.
2. To investigate conditions under which pirssonite precipitates from the solution by conducting experiments.
3. To obtain thermodynamic data for pirssonite formation and incorporate the data into a commercially available program, OLI, to predict conditions leading to scale formation.

This thesis is composed of a number of chapters, which are structured as follows:

- **Chapter 2** gives an overview of the literature relevant to this work. It offers a background of scale formation theory, summarizes green liquor solution chemistry, describes pirssonite mineralogy and its various properties, and outlines previous studies conducted by other researchers on pirssonite solubility. This chapter provides all the basics and background required to understand the work presented in this thesis.
- **Chapter 3** discusses the characterization of green liquor scale samples obtained from various kraft mills. This chapter is based on the following conference paper that will be presented at the 2011 TAPPI PEERS conference to be held in Portland, Ore in October 2011:

  - Zakir, T., Tran, H., and Papangelakis, V. “Characterization of hard scale formed in the kraft mill green liquor processing equipment”, 2011 TAPPI PEERS conference, Portland, Ore, Oct. 2-5, 2011 [8].

- **Chapter 4** describes the experiments conducted in this work to investigate the solubility of pirssonite. The solubility data presented in this chapter are incorporated in Chapter 5 to validate a database created for pirssonite compound in the OLI software.
- **Chapter 5** focuses on the chemical modeling performed in this work using the Mixed Solvent Electrolyte (MSE) framework of the OLI software. A database for pirssonite was created in this work that is capable of accurately predicting the solubility behavior of pirssonite under green liquor conditions.
- Finally, **Chapter 6** summarizes the major conclusions drawn from this work and **Chapter 7** provides a list of recommended future works.

Chapter 2

2 Literature Review

2.1 Scale Formation Theory

Scaling occurs when dissolved species from solutions deposits on equipment surfaces. The main three factors that lead to scale formation are as follows [9, 10]:

- Supersaturation
- Nucleation
- Crystal growth

Supersaturation:

The primary cause of chemical scale deposition is supersaturation [10, 11]. Temperature fluctuations, pressure drops, solution concentration, pH changes, impurities are some of the factors that can supersaturate a solution triggering the scaling process in an industrial environment [10]. Supersaturation, ΔC, is defined as

$$\Delta C = C - C_{eq} \tag{2-1}$$

where C is the concentration of the species that precipitates and C_{eq} is the equilibrium concentration of the precipitating species. A saturated solution is one which is in equilibrium with its solute. Supersaturated solutions are solutions that contain higher concentrations of dissolved solute than their equilibrium concentration. Supersaturation ratio [10], S, is a dimensionless term and is defined as

$$S = \frac{C}{C_{eq}} \tag{2-2}$$

Supersaturated solutions (S>1) are thermodynamically unstable where spontaneous crystallization is probable [10].

Nucleation:

Nucleation is defined as the birth of new crystals. The phase transition from liquid to solid will not usually occur at the instant the solution becomes supersaturated, but will initiate only after a

cluster of ions (or molecules) has reached a critical size in the liquid phase. It is only after this event that the solid phase can grow in volume enabling the phase transition to go to completion [10]. The process of nucleation can be divided into the following two main categories [10, 11]:

- Primary nucleation
    - Homogeneous
    - Heterogeneous
- Secondary nucleation

Primary nucleation is defined as the process where the precipitating solid phase is not required to be present in the liquid phase to start nucleation. Primary nucleation is further divided into two types: homogeneous and heterogeneous nucleation. In homogeneous nucleation, no solid phase is required at all while heterogeneous nucleation is initiated by the presence of a foreign substrate such as vessel walls, dust or other solid particles. Secondary nucleation requires the precipitating solid phase to co-exist in the liquid phase in order to commence nucleation [10, 11].

Crystal Growth:

Crystal growth is the third stage in the crystallization process after a solution has become supersaturated and nucleation has started. Crystal growth is a complex process and many theories on growth mechanisms are available in the literature. Dirksen and Ring [11] considered the following stages of crystal growth and discussed various types of growth mechanisms that are dependent upon the rate-limiting step. A detailed discussion on each of these stages is beyond the scope of this thesis.

1. Transport of solute from the bulk solution to the crystal surface
2. Adsorption on the crystal surface
3. Diffusion over the surface
4. Attachment to a step (point where two bonds are made between the solute and the crystal surface)
5. Diffusion along a step
6. Integration into the crystal at a kink site
7. Diffusion of coordination shell of solvent molecules away from the crystal surface
8. Liberation of heat of crystallization and its transport away from the crystal

The level of solution supersaturation determines the rate-limiting step which in turn dictates the shape of the crystals. For example, a solution with high supersaturation will make step 1 to be the rate-limiting step and hence, will have a diffusion-controlled growth, which will ultimately lead to the formation of dendritic type crystals [11].

2.2 Recausticizing Plant Chemistry

The main chemicals involved in the recausticizing process are sodium carbonate, sodium hydroxide and sodium sulfide. Sodium carbonate and sodium sulfide enter the causticizing plant as smelt where sodium carbonate in smelt is converted into sodium hydroxide through the causticizing reaction. Slaking (Equation 1-1) and causticizing (Equation 1-2) reactions occur simultaneously and can be described by the following simple chemical reaction:

Green Liquor + Lime = Lime Mud + White Liquor

$$Na_2CO_3 + Na_2S + CaO + H_2O = CaCO_3 + 2NaOH + Na_2S \quad (2\text{-}3)$$

Sodium sulfide does not participate in the causticizing reaction. However, a small amount of it hydrolyzes to produce NaOH and NaHS according to the following reaction.

$$Na_2S + H_2O \rightarrow NaOH + NaHS \quad (2\text{-}4)$$

2.2.1 Total Titratable Alkali (TTA)

Total Titratable Alkali or TTA is the total concentration of Na_2CO_3, NaOH and Na_2S present in green and white liquor. In North America, the total concentrations of these chemicals are expressed as equivalent concentration of sodium oxide (Na_2O). In other parts of the world, some mills express the concentration in terms of sodium hydroxide (NaOH). The units of choice to express TTA are usually g/L or lb/ft^3. In this study, TTA is expressed as g/L of Na_2O. The values of TTA typically range between 110 and 135 g/L of Na_2O [12, 13].

Green liquor is mostly composed of Na_2CO_3 and Na_2S with a small amount of NaOH. As the causticizing reaction progresses most of the carbonate in green liquor converts into equivalent moles of hydroxide. Therefore, the value of TTA remains constant throughout the process despite the changes in concentration of individual chemicals in the liquor cycle.

Active Alkali (AA) and Effective Alkali (EA)

Sodium hydroxide is the main constituent of white liquor. At high temperature and pressure it dissolves the lignin that bonds wood fiber together. Sodium sulfide is the other constituent in white liquor that helps reduce the damage to the cell walls of the wood fibers during the cooking process in the digester [3]. The strength of white liquor is measured by the concentration of these two chemicals. Active Alkali (AA) and Effective Alkali (EA) are the two measures that kraft mills use to determine the amount of white liquor required in the digester. AA and EA are defined as following:

$$AA = [NaOH] + [Na_2S] \tag{2-5}$$

$$EA = [NaOH] + \tfrac{1}{2}[Na_2S] \tag{2-6}$$

Where concentration, [ ], is expressed as g/L of Na_2O.

2.2.2 Sulfidity

Sulfidity is used by the mills to specify the amount of Na_2S present in the system. Sulfidity is usually defined in one of two ways: total amount of sodium sulfide over AA or total amount of sodium sulfide over TTA. The two sulfidity values are not the same since AA does not take into account the amount of sodium carbonate present in the solution. The advantage of using TTA based sulfidity over AA based is that TTA remains constant throughout the process causing the same effect for sulfidity. The sulfidity used in this study is TTA based which is defined by the following equation:

$$\%\, Sulfidity = \frac{[Na_2S]}{[NaOH] + [Na_2CO_3] + [Na_2S]} \times 100 \tag{2-7}$$

Typical values of sulfidity based on TTA are about 30% in North America and 40% in Scandinavia [12].

2.2.3 Causticizing Efficiency (CE)

Causticizing Efficiency or CE measures the extent of production of NaOH in the causticizing reaction. It is expressed as a percentage value and is defined as:

$$\% CE = \frac{[NaOH]}{[NaOH] + [Na_2CO_3]} \times 100 \quad (2\text{-}8)$$

CE refers to the efficiency of the causticizing reaction that never reaches full conversion due to the reversible nature of the equilibrium reaction. It is important to note that all concentrations should be converted into equivalent grams of Na_2O per liter of solution before Equation 2-8 can be used to calculate percent CE. Typical values of CE are around 80% [3, 4].

While CE indicates the amount of NaOH present in white liquor resulting from the causticizing reaction, causticity measures the amount of NaOH that exists in green liquor before it goes to the slaker/causticizers. The origin of NaOH in green liquor is through weak wash, which contains a small amount of dissolved sodium hydroxide in it. For the purpose of mathematical relationship, the equation that is used to determine CE can be used to calculate causticity (Equation 2-8). An important distinction between CE and causticity is that CE refers to NaOH present in white liquor whereas causticity measures NaOH in green liquor. Typical causticity of green liquor is between 5 and 10%.

2.3 Pirssonite

Pirssonite is a double salt of sodium and calcium carbonates with the chemical formula $Na_2CO_3 \cdot CaCO_3 \cdot 2H_2O$ or $Na_2Ca(CO_3) \cdot 2H_2O$. It is named after American geologist Louis Valentine Pirsson. It forms in non-marine evaporite deposits. Pirssonite is brittle and has a hardness of 3-3.5. It is optically transparent, viterous and its color is white to colourless [14, 15]. It has an orthorhombic crystal structure and its crystal habit is shown in Figure 2-1.

Figure 2-1: *Crystal habit of pirssonite [16]*

Pirssonite is found in the USA in Searles Lake, Borax Lake, Deep Spring Lake and Owens Lake in California and in Green River, Wyoming. It is also distributed in Argentina, Peru, Namibia, Turkey, and Russia [15]. Pirssonite can also be prepared in the laboratory. Bury and Redd [17] obtained pirssonite from a slurry of sodium carbonate, calcium carbonate and water only. Allen [18] and Dickens and Brown [19] prepared pirssonite from a mixture of sodium carbonate, sodium hydroxide, calcium carbonate and water. Dheilly and Tudo [20] synthetically produced pirssonite from a mixture of $NaHCO_3$, CaO and H_2O.

Gaylussite [21] is another double salt of sodium and calcium carbonates that has five moles of water in it with the chemical formula $Na_2CO_3 \cdot CaCO_3 \cdot 5H_2O$ or $Na_2Ca(CO_3)_2 \cdot 5H_2O$. Upon heating either pirssonite or gaylussite, the anhydrous double carbonate forms with the formula $Na_2CO_3 \cdot CaCO_3$ or $Na_2Ca(CO_3)_2$ [20, 22, 23]. Smith et al. [24] studied the thermal behavior of $Na_2CO_3 \cdot CaCO_3$. By heating a mixture of the constituent carbonates up to 500^oC they showed that as a sample of the carbonate mixture is heated, a new X-ray Diffraction pattern replaces the patterns of the two separate carbonates. Figure 2-2 illustrates the differences between the XRD patterns for the double carbonate and a mixture of the two constituent carbonates.

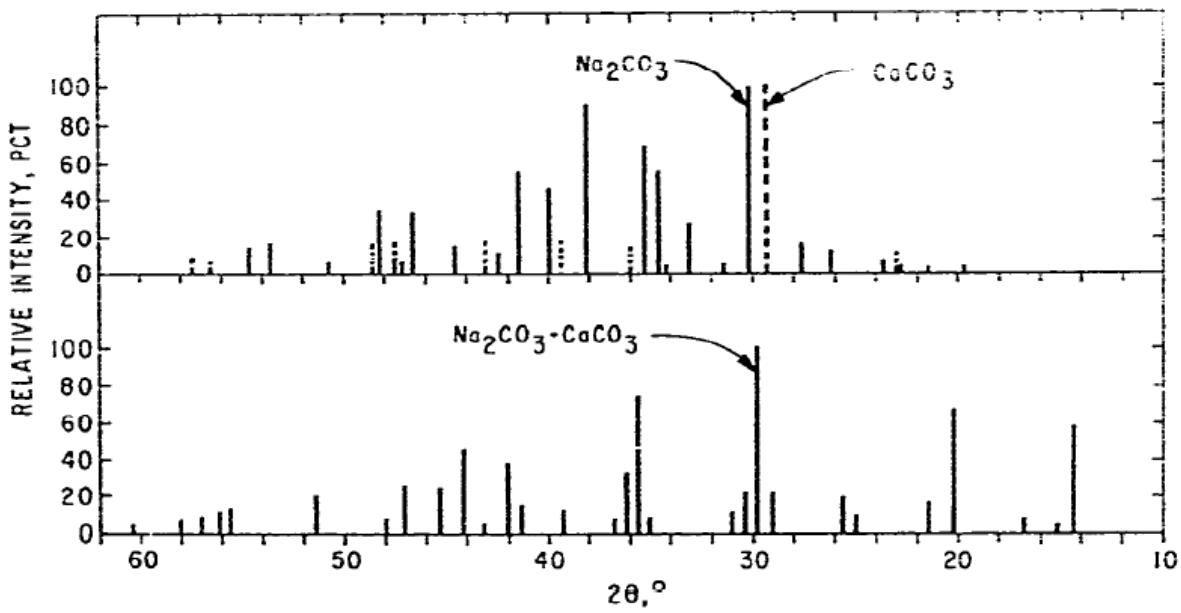

Figure 2-2: *XRD patterns of the mixed carbonates and the double carbonate compound [24]*

The double carbonate, $Na_2CO_3 \cdot CaCO_3$, has two polymorphs named nyerereite and zemkorite [22, 23]. The double carbonate goes through crystal phase transformation of these two polymorphic forms upon heating of it at a temperature range of 350°C-450°C [23- 25]

2.4 Previous Studies on Pirssonite Solubility

A review of the pertinent literature reveals that not a great amount of work has been done to study the solubility of pirssonite. In the pulp and paper industry, Frederick et al. [6] were the first to investigate pirssonite solubility under green liquor conditions. Their work was further extended by Ulmgren et al. [23] where they studied the solubility of pirssonite in green liquor solution generated from a pressurized black liquor gasifier instead of a conventional recovery boiler. Bury and Redd [17] and Littman and Gaspari [26] are the other groups of researchers that contributed to pirssonite solubility studies.

Bury and Redd examined the solubility of pirssonite in the system of Na_2CO_3, $CaCO_3$ and water in a temperature range of 15°C-95°C and published the following phase diagram (Figure 2-3). Their work shows pirssonite forms in a highly concentrated solution of Na_2CO_3 (>20wt%) at temperatures above 40°C.

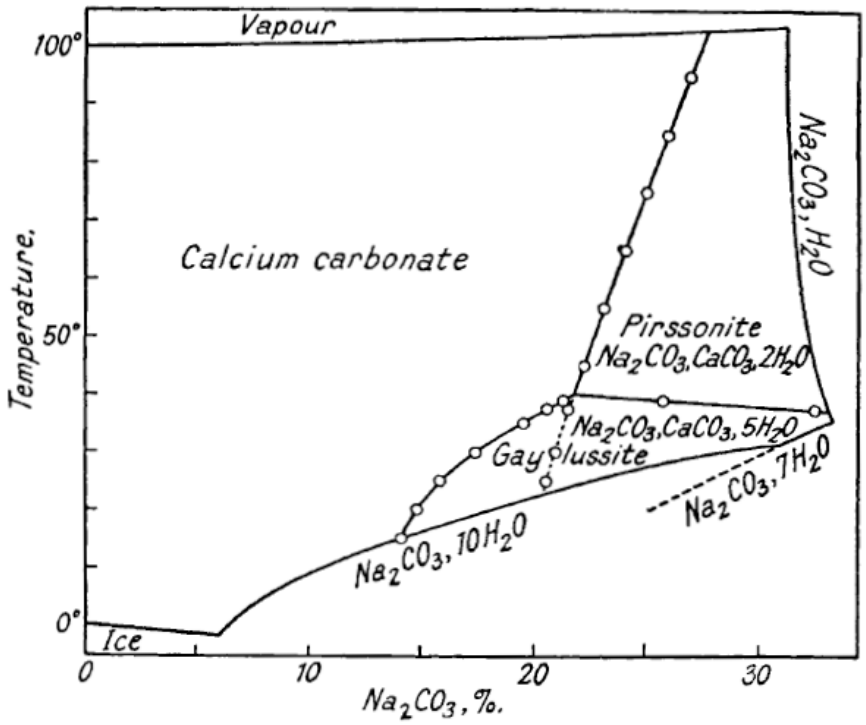

Figure 2-3: *System of $CaCO_3$-Na_2CO_3-H_20 [17]*

Littman and Gaspari studied the causticizing reaction in depth and postulated the formation of pirssonite from a solution of Na_2CO_3-$Ca(OH)_2$-NaOH at 95^{o}C. Figure 2-4 shows the phase diagram generated by Littman and Gaspari, where PQ line corresponds to pirssonite solubility in a solution of Na_2CO_3 and NaOH at 95^{o}C.

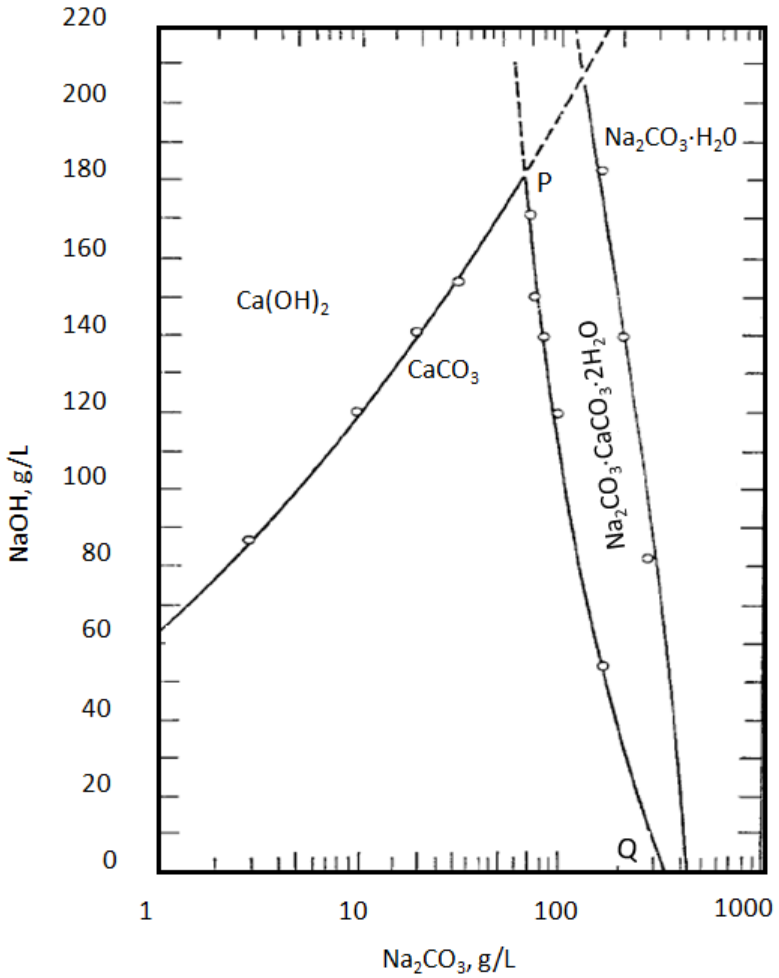

Figure 2-4: *System of $Ca(OH)_2$-NaOH-Na_2CO_3 in water at 95^oC [26]*

Frederick et al. investigated the effect of temperature and other sodium salts, such as NaOH, Na_2S and Na_2SO_4 on pirssonite solubility. They showed that pirssonite solubility increases with temperature and decreases with increased concentrations of other sodium salts. Figure 2-5 shows the effect of other sodium salts on pirssonite solubility at 95^{o}C and Figure 2-6 extends the same graph at different temperature levels showing the effect of temperature on pirssonite solubility. Based on these two graphs, they provided regression equations at three different temperatures (55^{o}C, 75^{o}C and 95^{o}C) that can be used to determine the solubility limit of pirssonite from a solution of sodium carbonate and other salts as mentioned above. Since pirssonite solubility curves in Figure 2-6 were extrapolated under dilute conditions where the concentrations of other salts become zero, the validity of the regression equations is dependent upon the accuracy of the extrapolated solubility curves.

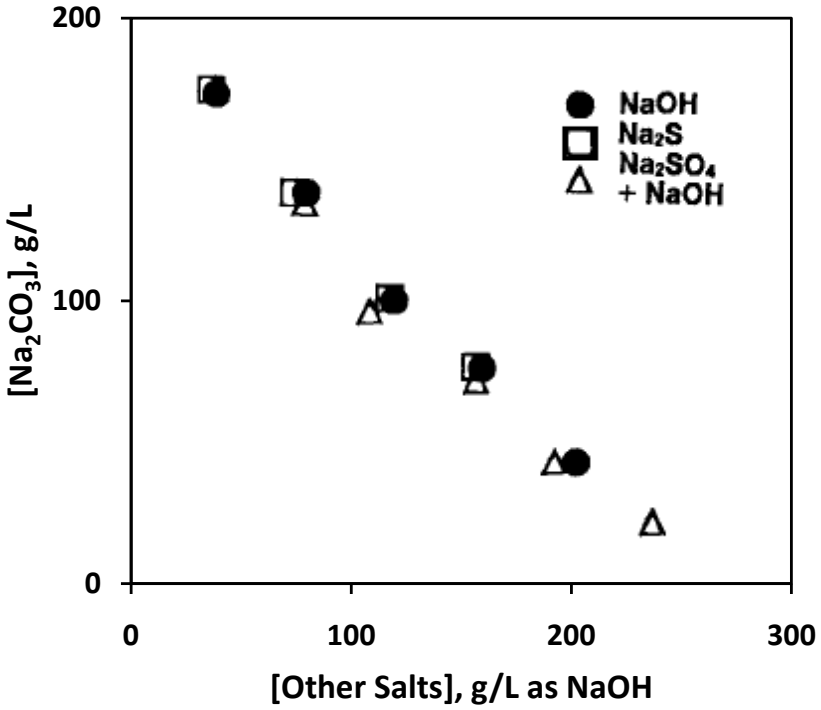

Figure 2-5: *The effect of different sodium salts on pirssonite solubility at 95°C [6]*

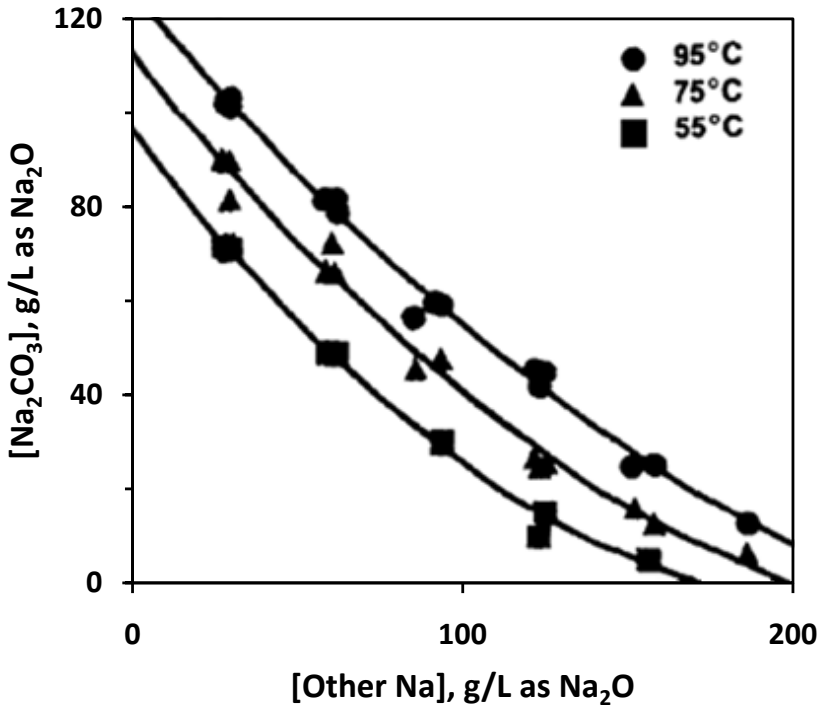

Figure 2-6: *The effect of temperature on pirssonite solubility [6]*

Frederick et al. compared their pirssonite solubility data (NaOH data at 95^{o}C as shown in Figure 2-5) with those published by Littman and Gaspari (Figure 2-4). The comparison plot is shown in Figure 2-7 where open circles represent the solubility values of pirssonite published by Littman and Gaspari and filled circles represent the work of Frederick et al. Both sets of data are in good agreement. However, it is noteworthy that pirssonite solubility in pure Na_2CO_3 solution (when NaOH concentration is zero) was not compared in this figure. This solubility behavior is shown by point "Q" in the phase diagram published by Littman and Gaspari, which has a value of about 335 g/L of Na_2CO_3. The same solubility data can be obtained from Frederick et al. (Figure 2-6), by reading the y-axis value of the extrapolation curve at x = 0, which corresponds to about 129 g/L of Na_2O or 221 g/L of Na_2CO_3. This value is considerably lower than 335 g/L of Na_2CO_3 indicating possible errors associated with the extrapolation lines through Frederick et al.'s experimental points.

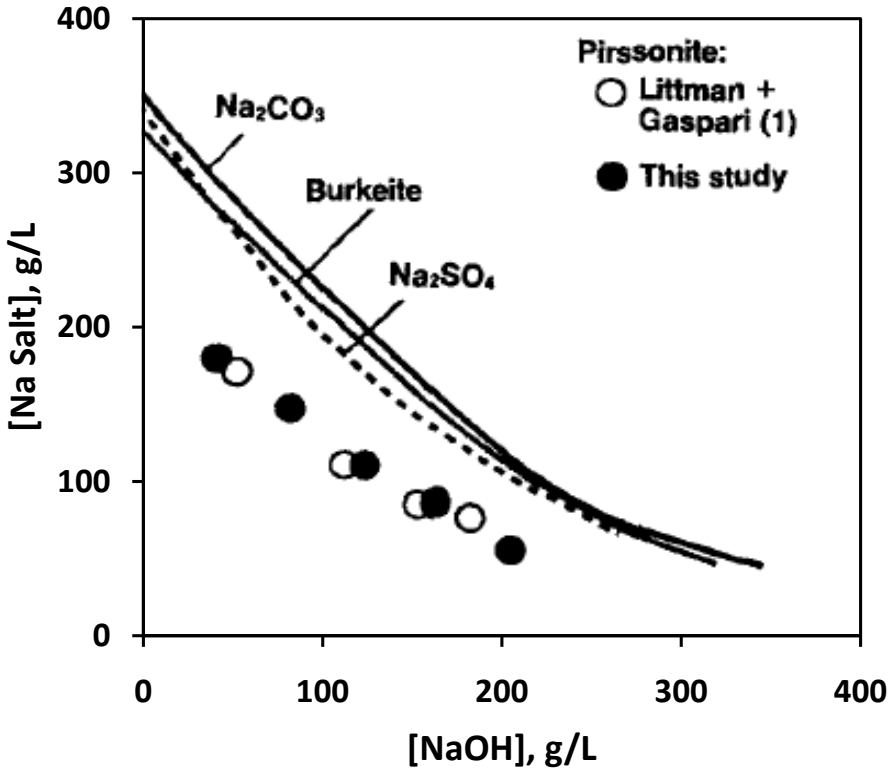

Figure 2-7: *Solubility of pirssonite in NaOH solutions at 95^{o}C [6]*

As mentioned earlier, Ulmgren et al. extended the work done by Frederick et al. to accommodate for green liquor solution generated from a gasifier. They studied the solubility of pirssonite in a temperature range of 95^{o}C-125^{o}C and published a linear model based on their experimental data

that calculates pirssonite solubility in green liquor solutions. However, like Frederick et al., they did not have any experimental data points in regions where the concentrations of other sodium salts are very low (Figure 2-8). This brings the validity of their linear solubility model in question.

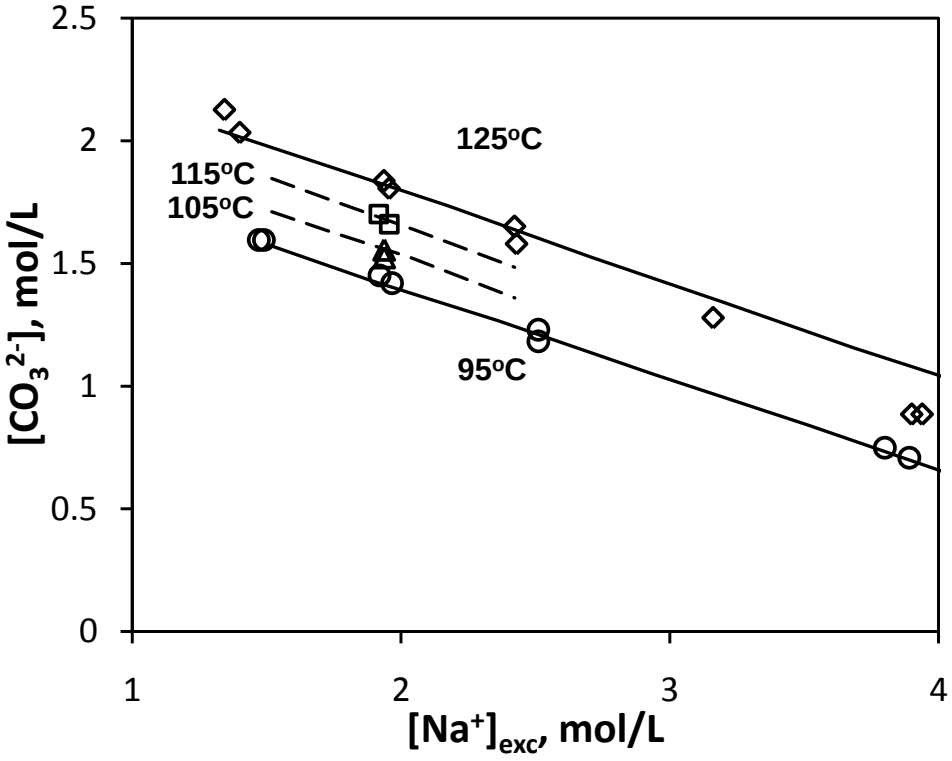

Figure 2-8: *Solubility of pirssonite reproduced from Ulmgren et al. [23]*

It is, therefore, important to revisit the solubility behavior of pirssonite under lower concentrations of sodium salts (Na_2S and NaOH) present in the solution.

Chapter 3

3 Scale Characterization

While pirssonite has often been cited in the literature to be the major component of green liquor scale, only a few papers actually provided the evidence of its presence. Frederick et al. [6] discussed pirssonite deposition problems in great detail but did not mention the deposit composition. Taylor and McGuffie [27] found both calcite and pirssonite in the green liquor scale samples that they collected at the Elk Falls mill in British Columbia. They reported that the deposit sample collected from the dissolving tank primarily composed of pirssonite (91.6 wt%) while the sample obtained from the green liquor clarifier line mainly contained calcite (85.1 wt%). Martins et al. [28] reported the presence of pirssonite along with calcite ($CaCO_3$), portlandite ($Ca(OH)_2$), larnite (Ca_2SiO_4) and brucite ($Mg(OH)_2$) in the slaker grit sample obtained from a kraft mill in Brazil.

The composition of green liquor scale must be known at individual mills, particularly those that experienced severe scaling problems. However, from the published literature information it is unclear if the scale consists of mainly pirssonite or a mixture of pirssonite, $CaCO_3$ and other compounds that are typically found in grits, dregs and lime mud. This chapter aims to identify and characterize the major phases present in green liquor scale.

3.1 Experimental Procedures

A total of 12 scale samples obtained from 10 different kraft pulp mills in Canada, United States, Brazil and New Zealand were characterized. A small amount (about 5 grams) was chiseled out from each of the scale samples, dried at 110^{o}C for 6 hours, ground into fine powder and kept in a sealed glass container until it was subjected to analysis. The analysis was performed using a simultaneous TGA/DSC Analyzer (Thermogravimetric Analysis/Differential Scanning Calorimetry). Selected samples were further analyzed using X-ray fluorescence (XRF), X-ray powder diffraction (XRD) spectrometer, Electron Micro Probe Analyzer (EPMA) and Scanning Electron Microscopy (SEM) to confirm the results obtained with TGA/DSC.

In TGA/DSC experiments, the sample was heated up to 1000^{o}C in N_2 at a heating rate of 20^{o}C/min. Changes in sample weight and thermal events that occurred during heating were

continuously monitored. The TGA/DSC thermal profile for each sample was compared against the thermal profiles for two standard chemicals: the analytical grade $CaCO_3$ from Fisher Scientific and pirssonite from Mineralogical Research Company.

3.2 Results and Discussions

Thermal Profile for $CaCO_3$

As shown in Figure 3-1, the thermal profile of the standard $CaCO_3$ consists of a single endothermic peak, corresponding to the decomposition of $CaCO_3$ into CaO and CO_2. This decomposition occurs in N_2 between 600^{o}C and 830^{o}C. The weight loss resulting from CO_2 escaping from the sample is about 43 wt%, which is close to 44 wt%, the theoretical weight loss of $CaCO_3$.

Thermal Profile for Pirssonite

The thermal profile of the standard pirssonite is shown in Figure 3-2. It consisted of four main events: i) the dehydration of pirssonite between 150^{o}C and 230^{o}C that resulted in a 15% weight loss of the sample, ii) two solid-solid phase transitions of anhydrous $Na_2Ca(CO_3)_2$ at 360^{o}C and 430^{o}C, iii) the decomposition of $CaCO_3$ into CaO and CO_2 between 670^{o}C and 870^{o}C that resulted in an additional 18% weight loss, iv) the melting of the Na_2CO_3 at around 850^{o}C with no weight loss. There was a slight overlap between the events iii) and iv).

The approximate weight changes and the chemical reactions involved in the above four steps are summarized in Table 3-1. The profile obtained in this study was similar to that of pirssonite obtained by Ulmgren et al [23].

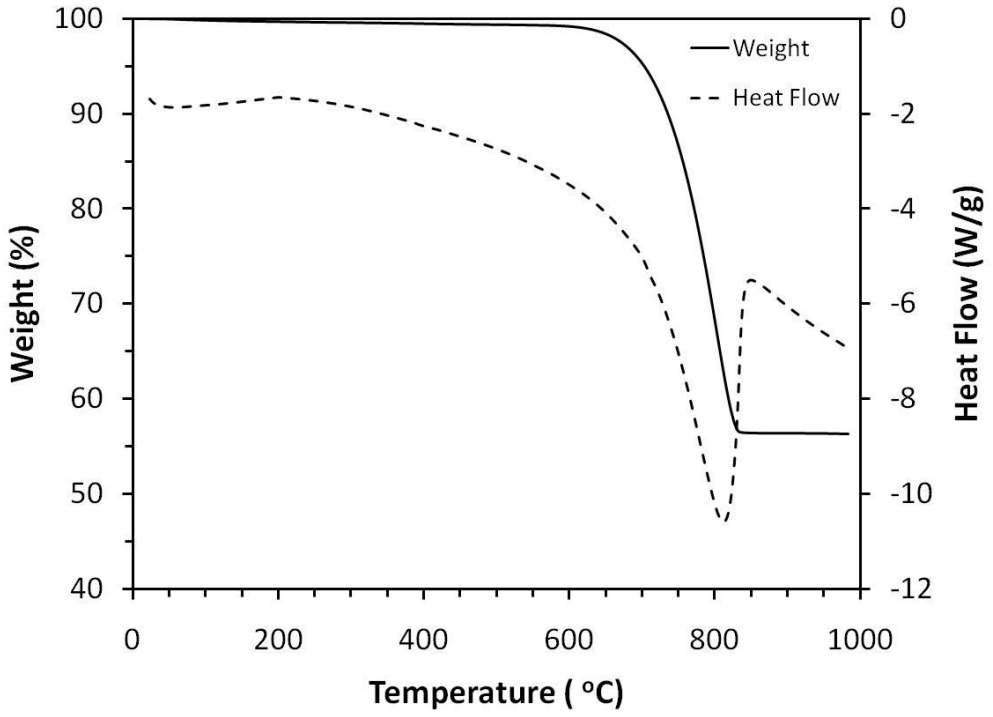

Figure 3-1: *TGA/DSC thermal profile for the pure $CaCO_3$ used as standard*

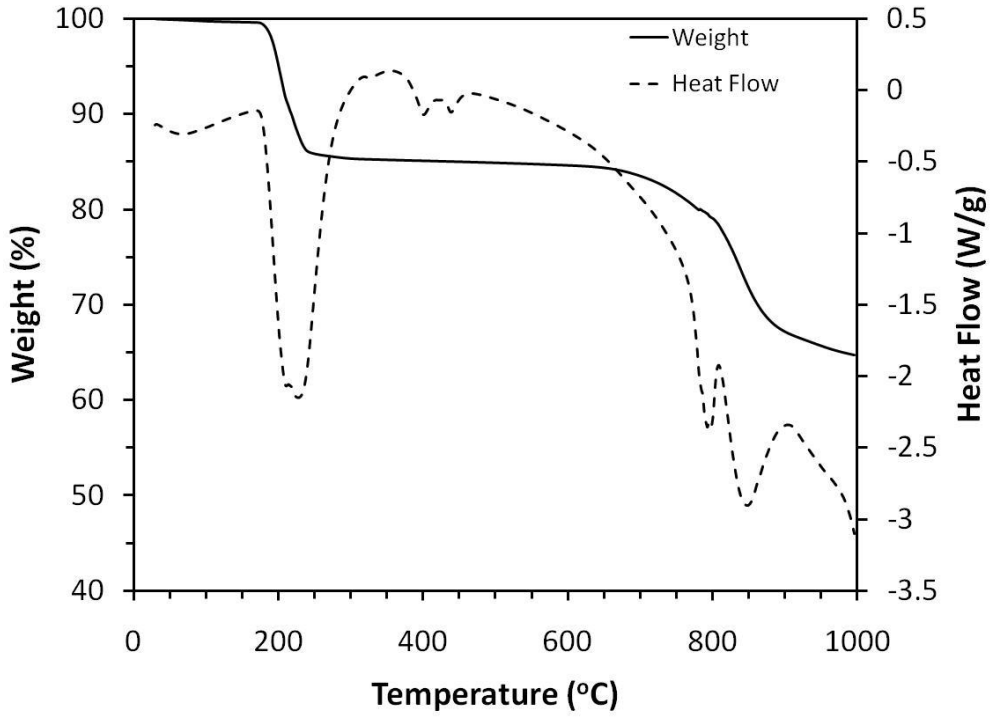

Figure 3-2: *TGA/DSC thermal profile for the commercial pirssonite crystal used as standard*

Table 3-1: *Thermal events and reactions that occur during the heating of pirssonite*

Temperature Range	Steps	Reactions	Weight Change
150°C – 230°C	Dehydration	$Na_2CO_3 \cdot CaCO_3 \cdot 2H_2O \rightarrow Na_2CO_3 \cdot CaCO_3$	15% loss
360°C, 430°C	Solid-solid phase transitions	From one form of $Na_2CO_3 \cdot CaCO_3$ to another	No change
670°C – 870°C	Decomposition of $CaCO_3$ in anhydrous pirssonite	$Na_2CO_3 \cdot CaCO_3(s) \rightarrow Na_2CO_3 + CaO + CO_2$	18% loss
850°C	Melting of Na_2CO_3	$Na_2CO_3(s) \rightarrow Na_2CO_3(l)$	No change

Scale Characterization

Figure 3-3 shows photos of the 12 scale samples characterized in this study. The alphabet letter and the Roman numeral below each photo represent the mill and sample identifications respectively. Six of the scale samples (A and Cii-G) were collected from the pipeline after the dissolving tank. Sample C-i was taken from the slaker. Sample H-i was taken from the feed tube of the centrifuge that takes the underflow of the clarifier. Sample H-ii was obtained from the dissolving tank agitator blade. Sample I was taken from the pump after the clarifier and sample J was collected from the valve of the pipeline that carries green liquor from the clarifier to the slaker. The extract location of sample B is not known.

Based on their TGA/DSC thermal profiles and elemental analysis results, four of these samples were identified as pirssonite (samples C-i, H-ii, I and J). The other eight consisted mostly of calcite ($CaCO_3$) and no pirssonite, except sample F which also contained calcite, but was mixed with some $CaSO_4$ and manganese oxide. Three (C-i, I and J) out of the four samples identified as pirssonite appeared to include large glassy crystals in them (Figure 3-4a) and were relatively brittle. The fourth sample (H-ii) was densely packed and did not contain large crystals, although, a closer look at the sample revealed its shiny surface with very small crystals in it (Figure 3-4b).

A: Calcite

B: Calcite

C-i: Pirssonite

C-ii : Calcite

D: Calcite

E: Calcite

F: Calcite and others

G: Calcite

H-i: Calcite

H-ii: Pirssonite

I: Pirssonite

J: Pirssonite

Figure 3-3: *Green liquor scale samples obtained from various kraft pulp mills*

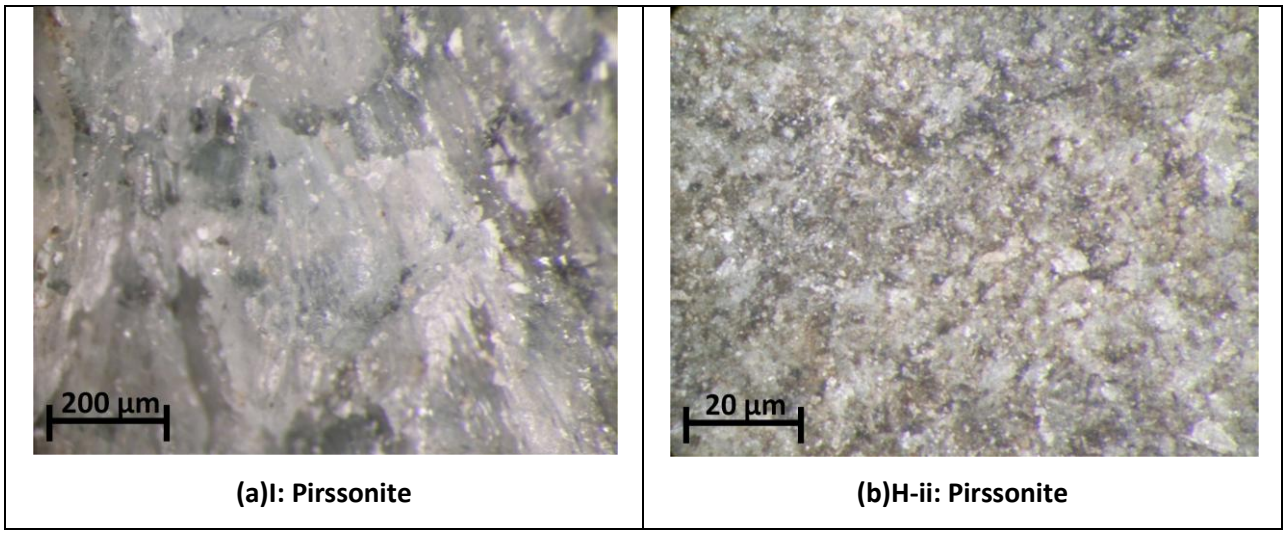

Figure 3-4: *Pirssonite scale samples observed using an optical microscope*

Samples identified as calcite were harder and contained many layers (see sample A in Figure 3-3). Despite its stratified appearance, sample A has a relatively uniform composition across the sample, which was verified by scanning the cross-section of the sample using an electron microprobe analyzer (EMPA). Figure 3-5 shows the cross-section of sample A embedded in an epoxy mount that was used in EMPA, where the white arrow indicates the direction of scan performed on this sample. Figure 3-6 shows the elemental map obtained on the scale sample across its 1.4 cm cross-section. The large amount of Ca (about 41 wt%) and a very small amount of Na (0.15 wt%) in the sample indicate that the sample contained mostly $CaCO_3$ along with some other calcium compounds in it.

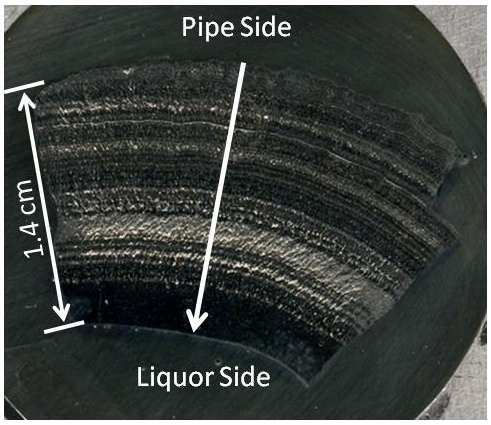

Figure 3-5: *Cross-section of sample A used in EMPA*

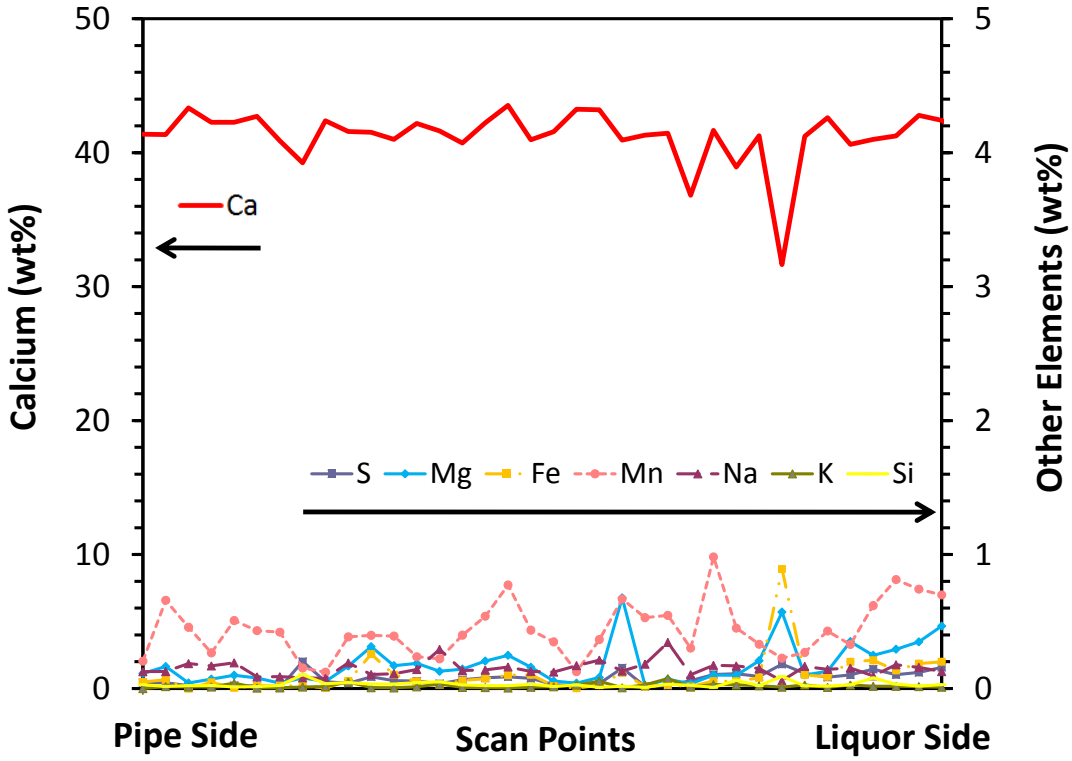

Figure 3-6: *EMPA analysis across scale sample A.*

Below are two representative examples of how TGA/DSC thermal profiles were used to characterize the scale samples in this study. One is shown in Figure 3-7 for sample A (calcite) and the other is in Figure 3-8 for sample I (pirssonite).

The thermal profiles for sample A in Figure 3-7 are strikingly similar to those for pure $CaCO_3$ (Figure 3-1). The major endothermic peak is observed between 620°C and 830°C, which is characteristic of $CaCO_3$. The weight loss associated with this peak is about 42% indicating the $CaCO_3$ content in sample A is about 95%. In Figure 3-8, the first four endothermic peaks summarized in Table 3-1 are clearly visible. The first weight loss associated with the dehydration of water is about 15% and the second weight loss associated with the decomposition of $CaCO_3$ is about 17%. Since a complete decomposition of $CaCO_3$ from pure pirssonite would have a weight loss of 18%, it can be concluded that sample I consists mostly of pirssonite (at least 95%) with some other minor impurities.

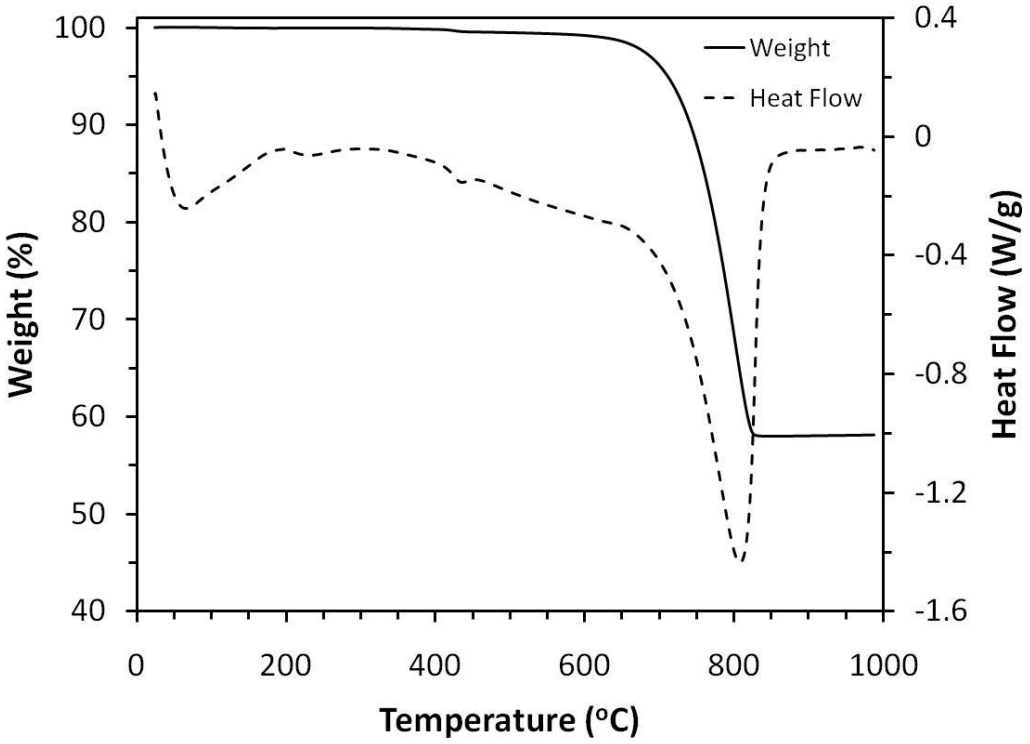

Figure 3-7: *Thermal profile for sample A*

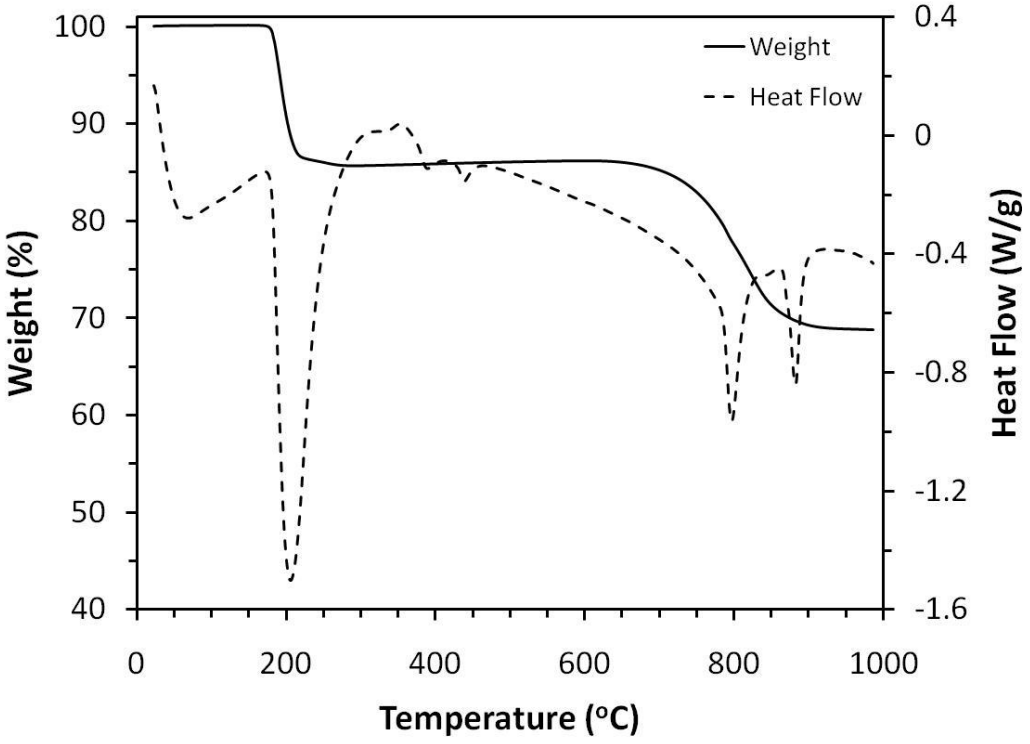

Figure 3-8: *Thermal profile for sample I*

Table 3-2 summarizes elemental compositions of samples A and I determined by XRF. Sample A contained 38.3 wt% Ca (or 96 wt% $CaCO_3$) with little Na. Sample I, on the other hand, contained less Ca but a much larger amount of Na. The Na_2/Ca molar ratio for this sample is (18.7/46)/(16/40) = 1.0, indicative of pirssonite. These results are consistent with TGA/DSC results, suggesting that sample A consists of mostly $CaCO_3$ and sample I mostly pirssonite.

Table 3-2: *Composition of sample A and I in wt%*

Elements (XRF)	Sample A	Sample I
Ca	38.3	16.0
Na	0.73	18.7
Mg	0.57	0.16
S	0.23	0.28
Mn	0.44	0.05
Fe	0.25	0.03
Al	0.07	0.03
Si	0.09	0.04
P	0.04	Trace
K	0.01	0.02
Sr	Trace	0.34
Ba	0.22	Trace
Other (Ni, Zn, Cu, Cl, etc.)	0.13	0.03

X-ray diffraction analysis was also used to confirm the mineral phases present in sample A and I. As shown in Figure 3-9 and 3-10, the XRD patterns for these two samples show the dominance of calcite in sample A and pirssonite in sample I.

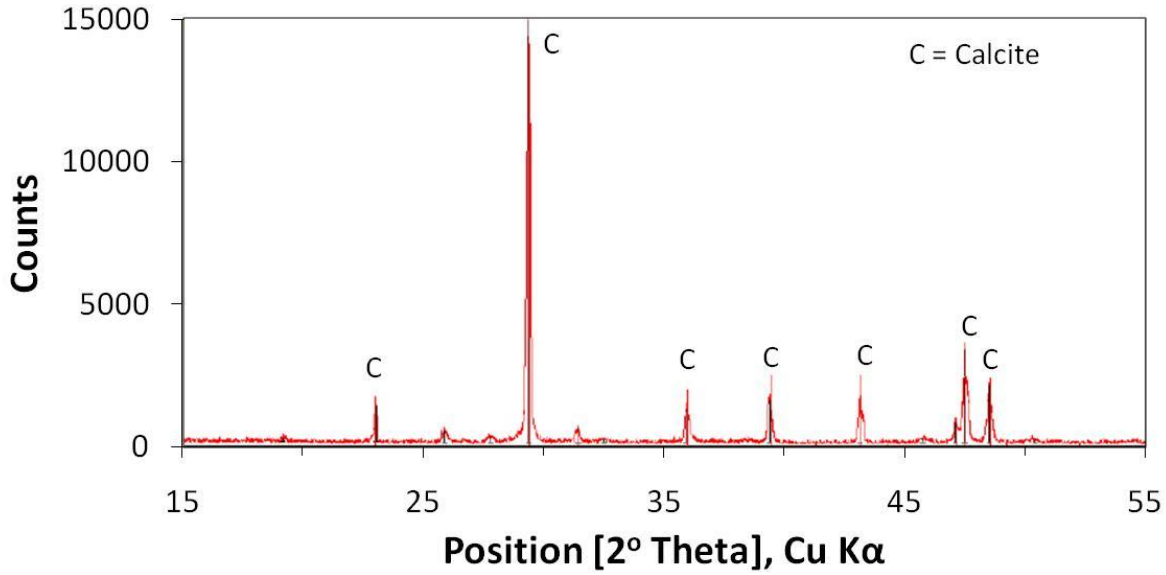

Figure 3-9: *XRD result for sample A-Calcite*

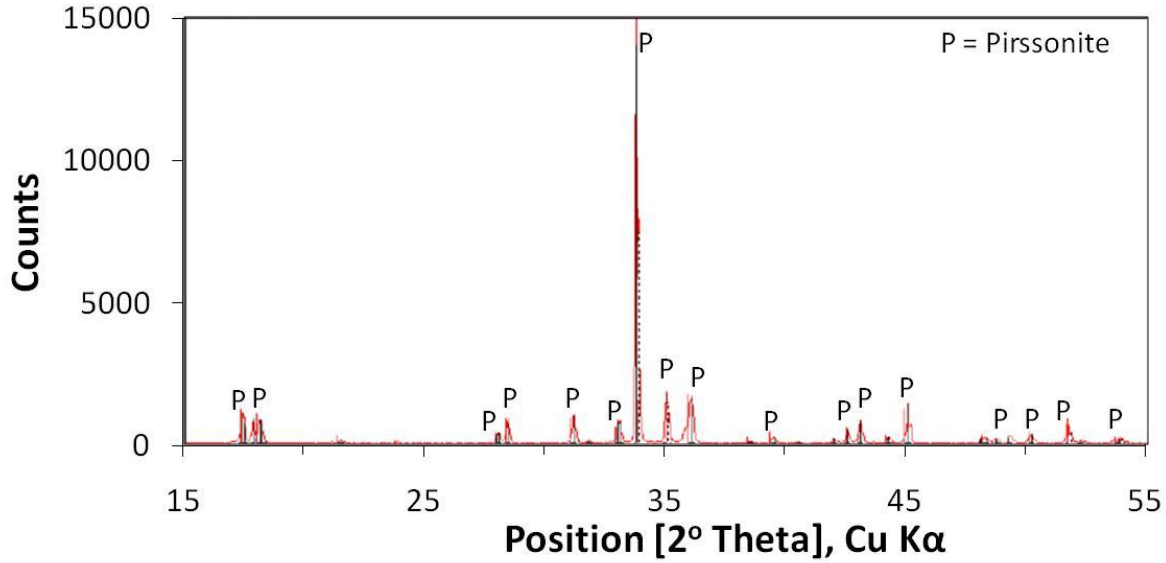

Figure 3-10: *XRD result for sample I-Pirssonite*

Figure 3-11 shows the SEM (Scanning Electron Microscope) images obtained for sample A and I. The size of the calcite grains is approximately 1 micron with smooth inter-grown blocks. The grains for pirssonite are much larger than calcite with its grain size ranging from about 100-300 microns. The hexagonal crystal habit observed in sample I is characteristic of pirssonite crystal as reported in the literature [16].

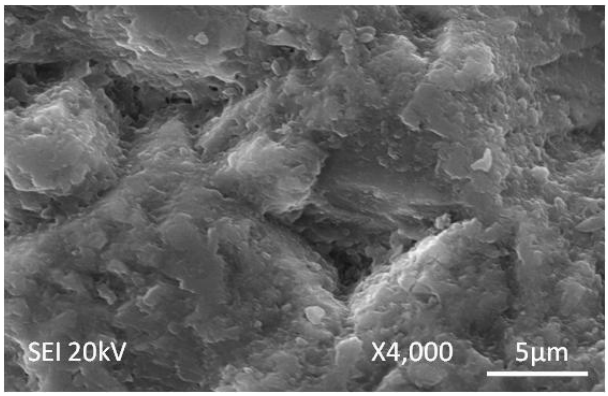

A: Calcite

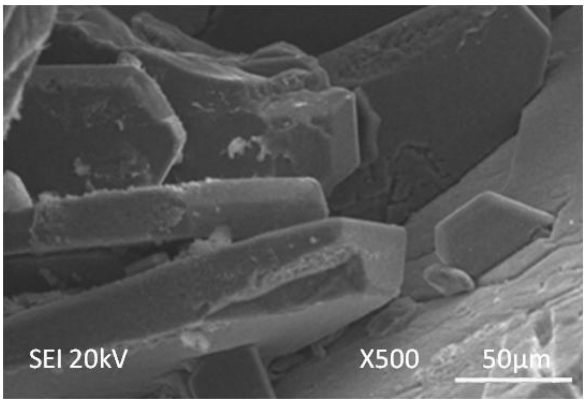

I: Pirssonite

Figure 3-11: *SEM micrograph of sample A& I*

IMPLICATIONS

Scaling in a pipeline occurs when crystals of a compound precipitate from the liquid that flows through the pipeline as a result of supersaturation of that compound in the liquid. The three compounds that form pirssonite in the green liquor handling systems are Na_2CO_3, $CaCO_3$ and H_2O. Na_2CO_3 and H_2O are the main components of the green liquor and hence are inherently present, while $CaCO_3$ originates from calcium compounds in smelt and/or from lime mud particles suspended in the weakwash.

Since Na_2CO_3 is highly soluble in green liquor and $CaCO_3$ has very low solubility, pirssonite may form through one of the following mechanisms: a) direct reaction between Na_2CO_3 in the solution and the surface of $CaCO_3$ particles or b) continuous dissolution of $CaCO_3$ particles to sustain the amounts of free Ca^{2+} ions in the solution which subsequently react with the Na^+ and the CO_3^{2-} ions to precipitate pirssonite as a new phase. The transformation of calcium carbonate to pirssonite through this continuous dissolution and re-precipitation mechanism was also postulated by Bialik et al [29]. These two mechanisms are discussed in details in section 4.3 of Chapter 4.

In this work, only 4 out of 12 scale samples were found to consist of pirssonite; the remaining mostly composed of $CaCO_3$. The predominant presence of $CaCO_3$ in the scale samples may be explained as follows.

Since the solubility of pirssonite is governed by temperature and Na_2CO_3 concentration of the green liquor [6, 7, and 14], it is possible that Na_2CO_3 incongruently dissolves from the pirssonite scale when the aqueous Na_2CO_3 concentration in the green liquor falls below the solubility limit of pirssonite. It is a common practice in many kraft mills to prevent scaling by switching green liquor and weak wash flows in the pipelines between the dissolving tank and the green liquor clarifier on a weekly basis [30]. It is possible that the pirssonite scale first forms during upset conditions (low temperature and high TTA). The formed pirssonite selectively leaches out its Na_2CO_3 part when the TTA is back to normal or during the weak wash switch, leaving the $CaCO_3$ part behind. The same concept may also be applied to the scale samples in the dissolving tank where localized and high TTA conditions may prevail leading to the precipitation of pirssonite, followed by incongruent dissolution of the pirssonite at a lower TTA level. This hypothesis has been investigated by conducting experiments. The experimental procedures to test this hypothesis and the results obtained are discussed in the next chapter.

3.3 Summary

A systematic study was carried out to characterize 12 green liquor scale samples collected from 10 kraft pulp mills. The results show that only one third (4) of the samples were pirssonite and two thirds (8) were predominantly calcite. It is not known why the majority of samples were made of mostly calcite. One explanation is that it may be a result of selective dissolution of Na_2CO_3 from the pirssonite scale during the time when the green liquor TTA was low, leaving the insoluble $CaCO_3$ behind.

Chapter 4

4 Experimental

This chapter focuses on the experiments conducted in this work with the following aims: (1) study the solubility of pirssonite in green liquor solution; and (2) investigate the incongruent dissolution of Na_2CO_3 from pirssonite, as speculated in Chapter 3. This chapter is sub-divided into two sections that describe the experimental procedures and the results obtained in each kind of tests.

4.1 Solubility of Pirssonite

4.1.1 Apparatus

Low temperature (< 75^{o}C) experiments were carried out in 1 L erlenmeyer flasks immersed in a water bath. The water bath temperature was controlled using a temperature controller. The water bath was placed on two stir plates to provide agitation in the solution in the erlenmeyer flask.

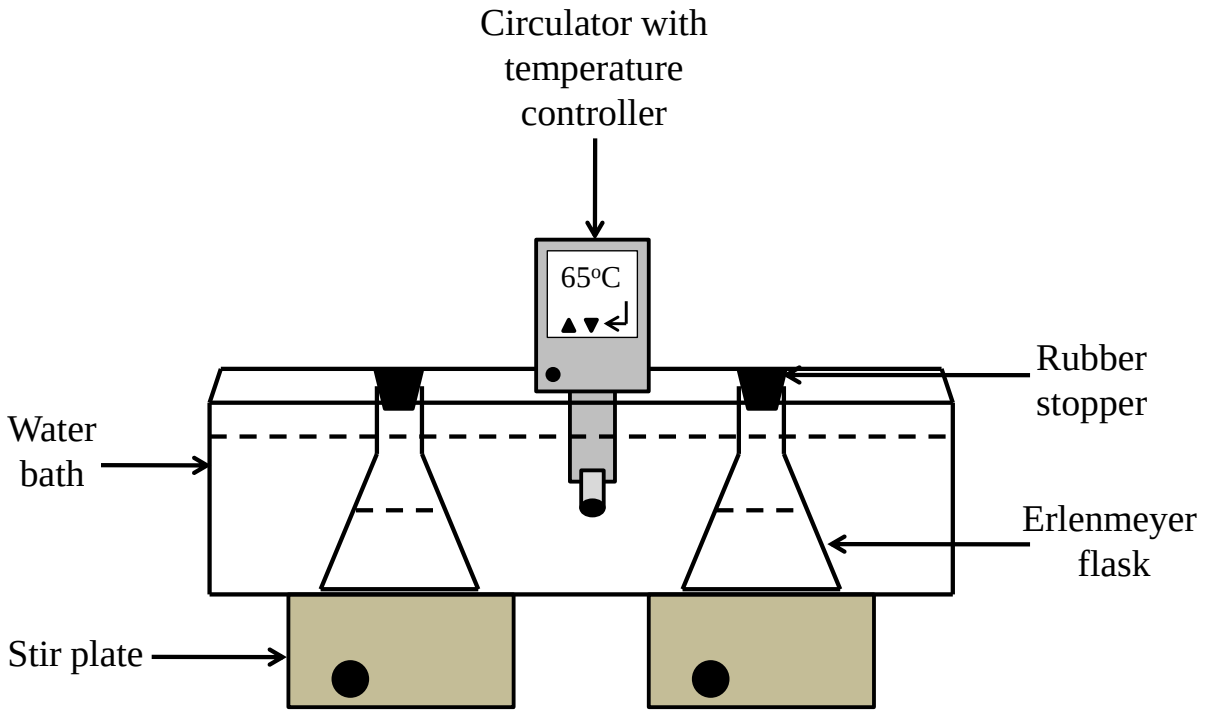

Figure 4-1: *Experimental set-up used for low temperature reactions*

High temperature experiments were carried out in 1 L jacketed reactor vessel. The heating in the reactor was provided by circulating oil through the jacket using a heated circulating bath that also has a temperature controller. Agitation was provided by inserting a shaft stirrer from the top of the reactor.

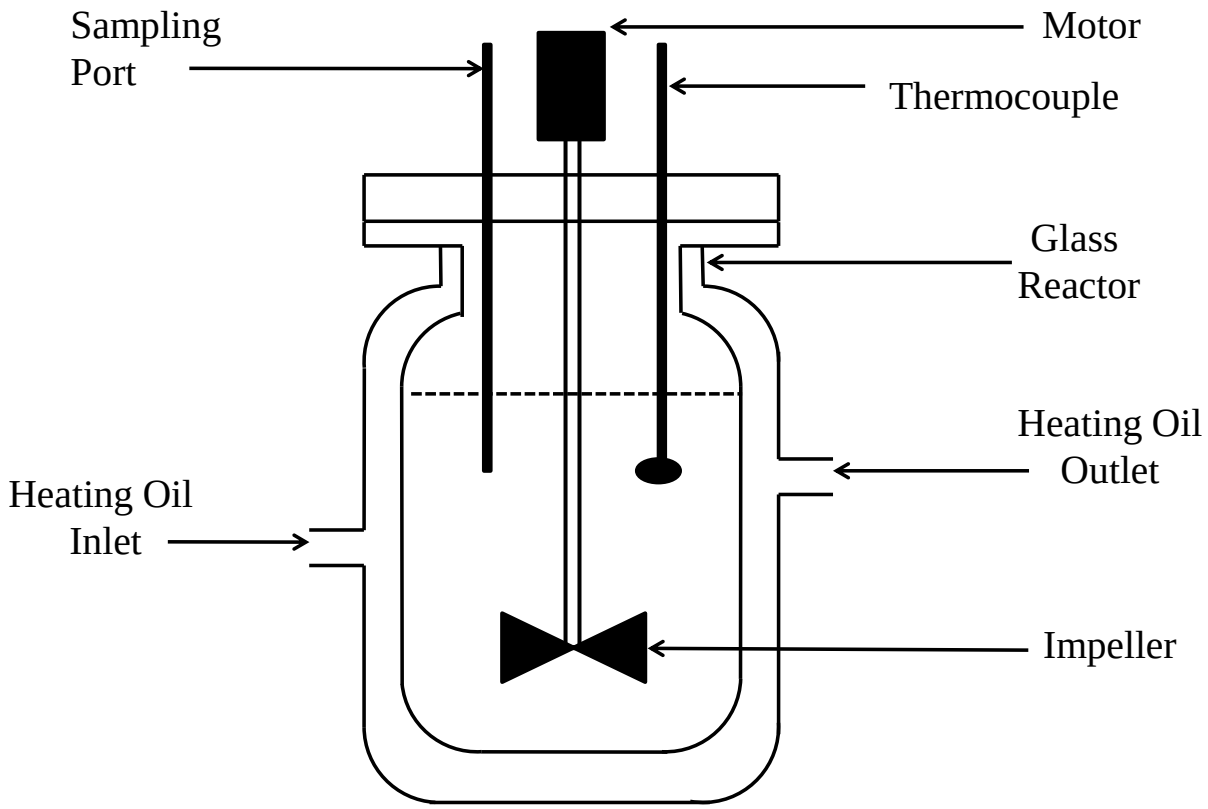

Figure 4-2: *Experimental set-up used for high temperature reactions*

4.1.2 Chemicals and Sampling Procedures

All chemicals used in this study were analytical grade obtained from Fisher Scientific unless otherwise specified. All solutions were prepared by dissolving reagent grade chemicals directly in deionized water without further purification. In both set-ups, liquid samples were withdrawn through a dip tube and a syringe. Filtrations were performed using a 0.45 µm nylon syringe filter. Liquid samples were immediately diluted with deionized water to prevent precipitation. Solid samples were also collected by filtering out solid from the liquid phase using 0.15 µm filter paper. Syringe, dip-tube and syringe filters were pre-heated to the solution temperature in order to ensure the withdrawn sample was maintained at the solution temperature.

4.1.3 Na_2CO_3-$CaCO_3$-H_2O System

The Na_2CO_3-$CaCO_3$-H_2O system was investigated at 55°C, 65°C, 75°C, 85°C and 95°C in order to reproduce the solubility curve published by Bury and Redd [17]. Excess amount of $CaCO_3$ was added in a solution of Na_2CO_3 and H_2O. A small amount of the solution was collected at a set time interval and the Na^+ concentration was determined using Atomic Absorption Spectroscopy. Calcium carbonate content in the solution was too small to detect. Solid samples were analyzed using Thermogravimetric analysis to determine their compositions.

Figure 4-3 shows the kinetic results for the reactions carried out at 85°C and 95°C. The sodium concentration decreases with time until it reaches a plateau indicating that equilibrium has been established. The equilibrium Na_2CO_3 concentration in the solution at 95°C is about 172 g/L of Na_2O, slightly higher than that at 85°C. It should also be noted that the kinetics of this system are rather slow. It takes about 9-12 hours to reach equilibrium.

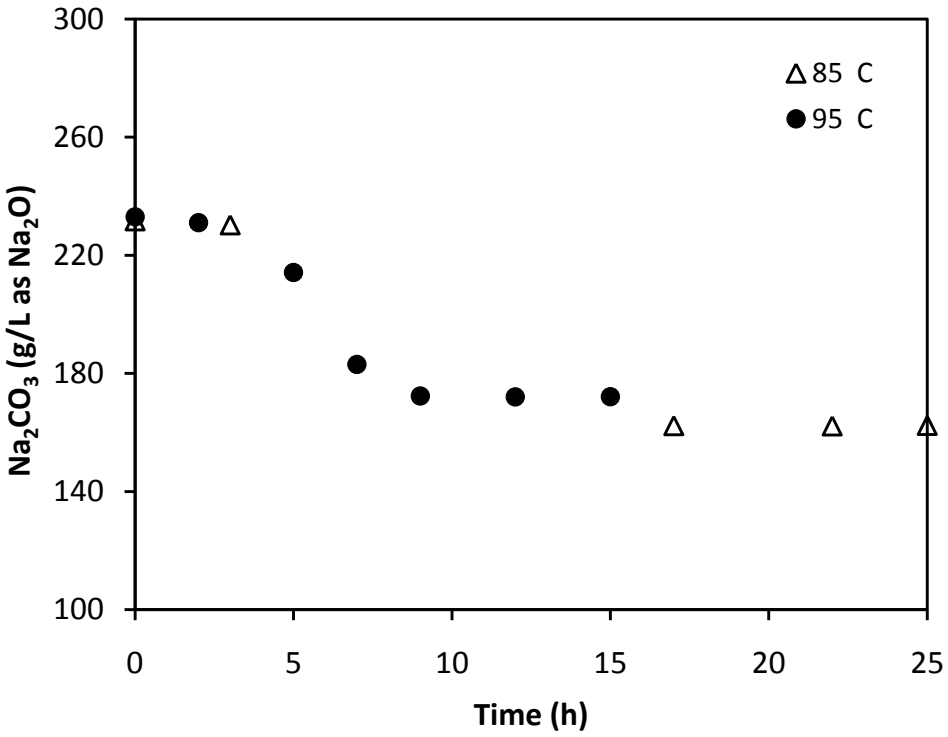

Figure 4-3: *Reaction kinetics at 85°C and 95°C*

Figure 4-4 shows the equilibrium Na_2CO_3 concentrations at all 5 temperatures obtained in this study (open triangles) and those published by Bury and Redd (filled squares).

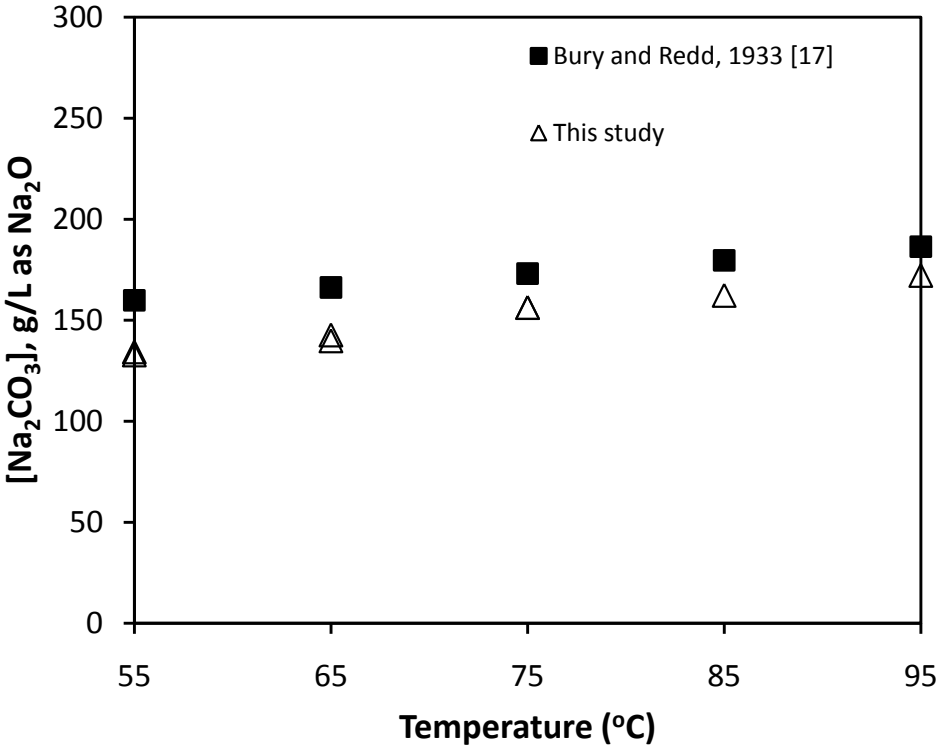

Figure 4-4: *Solubility of pirssonite obtained from this work and the literature [17]*

Solid samples were also collected from the reaction vessel at different time intervals and were analyzed using TGA/DSC. The results are shown in Figures 4-5, 4-6, 4-7 and 4-8, respectively for solid samples taken at t = 2, 5, 9 and 15 hours at 95^{o}C.

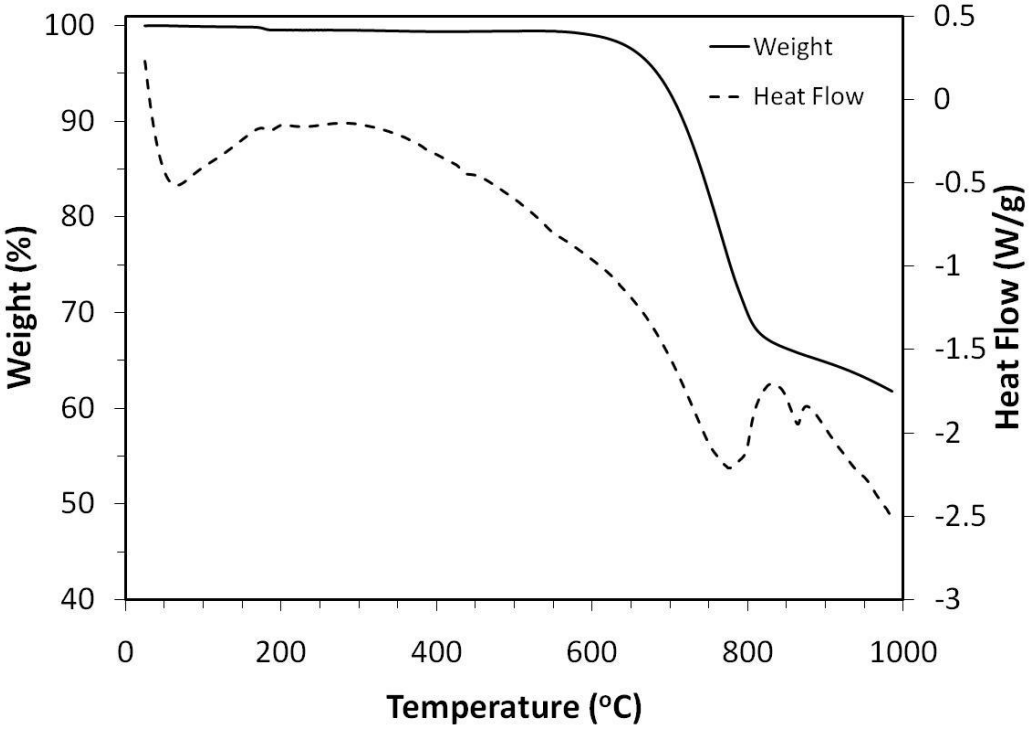

Figure 4-5: *Thermal profile of the solid sample collected at t = 2 h at 95°C*

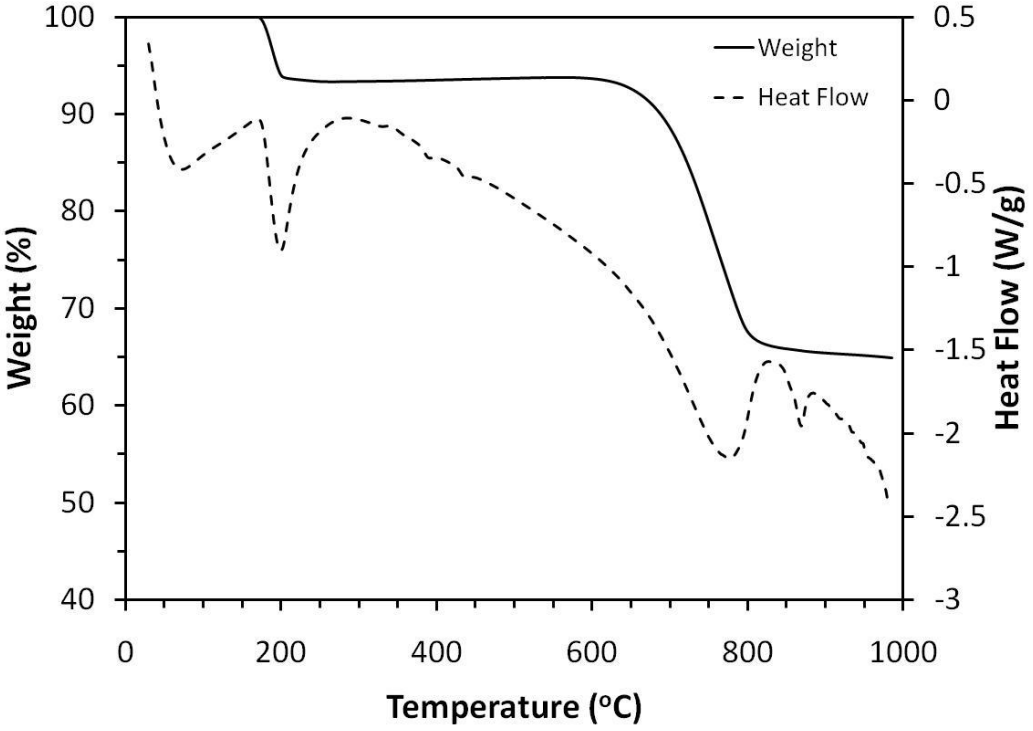

Figure 4-6: *Thermal profile of the solid sample collected at t = 5 h at 95°C*

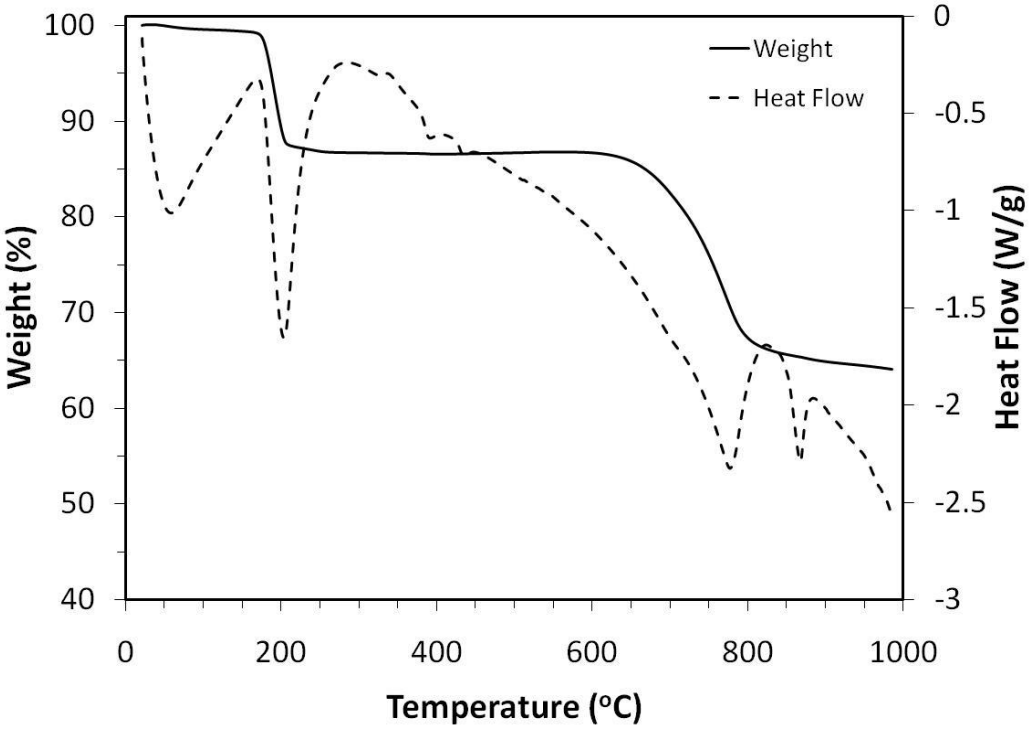

Figure 4-7: *Thermal profile of the solid sample collected at t = 9 h at 95°C*

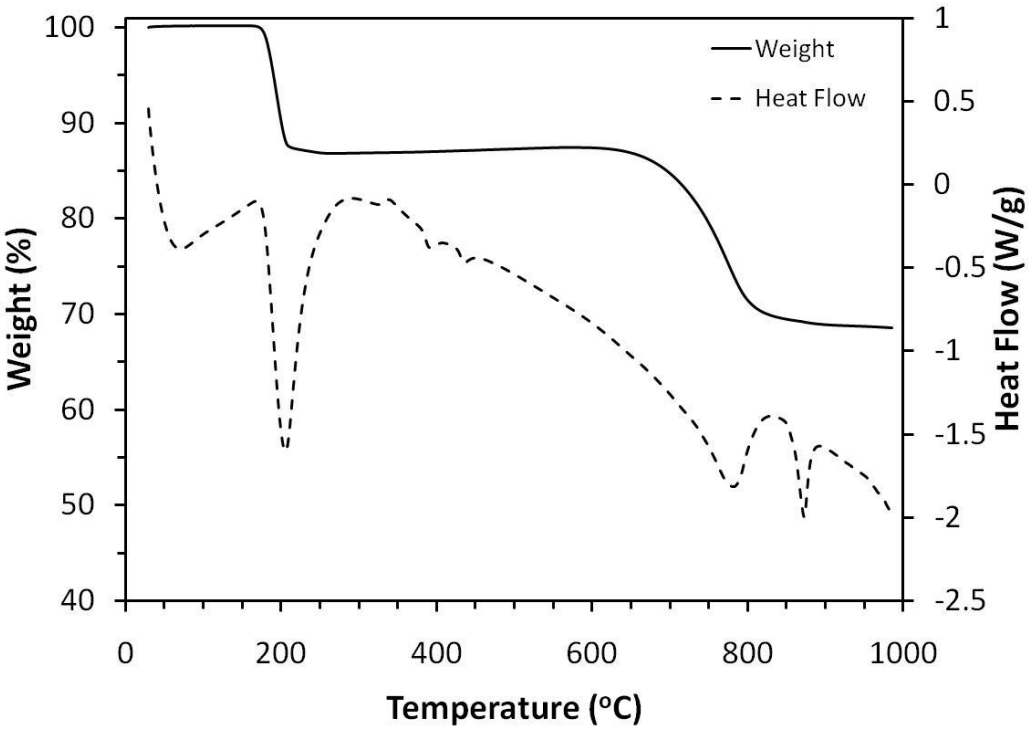

Figure 4-8: *Thermal profile of the solid sample collected at t = 15 h at 95°C*

All these four figures show the presence of pirssonite when the thermal profiles are compared to the standard profile for pirssonite (Figure 3-2). A more pronounced pirssonite thermal profile is observed as the reaction progresses, indicating a greater conversion of calcium carbonate to pirssonite. The solid sample collected at the beginning of the reaction (t=2 h) contains mostly unconverted calcium carbonate. This behavior is also seen in the kinetic profile obtained at 95^{o}C as shown in Figure 4-3, where the concentration of sodium carbonate in the solution remains unchanged from its initial concentration indicating the reaction induction period. In Figure 4-6, a small weight loss is observed around 200^{o}C with majority of the weight being lost around 680-800^{o}C attributed to the presence of a large amount of calcium carbonate in the sample with a small amount of pirssonite in it. When the total amount of water losses due to the dehydration of pirssonite are compared in Figure 4-5 to 4-8, it has been observed that the percent of water losses increase from 0.4% to 6.6% to 12.8% to 13.2% as the reaction proceeds. Figure 4-9 shows the percent conversion of $CaCO_3$ to pirssonite with time. The other main feature of pirssonite is the presence of endothermic peaks around 360^{o}C-430^{o}C where crystal transformation of the double carbonate, $Na_2CO_3 \cdot CaCO_3$, occurs with no weight change as described in Chapter 3. The formations of these peaks are more distinct in Figure 4-7 and 4-8 than in Figure 4-6 as the reaction progresses. These peaks are virtually non-existent in Figure 4-5 when the reaction is at the induction period stage.

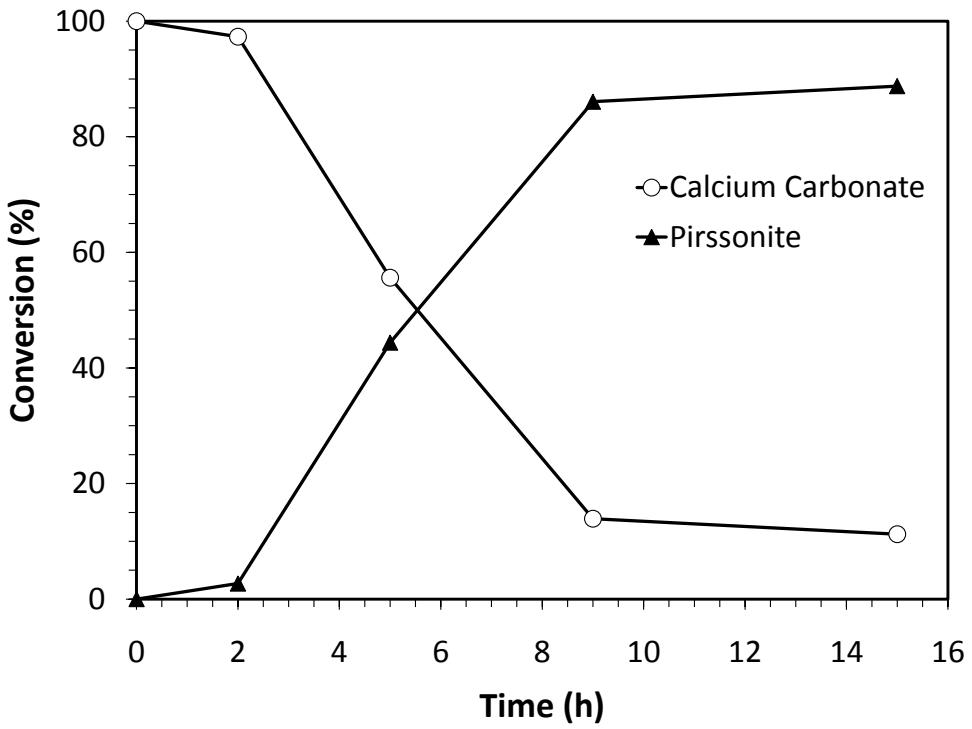

Figure 4-9: *Conversion of $CaCO_3$ to pirssonite with time at 95^oC*

The presence of pirssonite in the solid sample was also confirmed by X-Ray Diffraction technique. Figure 4-10 shows the diffractogram obtained for the sample collected at t = 15 h. Both pirssonite and calcite were identified by XRD analysis. The presence of calcite in the sample is due to the excess amount of calcium carbonate that was placed initially in the reactor in order to ensure pirssonite formation is dictated by the solubility limit of Na_2CO_3 (CO_3^{2-} ions) in solution only.

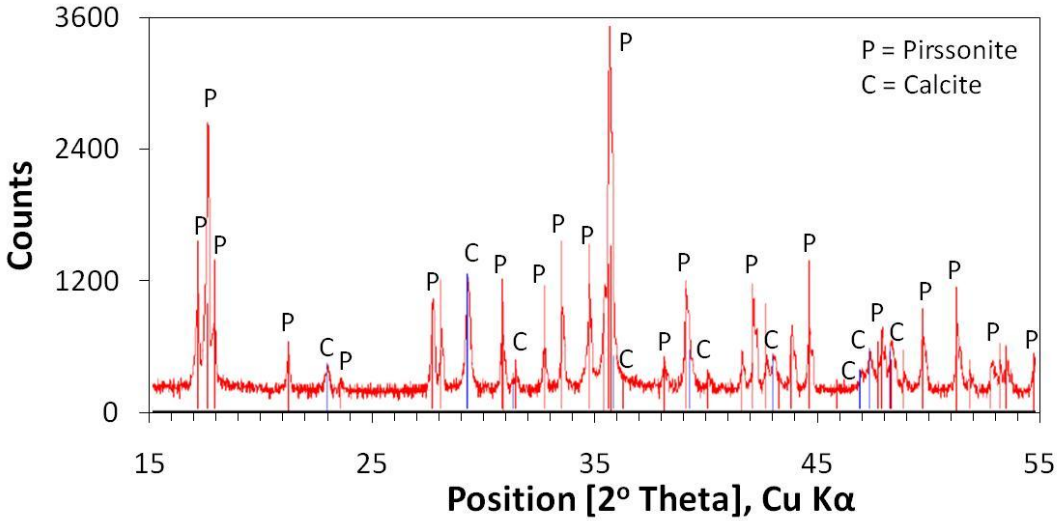

Figure 4-10: *XRD of the solid sample collected at t = 15 h at 95°C*

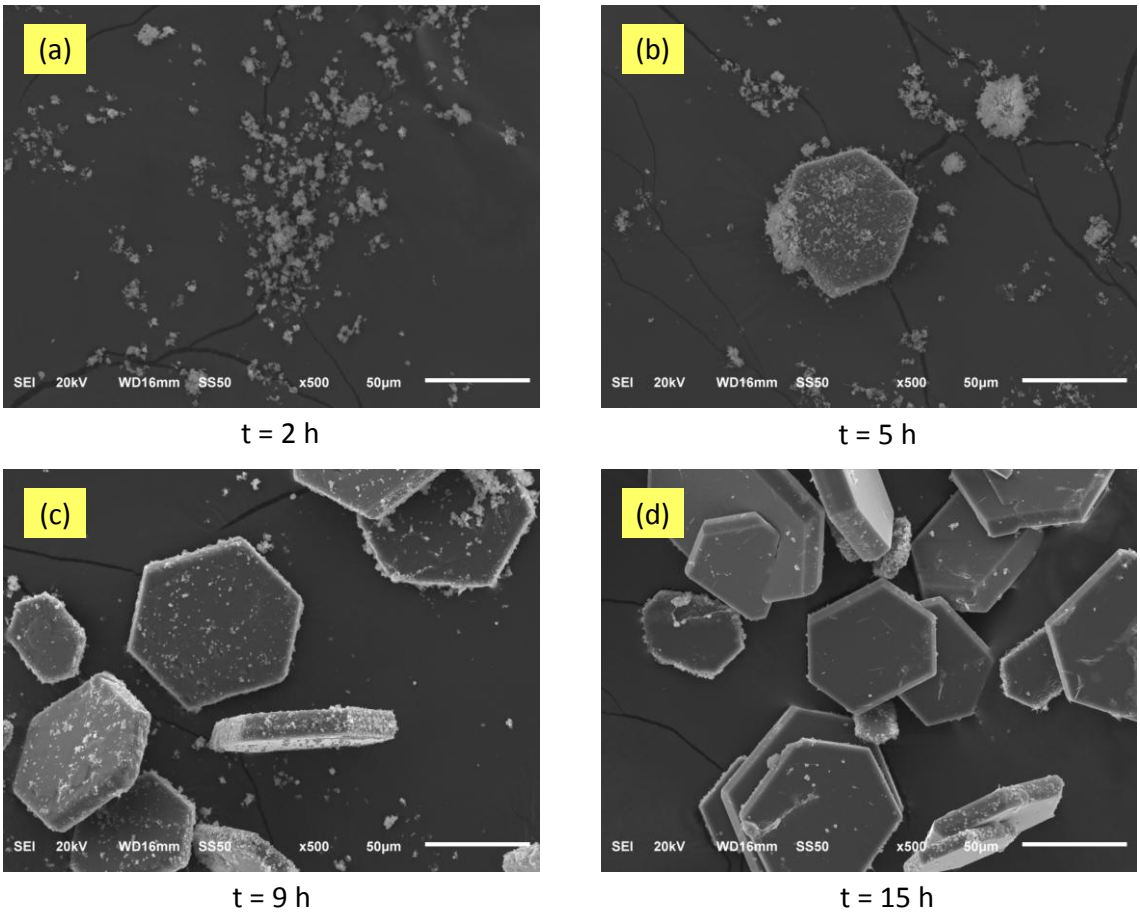

Figure 4-11: *SEM images of the solid samples taken at t = 2, 5, 9 and 15 h at 95°C*

Figure 4-11 shows the SEM images of the above-mentioned four solid samples. Two different crystal phases are observed and crystal transformation from one phase to another occurs as time progresses. The crystals seen in Figure 4-11a) are much smaller than the crystals observed in the other three images. The crystals observed in Figure 4-11a) have spherical shapes with size < 1µm and SEM-EDS performed on this sample confirmed that the sample mostly consists of $CaCO_3$ (See Figure B-1 in Appendix B). The hexagonal crystal habit of pirssonite is clearly visible in Figure 4-11b, c and d, with average crystal size of about 50 µm. The small calcium carbonate particles are more pronounced at t = 5 and 9 hours and become less visible at t = 15 hours, when the reaction reaches completion. Figure B-2 in Appendix B shows this behavior by comparing crystal phases at a lower magnification for solid samples collected at t = 9 and 15 hours.

4.1.4 Na_2CO_3-NaOH-$CaCO_3$-H_2O System

As mentioned earlier, Frederick et al. investigated the effect of other sodium salts such as NaOH and Na_2S on pirssonite solubility in the concentration range of 31 to 155 g/L of equivalent Na_2O at 95^oC (Figure 2-5 and 2-6). But Na_2S concentration in green liquor typically ranges from 25-50 g/L of Na_2O and NaOH concentration is about 5-16 g/L of Na_2O, which are mostly below their experimented range of concentrations. Frederick et al. extrapolated to these lower concentration regions as shown in Figure 2-6. However, a discrepancy in their extrapolated values and those published by Littman and Gaspari were observed under pure Na_2CO_3 solution conditions with no other sodium salts (NaOH = 0 g/L and Na_2S = 0 g/L) as discussed previously in section 2.4 of Chapter 2. Therefore, the effects of NaOH and Na_2S on pirssonite solubility were revisited in order to reproduce the solubility data under Frederick et al.'s conditions and to examine the dilute conditions that are more relevant to green liquor solution compositions.

Experiments were carried out in 1L jacketed reactor vessel at 95^oC. Known amounts of NaOH and Na_2CO_3 were dissolved completely in deionized water at 95^oC before excess amounts of $CaCO_3$ powder was placed in the reactor. The slurry was continuously agitated and samples were taken at regular intervals. The concentrations of OH^- and CO_3^{2-} ions in the liquid samples were determined by titrating with 1N HCL. The titrator used was the 751 GDP Titrino model from Metrohm. Solid samples were analyzed using TGA/DSC.

The effect of NaOH on the solubility of pirssonite was investigated at 95^{o}C. Figure 4-12 shows the kinetic results obtained for one of the experiments. NaOH in the solution remained constant while Na_2CO_3 decreased as more and more dissolved Na_2CO_3 from the solution reacted with $CaCO_3$ to form pirssonite until equilibrium was established. As seen in Figure 4-12, it took about 12 hours for the system to reach equilibrium. Figure 4-13 shows the equilibrium values of pirssonite solubility data with NaOH concentration varying from 0-108 g/L of Na_2O. The experiments were reproducible under Frederick et al.'s conditions, but, as shown in Figure 4-13, the solubility data in the dilute range (NaOH < 31g/L Na_2O) were much higher than those predicted by the extrapolation curve through Frederick's data points (Figure 2-6). The presence of pirssonite in the solid samples was confirmed by TGA/DSC analysis and the TGA profiles for one set of the experiments are presented in Appendix A (Figure A2-1 to A2-6).

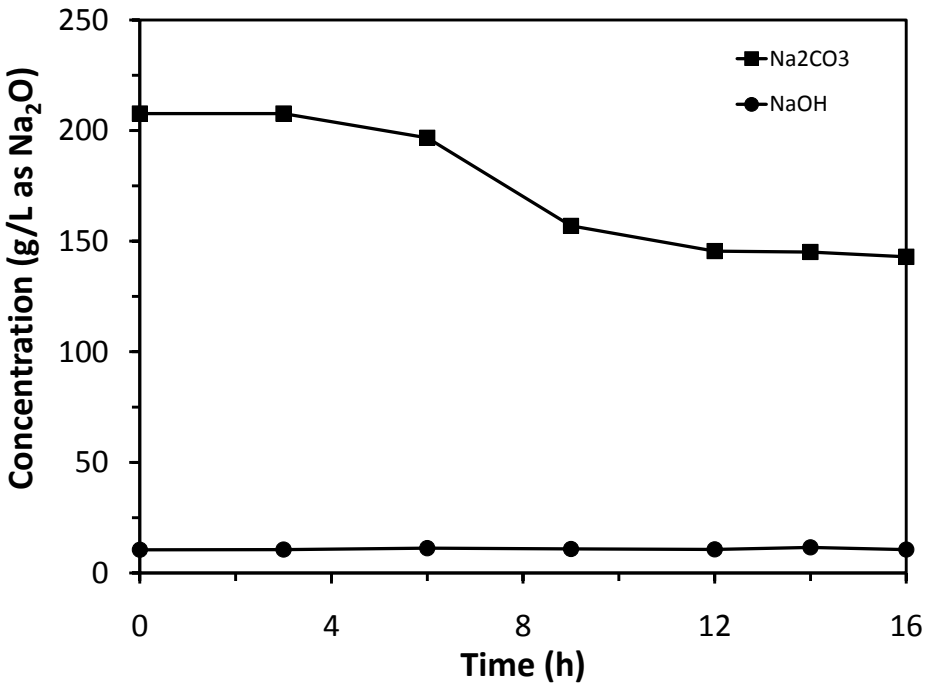

Figure 4-12: *Reaction kinetics for NaOH = 10.5 g/L of Na_2O at 95^{o}C*

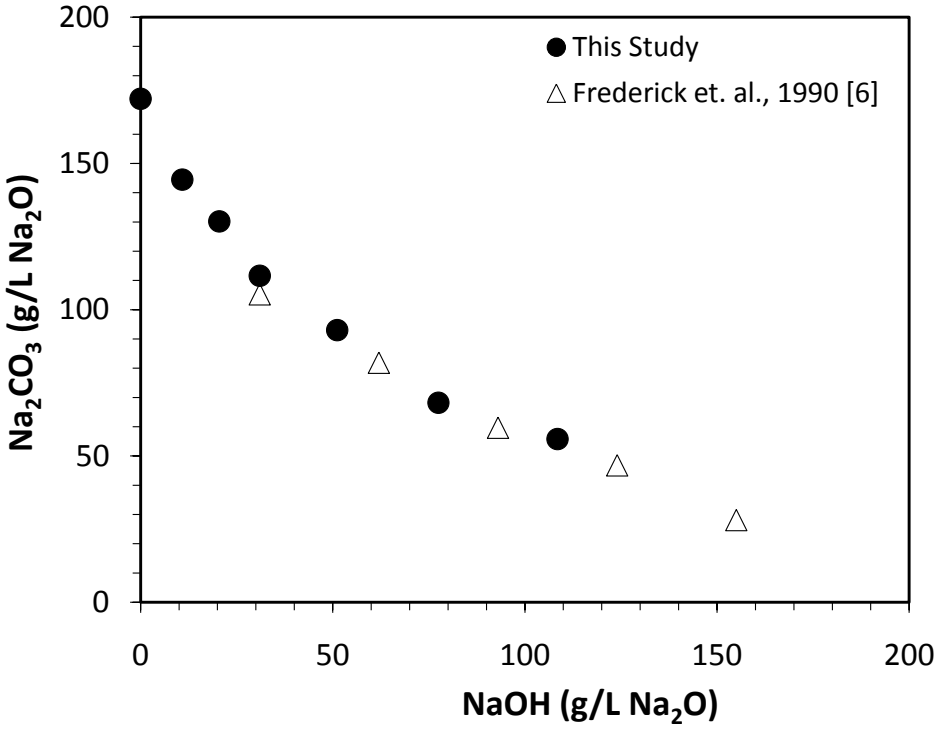

Figure 4-13: *Solubility of pirssonite in Na_2CO_3-NaOH-$CaCO_3$-H_2O system at 95^oC*

4.1.5 Na_2CO_3-Na_2S-$CaCO_3$-H_2O System

The effect of Na_2S on pirssonite solubility was examined in the double-jacketed 1 L reactor at 95^{o}C. Known amounts of Na_2S and Na_2CO_3 were dissolved completely in deionized water at 95^{o}C before calcium carbonate powder was introduced in the system. The concentrations of OH^-, HS^-, and CO_3^{2-} ions in the solution were determined using the ABC titration method in accordance with the TAPPI standard for green liquor analysis-T624os-68 [31]. The mode of operation of the Metrohm auto-titrator was "smelt", a programmed mode developed in the University of Toronto-Pulp and Paper Center to titrate green liquor solutions [32]. Figure 4-14 shows the kinetic behavior observed in one of the experiments conducted in this system where Na_2S concentration is about 40 g/L of Na_2O and Na_2CO_3 concentration decreases with time until it reaches equilibrium. It is interesting to observe that the kinetics are much slower in the presence of sodium sulfide, where it took about 48-54 hours of equilibration time in contrast to the other two systems where it took only about 9-12 hours to reach equilibrium. It was also observed that as soon as calcium carbonate powder was introduced in the clear solution of Na_2CO_3 and Na_2S, the slurry turned into a pastel green colour whereas in the other two systems

the slurry was white in colour. Figure 4-15 shows the solubility of pirssonite in the presence of Na_2S. It shows that Frederick et al.'s data is reproducible again in the sodium sulfide system and extends the graph in the lower concentration region where Na_2S concentration is less than 31 g/L of Na_2O. TGA profiles obtained on the solid samples collected from this system are shown in Appendix A (Figure A2-7 to A2-12).

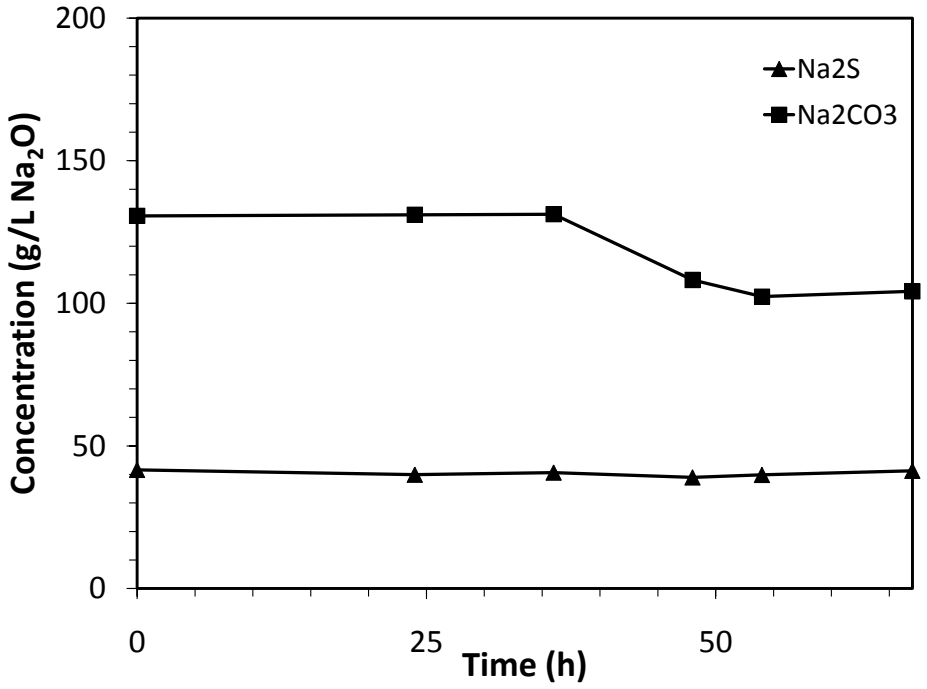

Figure 4-14: *Reaction kinetics for Na_2S = 40.5 g/L of Na_2O at 95^oC*

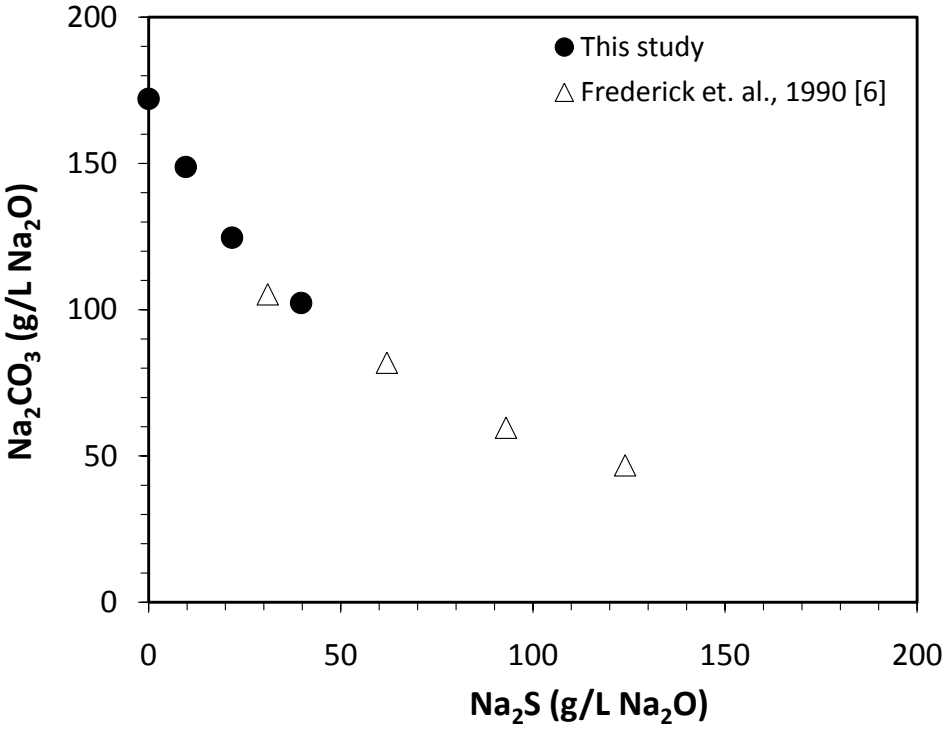

Figure 4-15: *Solubility of pirssonite in Na_2CO_3-Na_2S-$CaCO_3$-H_2O system at 95^oC*

4.2 Incongruent Dissolution of Pirssonite

The dissolution behavior of pirssonite was also examined. Theoretically, Na_2CO_3 from pirssonite should dissolve in water leaving $CaCO_3$ behind (Equation 4-1). Based on this, a hypothesis was postulated in Chapter 3 to explain the occurrence of $CaCO_3$ in most scale samples obtained from the mills.

$$Na_2Ca(CO_3)_2 \cdot 2H_2O(s) \rightarrow 2Na^+ + CO_3^{2-} + 2H_2O + CaCO_3(s) \quad (4\text{-}1)$$

Pirssonite Synthesis:

Pure pirssonite was synthesized in the laboratory from a solution of Na_2CO_3, $CaCO_3$ and H_2O. Stoichiometric amounts of the stated chemicals were placed in the low temperature reactor set-up at 75^{o}C (Figure 4-1) and agitated for 24 hours to ensure equilibrium had established. Precipitated solid phase was collected and dried. TGA/DSC and SEM analyses were performed on the solid phase to check for purity.

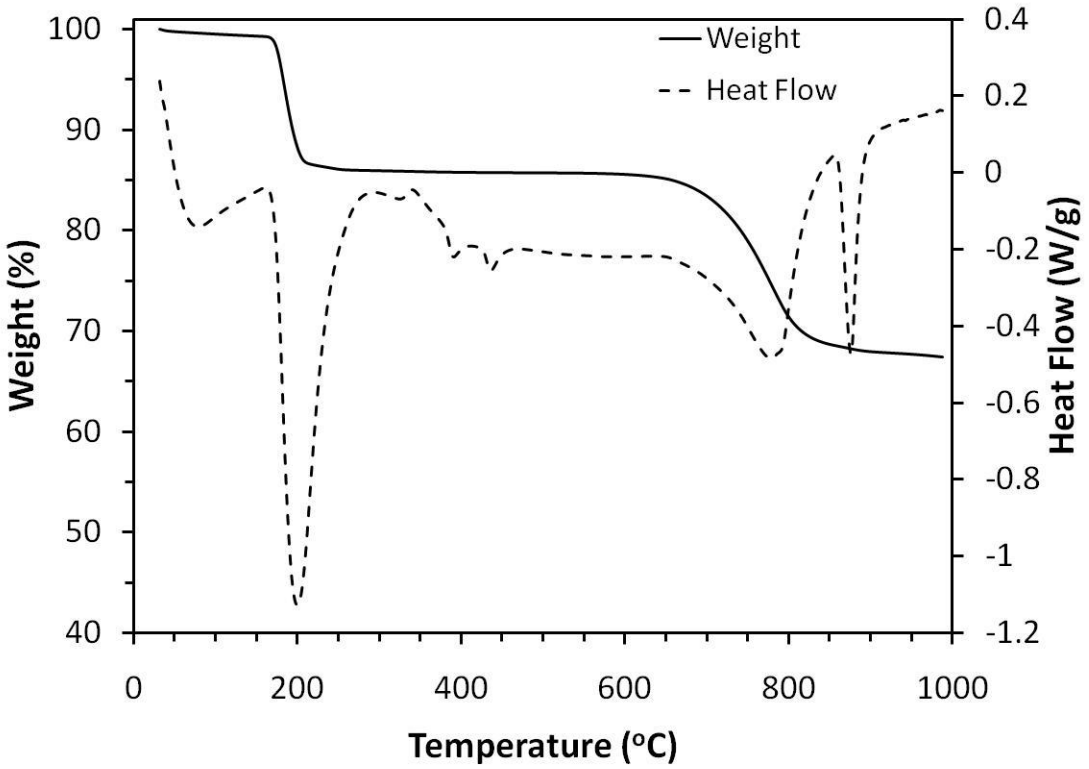

Figure 4-16: *Thermal profile for synthetic pirssonite prepared in the laboratory*

Figure 4-16 shows the TGA/DSC profile obtained on the solid phase. A weight loss of about 18% is observed due to the decomposition of $CaCO_3$ indicating the purity of pirssonite in the solid sample is about 99%. The predominance of pirssonite in the solid sample was also checked by SEM imaging. As seen in Figure 4-17 only pirssonite phase is observed at X250 magnification conforming to the TGA/DCS result.

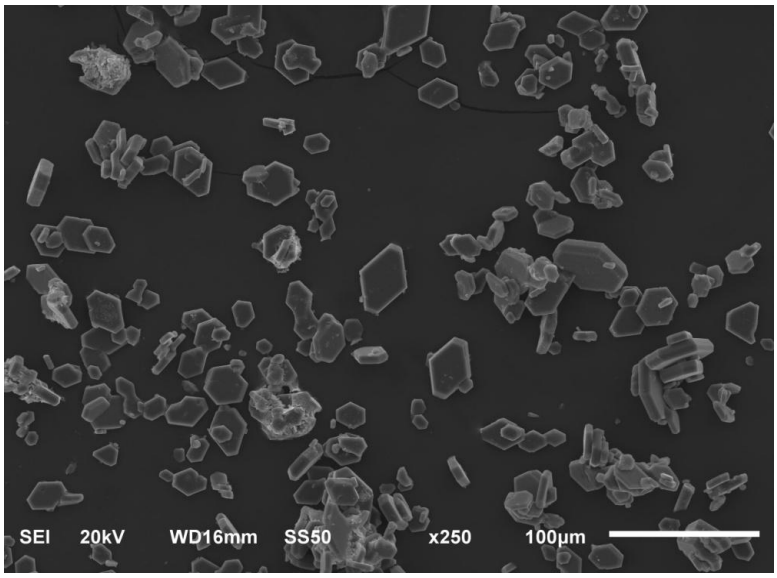

Figure 4-17: *SEM image of the synthetic pirssonite*

Dissolution Experiments:

Three kinds of experiments were performed to examine incongruent dissolution of pirssonite. Synthetic pirssonite was dissolved in deionized water and weak wash (5 g/L of NaOH); and one pirssonite sample (ID: I) obtained from one of the mills was dissolved in deionized water. All three experiments were conducted at 95^{o}C. Synthetically prepared pirssonite powder was introduced in water/weak wash and the slurry was agitated. As for the mill sample, a small piece of it was tied with the agitator shaft, immersed in deionized water and let it spin with the shaft in the water.

The kinetics for pirssonite dissolution in all three cases was observed to be very fast. It took less than 30 minutes for pirssonite powder (synthetic) to completely dissolve in deionized water/ weak wash. The surface of the mill sample was observed to be washed away leaving a white layer of soft $CaCO_3$ powder behind (Figure 4-18). Post dissolution solid samples were collected, dried and analyzed using TGA/DCS to verify incongruent dissolution of pirssonite. The presence of $CaCO_3$ in all three solid samples is clearly visible from TGA/DSC analysis as shown in Figure 4-19, 20 and 21.

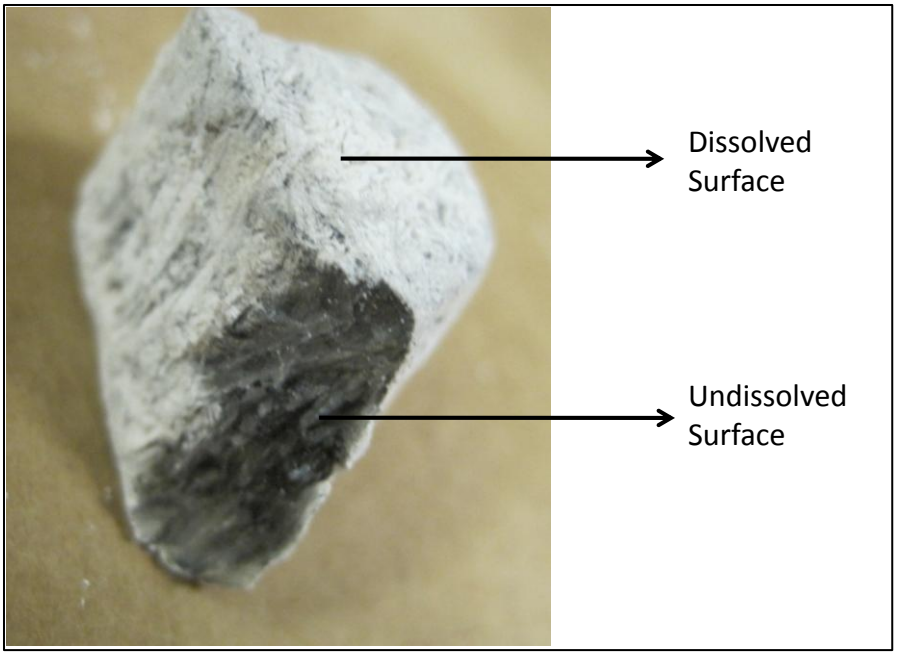

Figure 4-18: *Mill sample (ID: I) dissolved in deionized water*

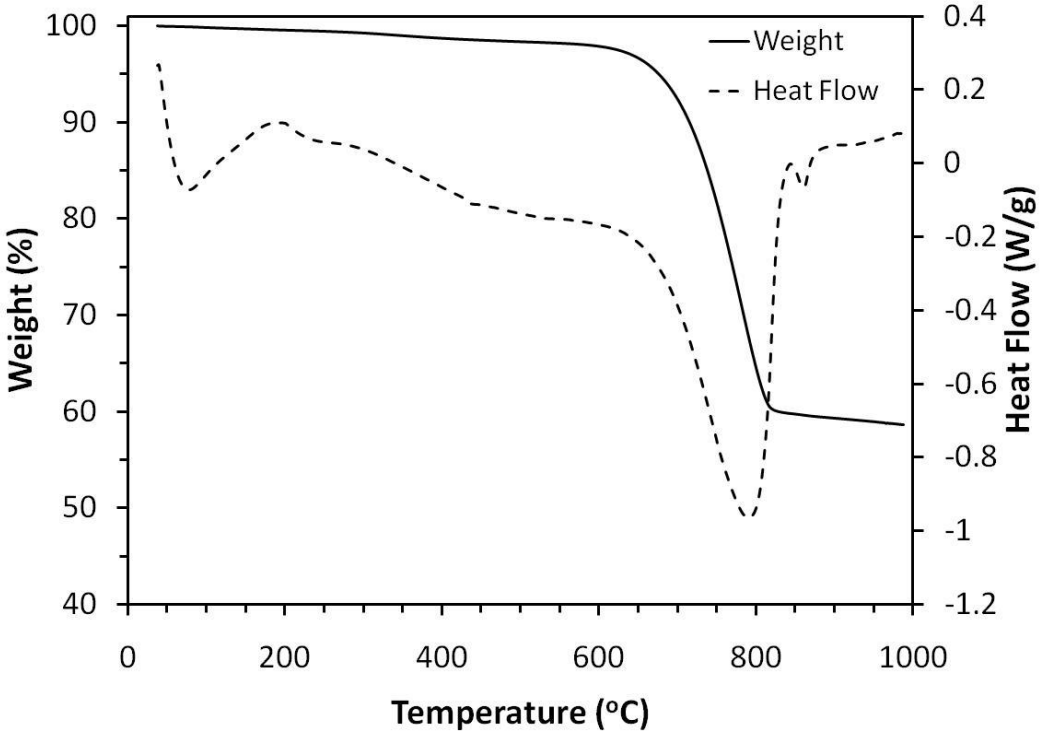

Figure 4-19: *Thermal profile of the solid sample obtained from dissolving synthetic pirssonite powder in deionized water at 95°C*

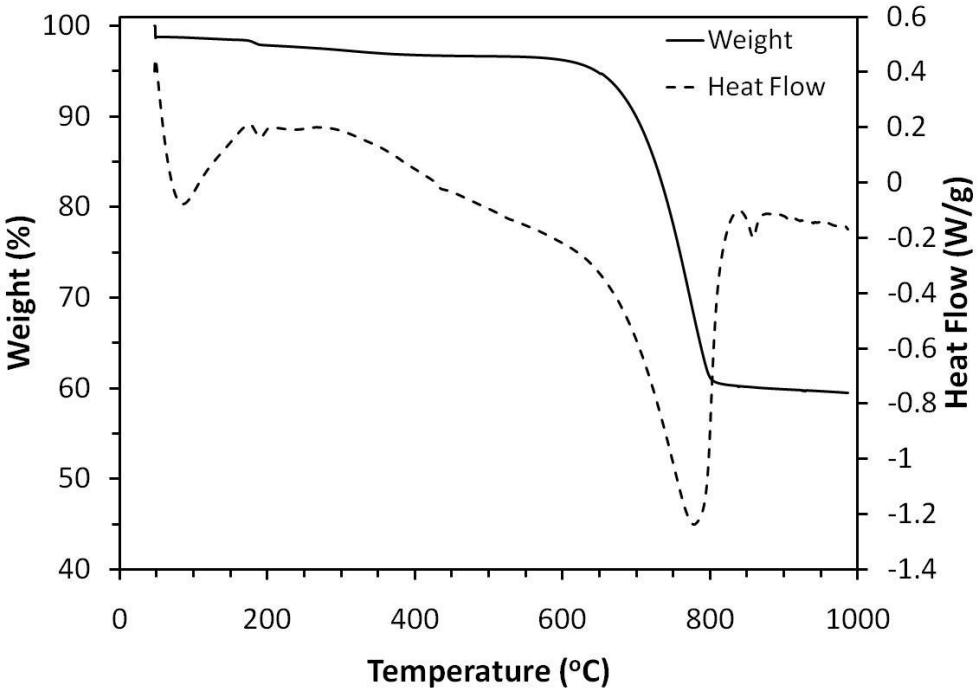

Figure 4-20: *Thermal profile of the solid sample obtained from dissolving synthetic pirssonite powder in weak wash (5g/L of NaOH) at 95°C*

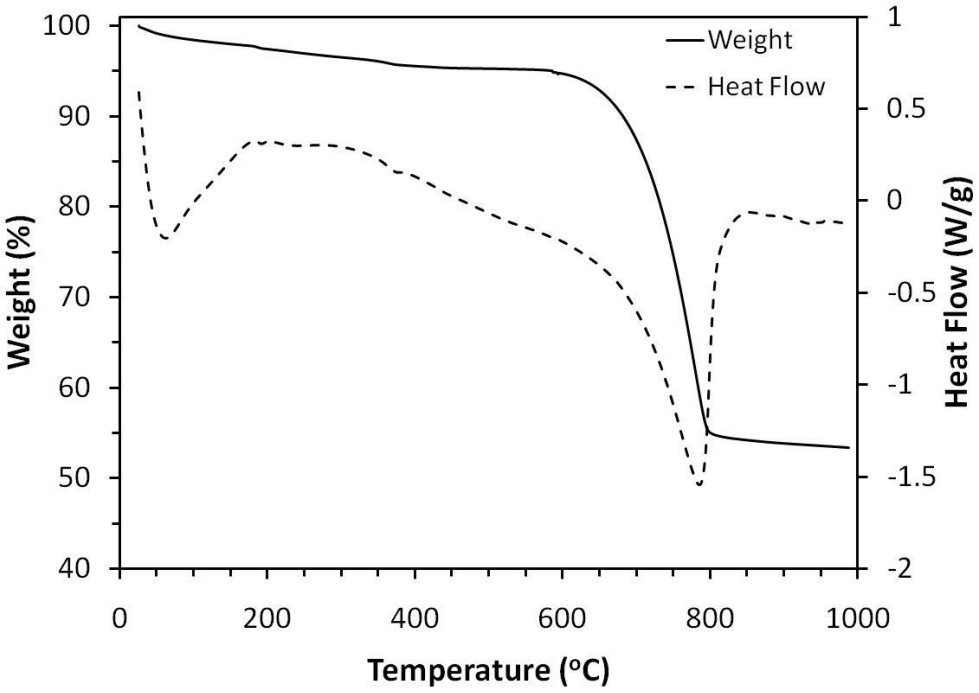

Figure 4-21: *Thermal profile of the solid sample obtained from dissolving scale sample # I in deionized water at 95°C (dissolved surface as shown in Figure 4-18)*

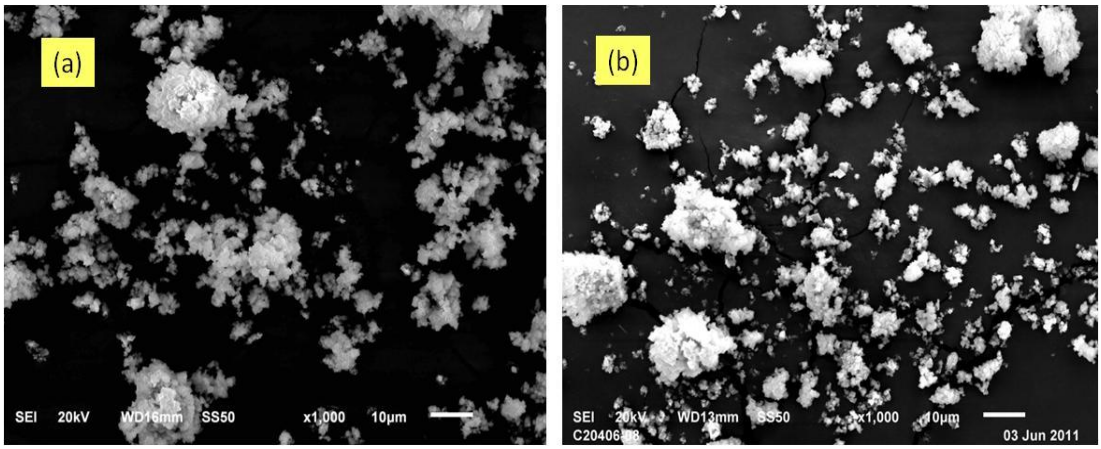

Figure 4-22: *SEM images of the solid samples collected from dissolving synthetic pirssonite in a) deionized water and b) weak wash solution at 95^{o}C*

Figure 4-22 shows the SEM images of the solid samples collected after synthetic pirssonite was dissolved in deionized water and weak wash. The crystal morphology observed in these images are similar to those observed in Figure 4-11a. SEM-EDS analysis showed the phases detected in these two solid samples as $CaCO_3$ and XRD analysis confirmed the solid phase as calcite (Figure 4-24). Figure 4-23 shows the SEM image of the solid sample that was obtained by dissolving mill sample in deionized water. The crystal morphology of this sample is needle like and looks quite different than the other two solid samples, although, SEM-EDS on this sample also showed the predominant presence of calcium in this sample. XRD analysis showed that the solid phase is composed of aragonite and calcite (Figure 4-25), explaining the different crystal morphology observed in this sample.

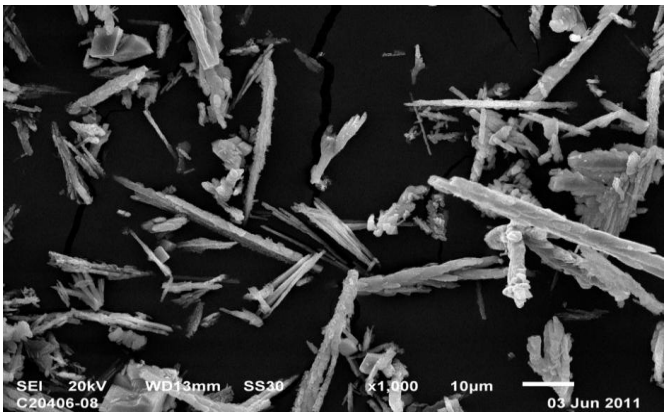

Figure 4-23: *SEM image of the solid sample collected from dissolving mill sample in deionized water at 95^{o}C*

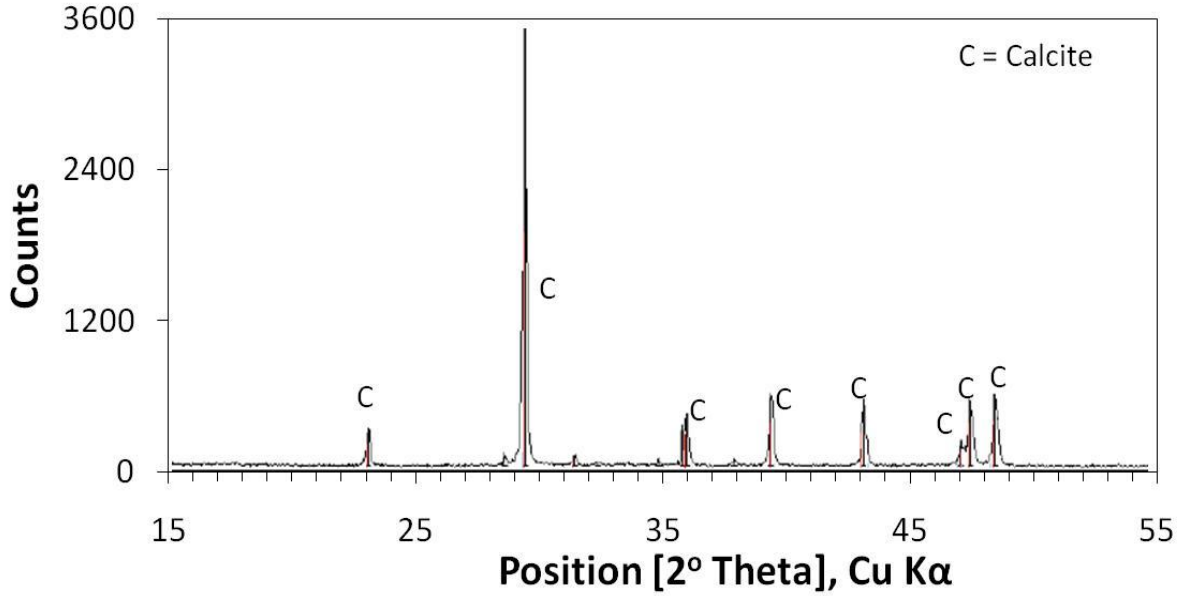

Figure 4-24: *XRD spectra of the solid phase obtained by dissolving synthetic pirssonite in weak wash at 95°C*

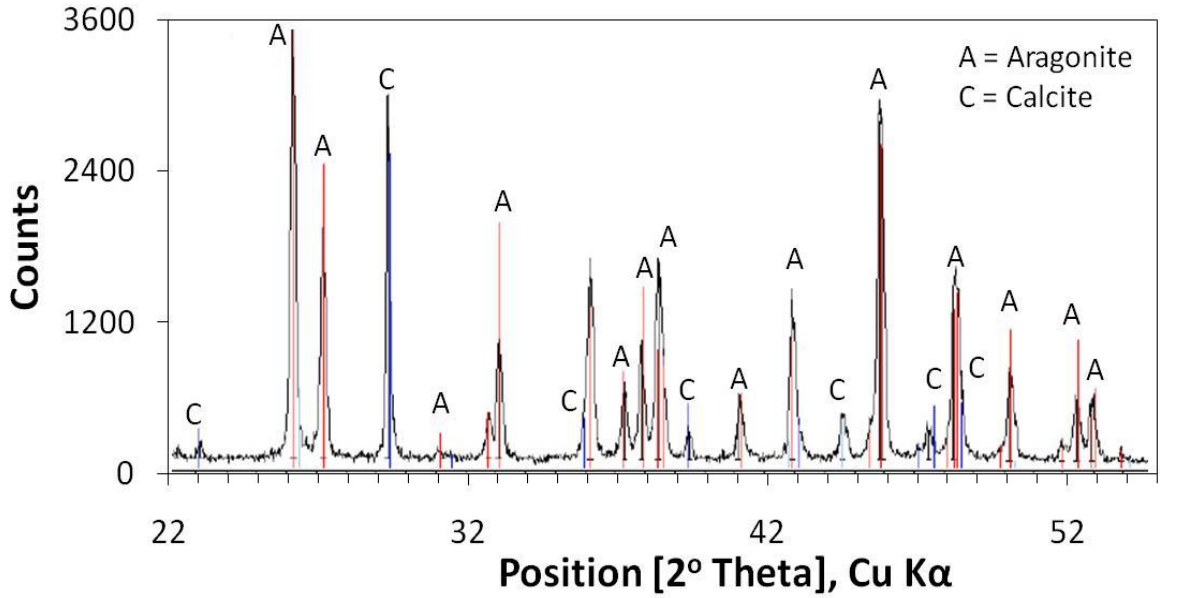

Figure 4-25: *XRD spectra of the solid phase obtained by dissolving mill sample in deionized water at 95°C*

4.3 Pirssonite Formation Mechanism

In Chapter 3, two possible mechanisms were introduced in order to describe the formation of pirssonite. These mechanisms are: a) direct reaction between Na_2CO_3 in the solution and the surface of $CaCO_3$ particles or b) continuous dissolution of $CaCO_3$ particles to produce Ca^{2+} ions in the solution which subsequently react with the Na^+ and CO_3^{2-} ions to precipitate pirssonite as a new phase. Figure 4-26 shows an SEM image of the solid sample collected at t = 5 hours from the system of Na_2CO_3-$CaCO_3$-H_2O. In this image, it can be observed that $CaCO_3$ particles agglomerate on a pirssonite crystal which is undergoing formation.

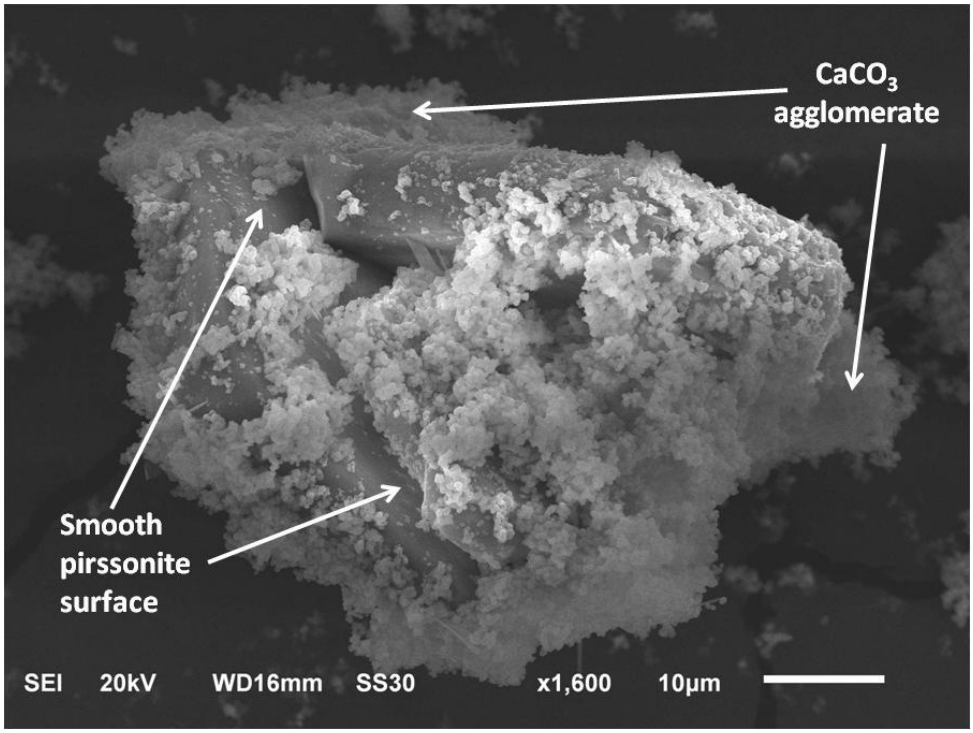

Figure 4-26: *SEM image of the solid sample collected at t=5 from Na_2CO_3-$CaCO_3$-H_2O system at 95^oC*

In order for mechanism a) to hold true, pirssonite should form around $CaCO_3$ particles keeping the morphology of the $CaCO_3$ particles intact. However, the opposite behavior is observed in Figure 4-26 where $CaCO_3$ particles are covering the smooth surface of pirssonite. It was also observed in Figure 4-11a, b, and c, where small $CaCO_3$ particles disappeared with time replacing them with large pirssonite crystals. Therefore, it is more likely for mechanism b) to take place. Figure 4-27 illustrates this mechanism where very small amounts of dissolved Ca^{2+} ions (from

$CaCO_3$) present in the solution react with the Na^+ and the CO_3^{2-} ions in order to initiate pirssonite crystallization through primary heterogeneous nucleation. Calcium carbonate suspended particles present in the solution and/or vessel walls act as nucleation sites. The formation of pirssonite crystals depletes Ca^{2+} ions from solution. This triggers more dissolution of $CaCO_3$ particles to maintain the crystallization process. The dissolution-re-precipitation reaction mechanism that takes place to form pirssonite is as follows:

Dissolution: $$CaCO_3(s) \rightarrow Ca^{2+} + CO_3^{2-} \quad (4\text{-}2)$$

Re-precipitation: $$Ca^{2+} + 2Na^+ + 2CO_3^{2-} + 2H_2O \rightarrow Na_2Ca(CO_3)_2 \cdot 2H_2O(s) \quad (4\text{-}3)$$

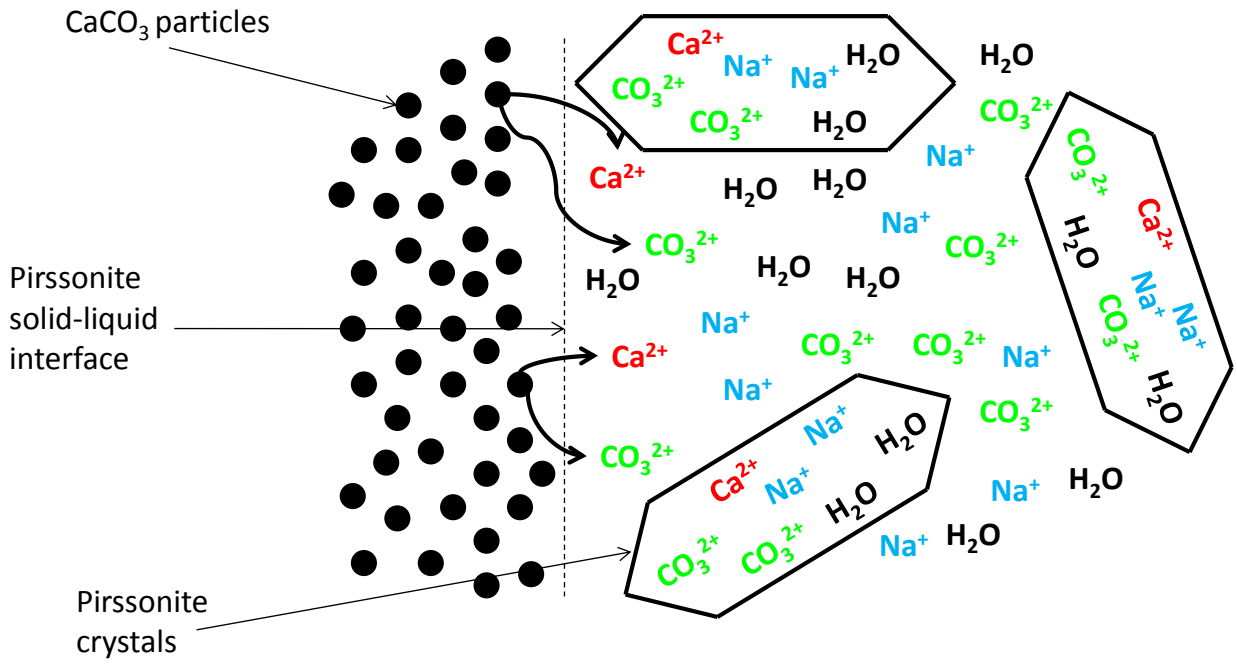

Figure 4-27: *Illustration of the pirssonite formation mechanism*

Although the above mentioned pirssonite formation mechanism is consistent with the SEM images obtained in this work, more work is required to confirm its existence and to better understand the growth kinetics and the mechanisms that lead to the hexagonal crystalline habit, as observed in this study.

4.4 Summary

In this chapter, it was shown through experimental evidence that the solubility of pirssonite increases with temperature and decreases with increasing concentration of sodium salts found in green liquor such as Na_2S and NaOH. Frederick et al.'s data on pirssonite solubility were verified for reproducibility and were extended to a more dilute range of concentrations that are prevalent in real green liquor solutions. This improved set of pirssonite solubility data are used in Chapter 5 to create a database for pirssonite in OLI that is subsequently used to generate graphs that can be used by the mills to prevent pirssonite deposition problems.

Incongruent dissolution of sodium carbonate from pirssonite was verified in the second part of this chapter. It was shown that both synthetic pirssonite (in powder form) and pirssonite scale sample dissolve rather quickly in water or weak wash, leaving $CaCO_3$ powder behind. The experimental results agree with the hypothesis generated in Chapter 3. However, the reason behind the hardness of the $CaCO_3$ scale found in the mills is still unknown, as according to this study it was observed that $CaCO_3$ left behind upon dissolution of pirssonite scale was in soft powder form.

The last part of the chapter gives a plausible mechanism for pirssonite formation from a solution containing sodium carbonate and calcium carbonate particles. This part of the study is still at its initial stage and requires further work.

Chapter 5

5 Chemical Modeling of Pirssonite Solubility in Green Liquor solutions

This chapter discusses the chemical modeling performed in this work to predict the solubility of pirssonite in green liquor solutions using the Mixed Solvent Electrolyte (MSE) framework of the OLI software. A primary database was created for pirssonite using the thermodynamic data available in the literature. It was further modified and validated against the experimental data presented in Chapter 4. This chapter describes the methodology used to create the database along with the validation curves. Finally, it presents the pirssonite solubility curves that can be utilized by the kraft mills as guidelines to prevent pirssonite deposition problems.

5.1 OLI Software

OLI is a thermodynamic based computer program that is widely used in various industries to simulate aqueous processes. OLI's specialty software is based on the OLI Engine. The specialty software includes OLI/Analyzer Line, ESP (Environmental Simulation Program) and CSP (Corrosion Simulation Program). Analyzer is a Windows-based software that can perform different types of calculations using its different program modules, such as Stream Analyzer, Corrosion Analyzer, and Score Analyzer. Stream Analyzer is used to perform equilibrium calculations for electrolyte chemistry. ESP, in contrast, is a tool that is used to design and simulate process flow sheets. OLI/ESP and OLI/Stream Analyzer were used in this work [33].

OLI software simulates electrolyte systems using either of the two available thermodynamic frameworks: Aqueous (AQ) and Mixed Solvent Electrolyte (MSE). The aqueous framework is based on the Bromley-Zemaitis activity coefficient model whereas the MSE framework is based on the excess Gibbs energy model [34]. The advantage of using the MSE model over the AQ model is that the MSE model is capable of accurately calculating thermodynamic properties from infinite dilution to pure fused salt electrolytes. The Aqueous model is applicable to dilute aqueous systems with a concentration range of up to 0.3 (mole fraction). The MSE model, on the other hand, can treat systems of any composition with mole fractions varying from 0 to 1 for any component [35]. In this work, the MSE model embedded in the OLI engine was used to investigate the solubility of pirssonite in green liquor solutions.

5.2 Pirssonite Database

OLI/MSE has a public database called MSEPUB that contains thermodynamic data for most common compounds such as Na_2CO_3, Na_2S. However, it does not have pirssonite in its database. Therefore, a database was created for pirssonite utilizing OLI/ESP. In order to create a new compound, its standard state properties (e.g. Gibbs free energy, enthalpy of formation, entropy and heat capacity) must be known. The standard state properties of pirssonite that were initially used to create the pirssonite database in OLI/ESP were obtained from the literature [36] and are summarized in the following table:

Table 5-1: *Standard state properties of pirssonite obtained from Königsberger et al. [36]*

	$\Delta_f H^o_{298}$ *kJ mol^{-1}*	S^o_{298} *J mol^{-1} K^{-1}*	$C^o_{p,\,298}$ *J mol^{-1} K^{-1}*
Pirssonite	-2955.84	239.05	329.43

In OLI/ESP, standard state properties as well as ion-interaction parameters can be regressed using various types of experimental data such as vapor pressure, solid solubility, heat of mixing [37]. In this work, the standard state properties of pirssonite and the ion interaction parameters between OH^- and CO_3^{2-} ions were regressed using the solubility data discussed in Chapter 4. Table 5-2 lists the regressed standard state properties and the ion interaction parameters that were used to update the pirssonite database in OLI/ESP. This updated database was used in OLI/Stream Analyzer to create pirssonite solubility curves that are discussed in section 5.3.

Table 5-2: *Regressed standard state properties and ion interaction parameters used to update the pirssonite database in OLI/ESP*

	$\Delta_f H^o_{298}$ *kJ mol^{-1}*	S^o_{298} *J mol^{-1} K^{-1}*	$C^o_{p,\,298}$ *J mol^{-1} K^{-1}*	*BMD0*	*CMD0*
Standard State Properties of Pirssonite	-2658.68	223.40	388.25	N/A	N/A
OH^- and CO_3^{2-} Ion Interaction Parameter	N/A	N/A	N/A	-154.15	222.88

Model Validation

Experimental solubility data obtained for the systems Na_2CO_3-$CaCO_3$-H_2O and Na_2CO_3-NaOH-$CaCO_3$-H_2O were used to regress the model parameters. Solubility data obtained in the presence of sodium sulfide were not used in the regression procedure but it were used to validate the regressed parameters. Figure 5-1, 5-2 and 5-3 show the model validation curves where the experimental solubility data are compared with OLI prediction results. The Absolute Average Relative Deviations (AARD%[1]) between the experimental data and the predicted results as shown in Figure 5-1, 5-2 and 5-3 are 4.26%, 7.91% and 4.64% respectively.

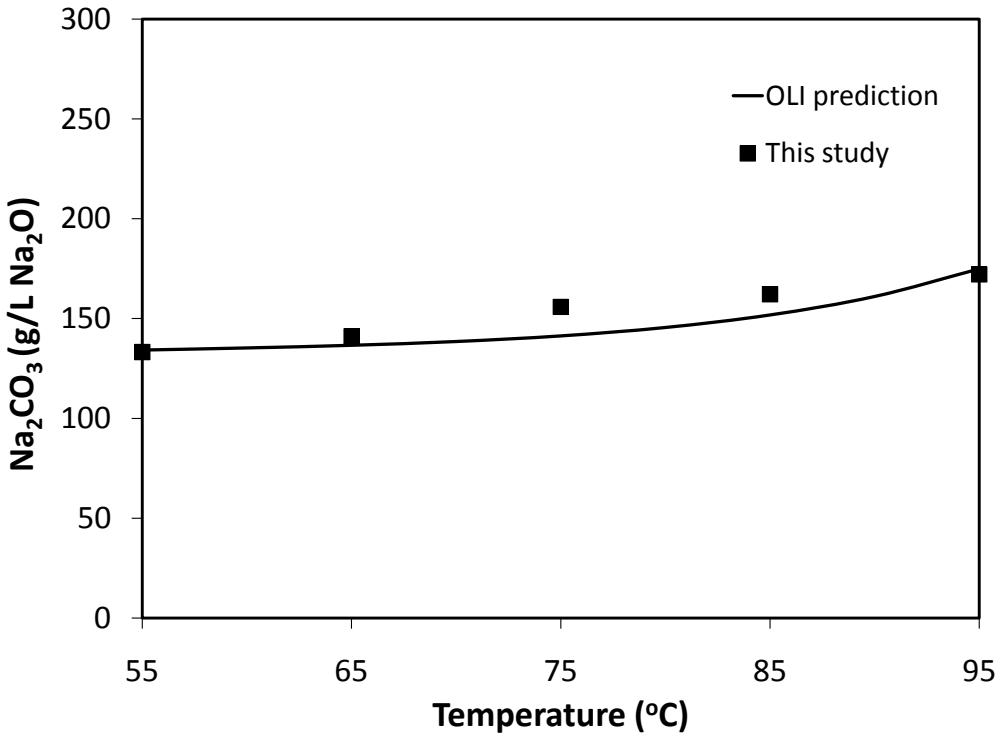

Figure 5-1: *Comparison of experimental data and OLI predictions for pirssonite solubility in Na_2CO_3-$CaCO_3$-H_2O system from 55°C-95°C*

[1] $AARD(\%) = \frac{100}{NP}\sum_i^{NP}\frac{|Exp.value - calculated\ value|}{Exp.value}$, NP: Total number of experimental points

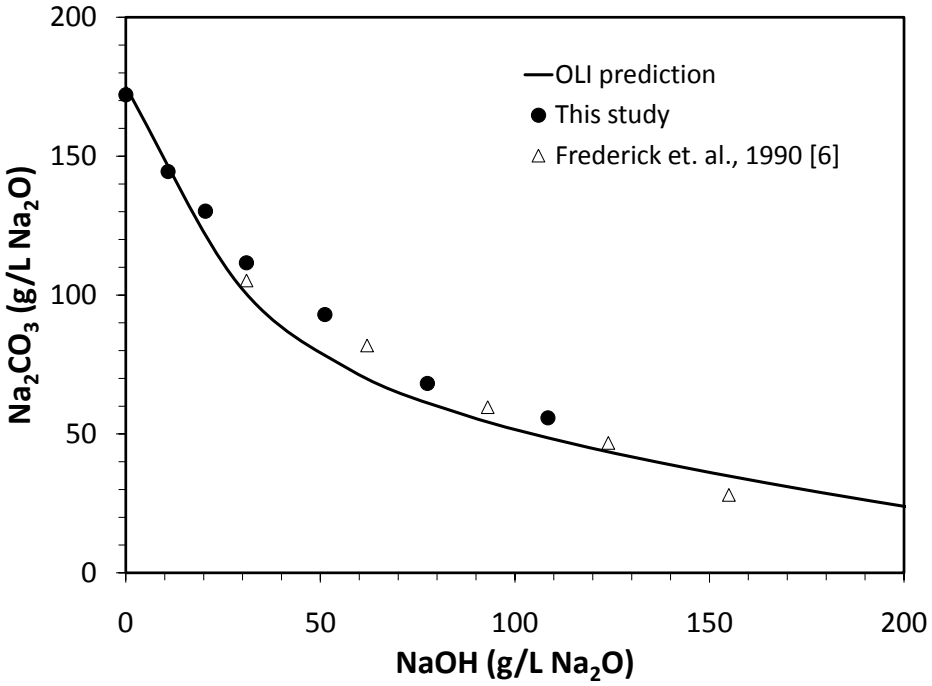

Figure 5-2: *Comparison of experimental data and OLI predictions for pirssonite solubility in Na_2CO_3-NaOH-$CaCO_3$-H_2O system at 95^oC*

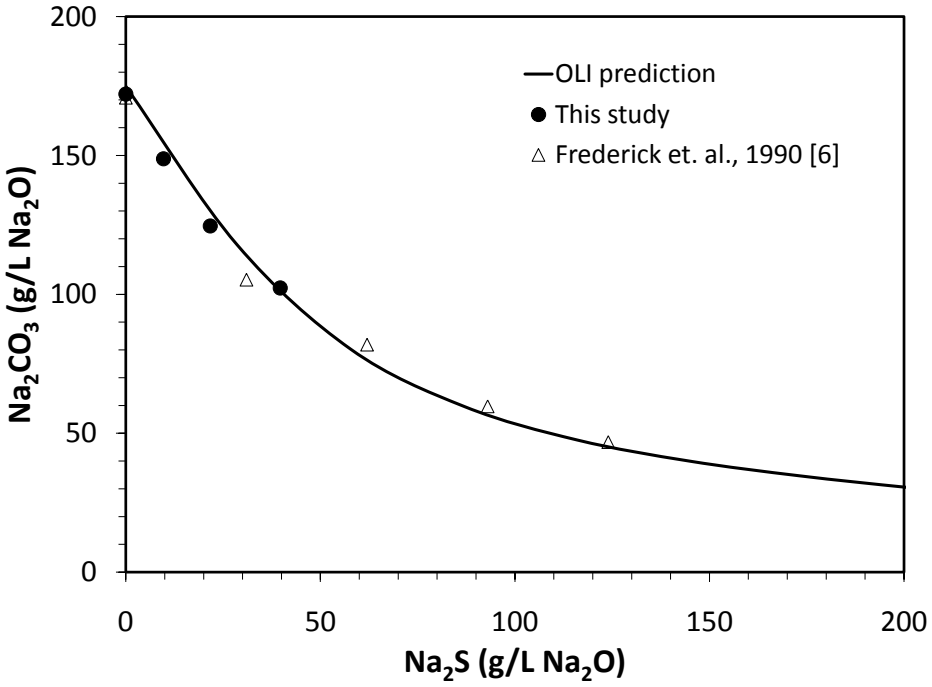

Figure 5-3: *Comparison of experimental data and OLI predictions for pirssonite solubility in Na_2CO_3-Na_2S-$CaCO_3$-H_2O system at 95^oC*

5.3 Modeling of Pirssonite Solubility Using OLI Stream Analyzer

Stream Analyzer was used to predict the solubility behavior of pirssonite under various mill operating conditions. At a fixed TTA, the concentrations of Na_2CO_3, Na_2S and NaOH are fixed by sulfidity and causticity of green liquor. The concentrations of all three constituent chemicals will increase as the TTA level increases in green liquor at fixed sulfidity and causticity. This behavior is depicted by the *mill operating* line *(solid)* in Figure 5-4 where sodium carbonate concentration in green liquor (y-axis) increases with an increasing TTA (x-axis) at 30% sulfidity and 10% causticity. However, as TTA increases, the solubility of pirssonite decreases as the increased level of sodium sulfide and sodium hydroxide due to TTA rise will depress the amount of sodium carbonate that can be present in the aqueous phase. This behavior is shown by the pirssonite *solubility* line *(broken)* in the following figure. The intersection between the *mill operating* and the *pirssonite solubility* lines represent the saturation point with respect to pirssonite in green liquor solutions. This point is called TTA_{sat} in this work. Pirssonite will precipitate from green liquor solutions as the TTA exceeds this TTA_{sat} point.

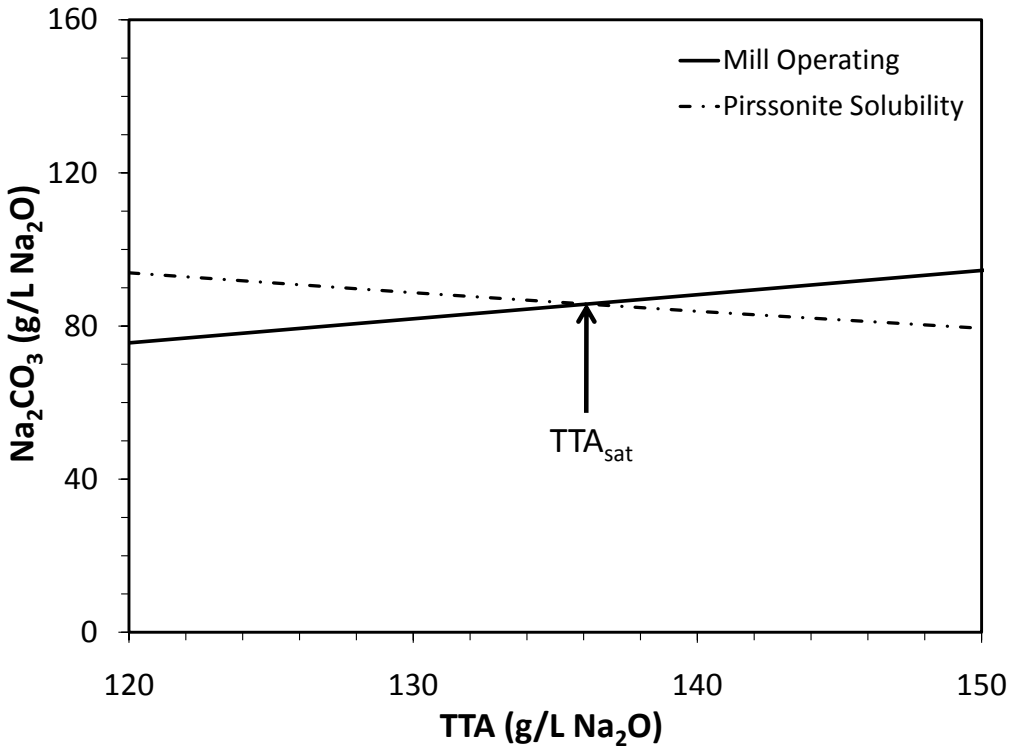

Figure 5-4: *Calculation of TTA_{sat} from green liquor solutions with 30% sulfidity and 10% causticity at 95^oC using OLI*

A series of graphs similar to Figure 5-4 were created with sulfidity ranging from 0-70% and causticity varying from 0-30% at 95°C. These graphs were used to determine the TTA_{Sat} points by intersecting the mill operating lines with the pirssonite solubility lines. Figure 5-5 was obtained by plotting TTA_{sat} points against sulfidity. The effect of causticity is shown by using different lines in the same plot. This graph is useful and can be easily read by mill operators/process engineers to determine the maximum level of TTA their operation can have before pirssonite will precipitate from a given sulfidity and causticity. For example, at 25% sulfidity and 5% causticity (green line), TTA_{sat} is about 138.5 g/L of Na_2O. Therefore, mills operating TTA must be below 138.5 g/L of Na_2O to prevent pirssonite deposition at 95°C.

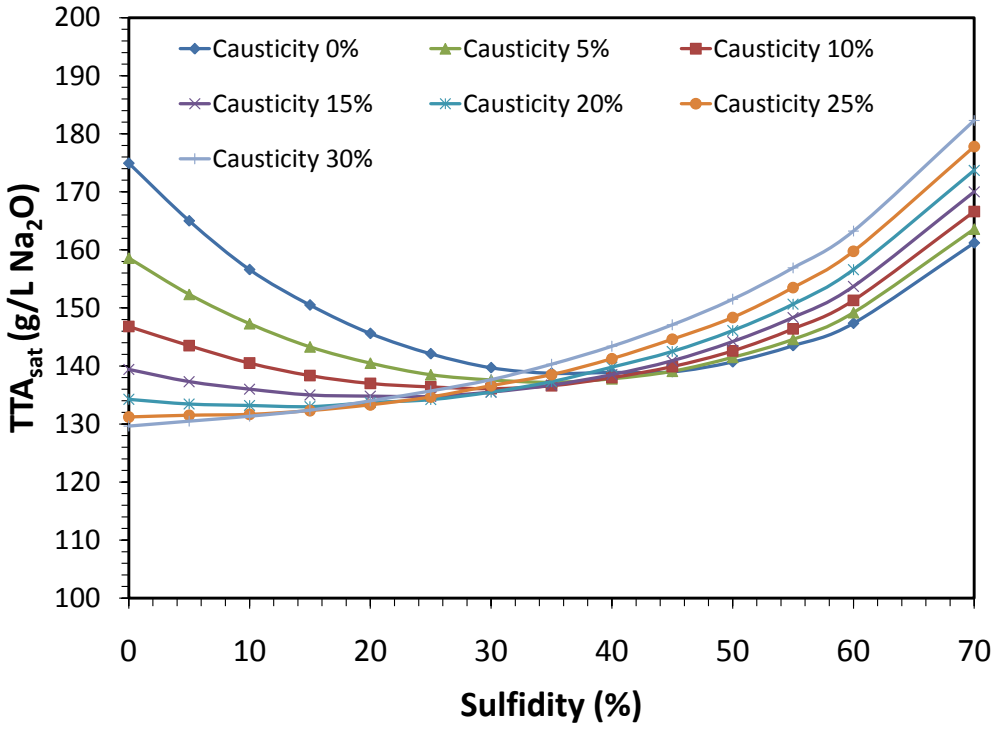

Figure 5-5: *OLI-generated pirssonite solubility curve for green liquor solutions with 0 mol% Cl/(Na+K) at 95°C*

It is interesting to note that the curve has a parabolic shape with TTA_{sat} points decreasing with an increasing level of sulfidity until it reaches a minimum when the trend is reversed. At low sulfidity, green liquor is mainly composed of sodium carbonate with a small amount of sodium sulfide. As the sulfidity of green liquor increases, so does the concentration of sodium sulfide lowering the solubility of sodium carbonate, and hence, pirssonite in green liquor which is

observed by the first half of the parabola. As the sulfidity is increased further, the sodium carbonate concentration in green liquor decreases to a point where there is not enough sodium carbonate present in the solution to initiate pirssonite precipitation. This is the minimum point shown in Figure 5-5. At this high sulfidity, green liquor TTA must be increased to raise CO_3^{2-} ion concentration in green liquor in order to attain saturation for pirssonite. This is the reason why TTA_{sat} increases after the minimum point as sulfidity continues to go up.

5.3.1 Effect of Chloride on Pirssonite Solubility

The effect of chloride on pirssonite solubility is of interest to many kraft mills particularly to those ones that are located in the coastal regions. Chloride (Cl^-) may exist as NaCl and/or KCl in green liquor. The concentration of chloride in green liquor is usually represented as Cl/(Na+K) mol% and may vary from 0.3 mol% for inland mills to as high as 18 mol% for coastal mills with seaborne logs [32]. Typically, the concentration of Cl^- in the system is about 1.5 Cl/(Na+K) mol % [38]. Chloride in green liquor is most likely to bond with Na^+ rather than K^+ due to higher sodium concentration. In this work, the effect of chloride on pirssonite solubility was investigated by introducing chloride as NaCl in OLI. Figure 5-6 and 5-7 represent the pirssonite solubility curves with 10 and 20 mol% Cl/(Na+K) respectively. Figure 5-5 shows the solubility curve for 0 mol% Cl/(Na+K). Figure 5-8 shows the effect of chloride on pirssonite solubility for green liquor solutions with 30% sulfidity and 5% causticity. By looking at this graph, it is evident that the higher the concentration of Cl^- in green liquor solutions, the lower the solubility of pirssonite becomes.

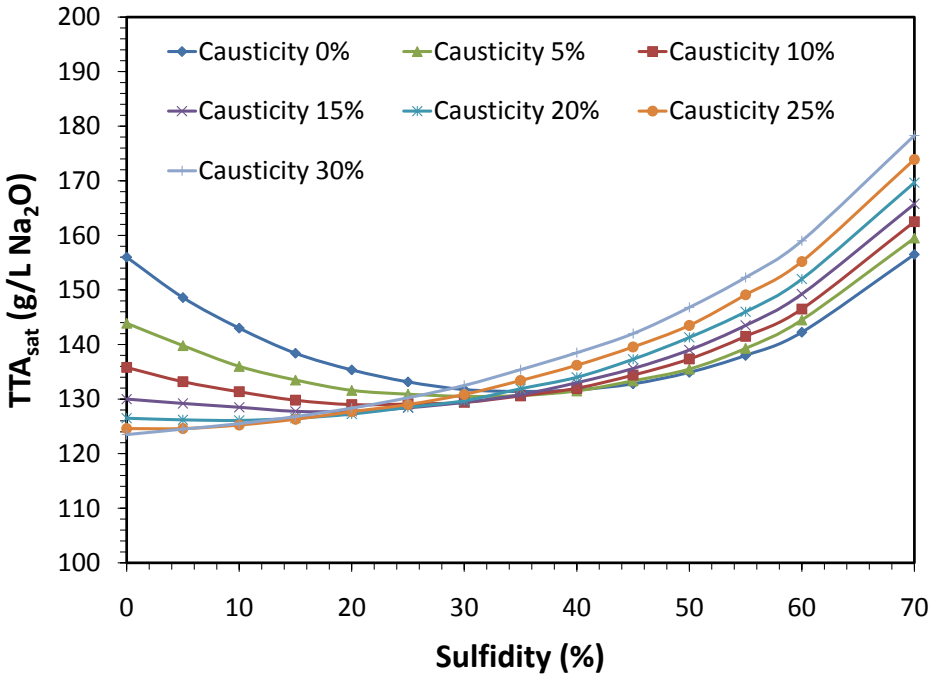

Figure 5-6: *OLI-generated pirssonite solubility curve for green liquor solutions with 10 mol% Cl/(Na+K) at 95°C*

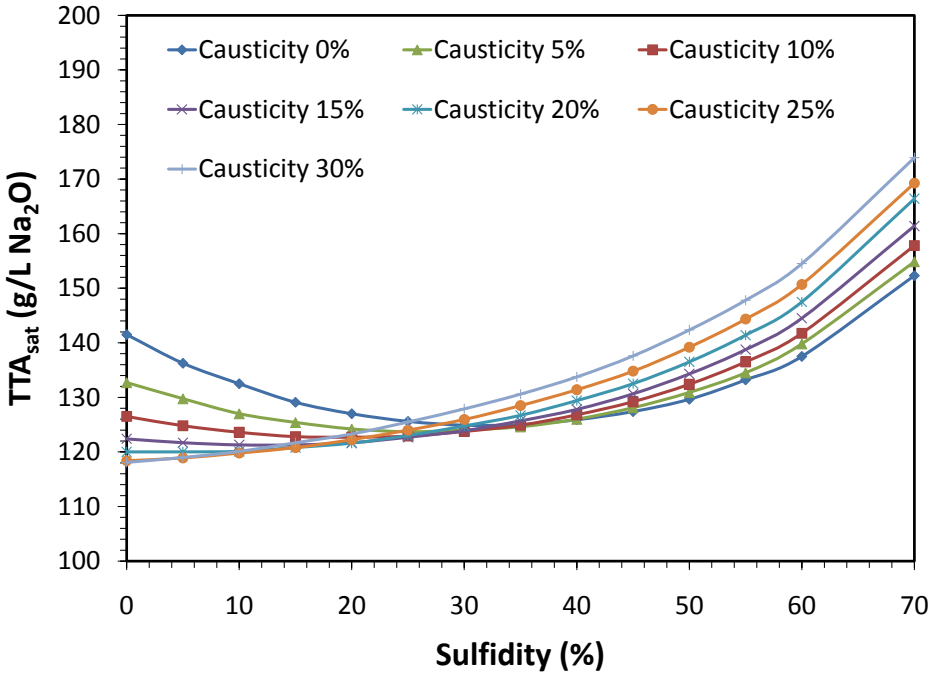

Figure 5-7: *OLI-generated pirssonite solubility curve for green liquor solutions with 20 mol% Cl/(Na+K) at 95°C*

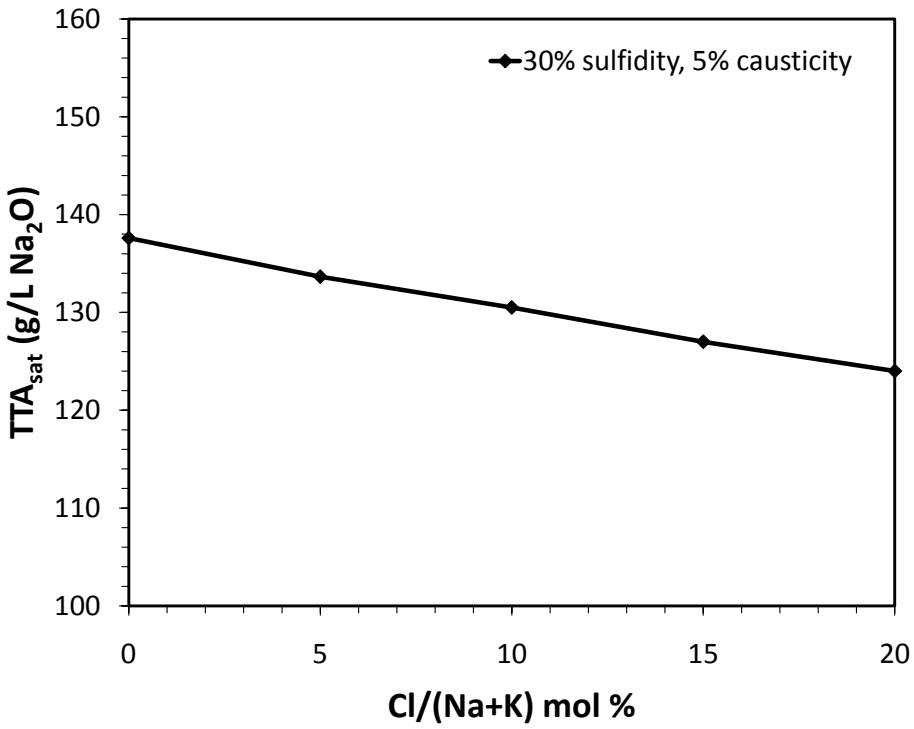

Figure 5-8: *Effect of chloride on pirssonite solubility at 95^{o}C with 30% sulfidity and 5% causticity (OLI-generated)*

5.3.2 Effect of Temperature on Pirssonite Solubility

The solubility of pirssonite increases with an increase in temperature [6, 23]. This behavior was also observed in this study and was shown that the solubility of pirssonite increases by about 10 g/L of Na_2O for every 10^{o}C increases in temperature. Green liquor temperature usually varies between 85^{o}C to 95^{o}C; therefore, it is important to know the TTA_{sat} points for this temperature range. Since the causticity of green liquor under normal conditions is between 5 and 10%, three solubility curves at three different temperature levels (75^{o}C, 85^{o}C, and 95^{o}C) were created using OLI and are shown in Figure 5-9 for 0% causticity, Figure 5-10 for 5% causticity and Figure 5-11 for 10% causticity. These graphs are useful for the kraft mills to determine the TTA saturation points at their corresponding green liquor temperature. Figure 5-12 shows the effect of temperature, ranging from 65^{o}C – 95^{o}C, on pirssonite solubility for green liquor solutions at 30% sulfidity and 5% causticity.

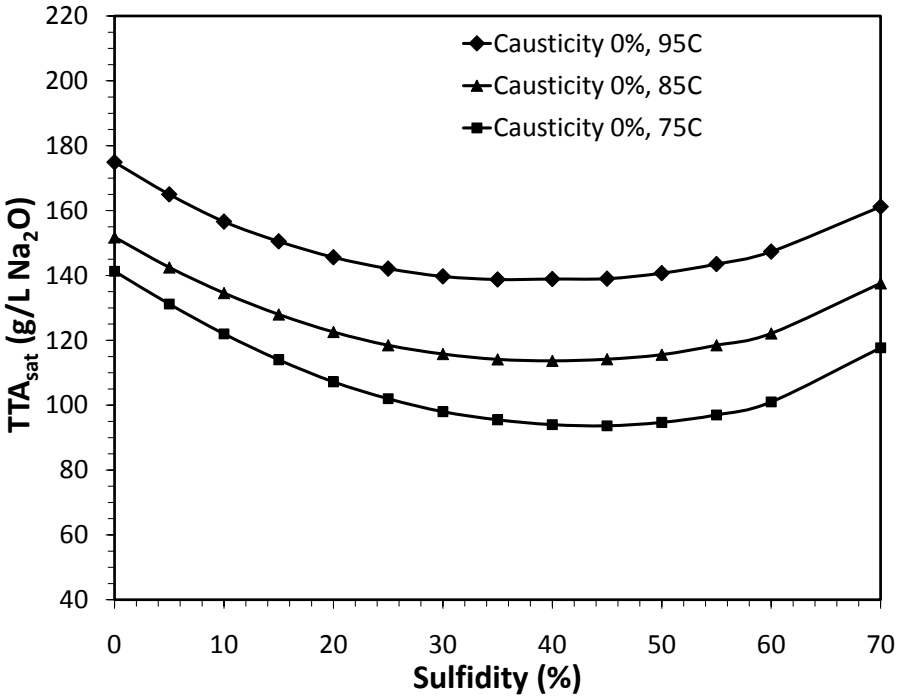

Figure 5-9: *Effect of temperature on pirssonite solubility at 0% causticity (OLI-generated)*

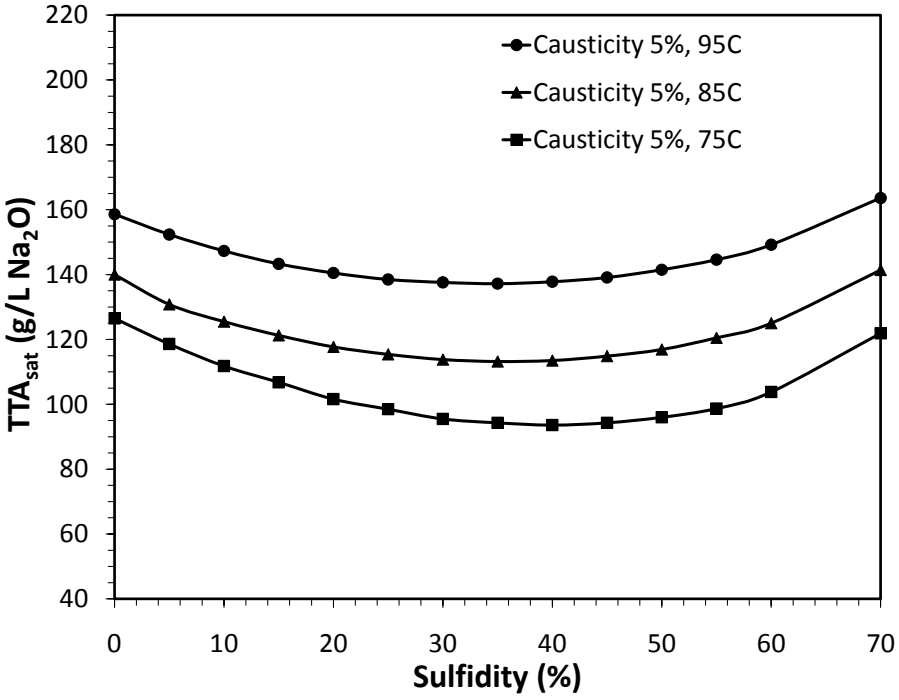

Figure 5-10: *Effect of temperature on pirssonite solubility at 5% causticity (OLI-generated)*

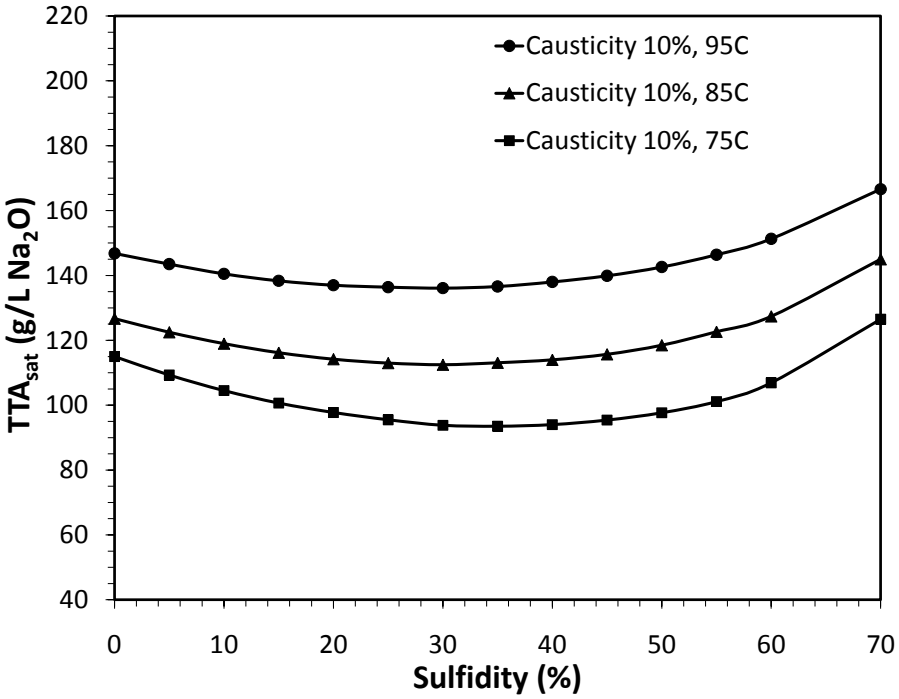

Figure 5-11: *Effect of temperature on pirssonite solubility at 10% causticity (OLI-generated)*

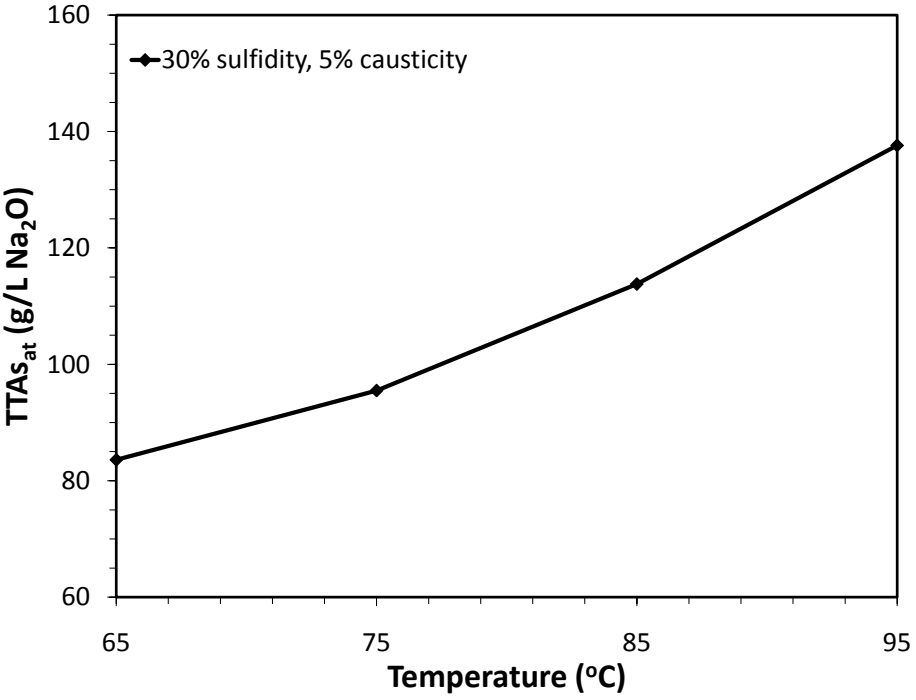

Figure 5-12: *Effect of temperature on pirssonite solubility at 30% sulfidity and 5% causticity (OLI-generated)*

5.4 Application of the Pirssonite Solubility Curves – A Case Study

Severe deposition problem was encountered in one of the kraft mills (mill I) at the beginning of this year. Scaling was first detected after the pump of the pipeline that carries clarified green liquor during the week of January 24, 2011. Scale sample (ID # I in this study) was collected and analyzed. Characterization of this sample revealed it to be purely consisting of pirssonite, as discussed in Chapter 3. The following figures present the actual mill data on clarified green liquor (TTA, sulfidity, causticity and temperature) from 1/1/2011 to 5/12/2011, the time line when deposition problems were severe.

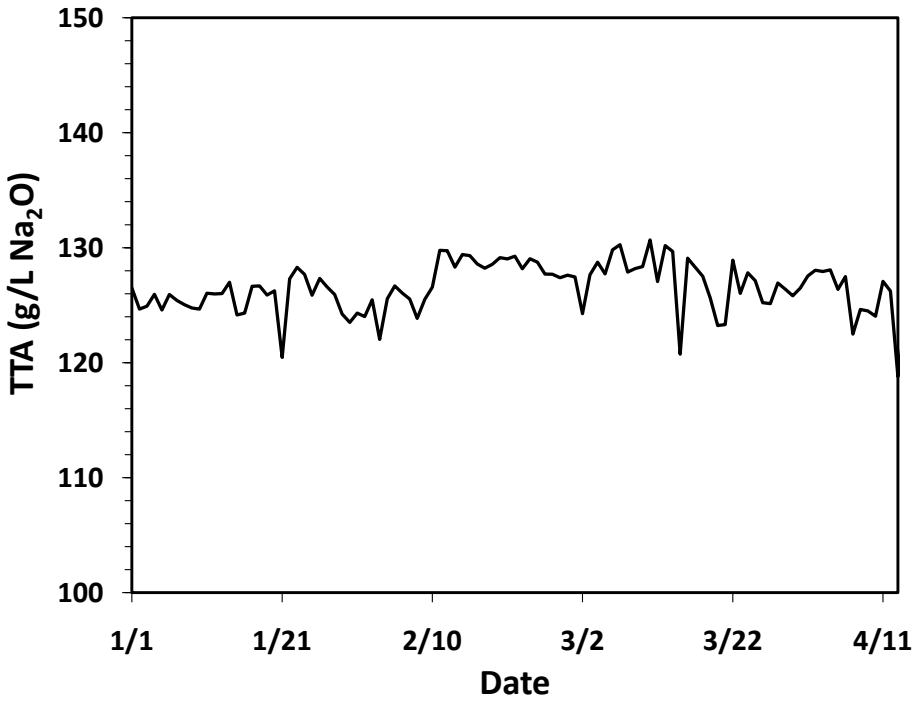

Figure 5-13: *Clarified green liquor TTA data for mill I*

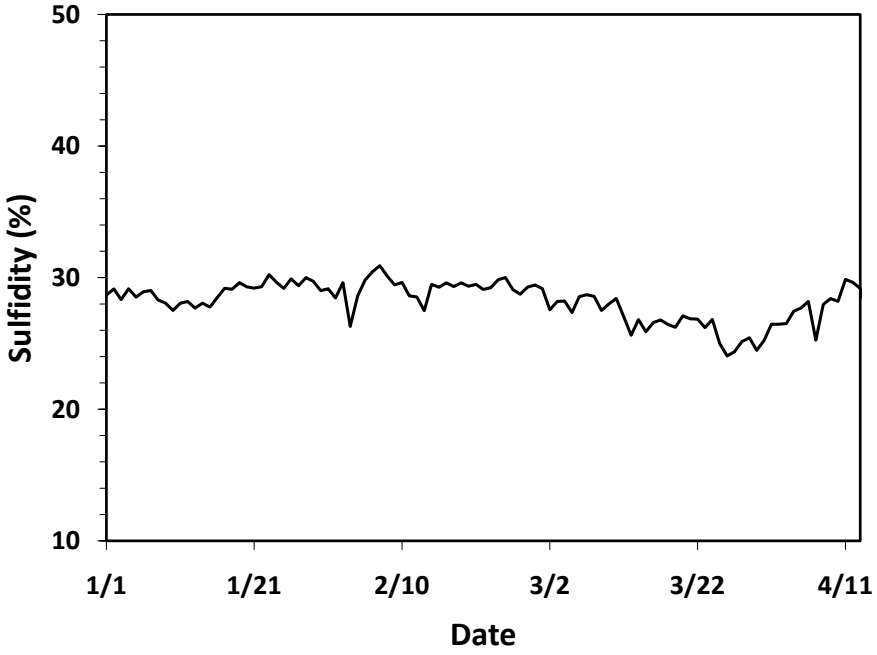

Figure 5-14: *Clarified green liquor sulfidity data for mill I*

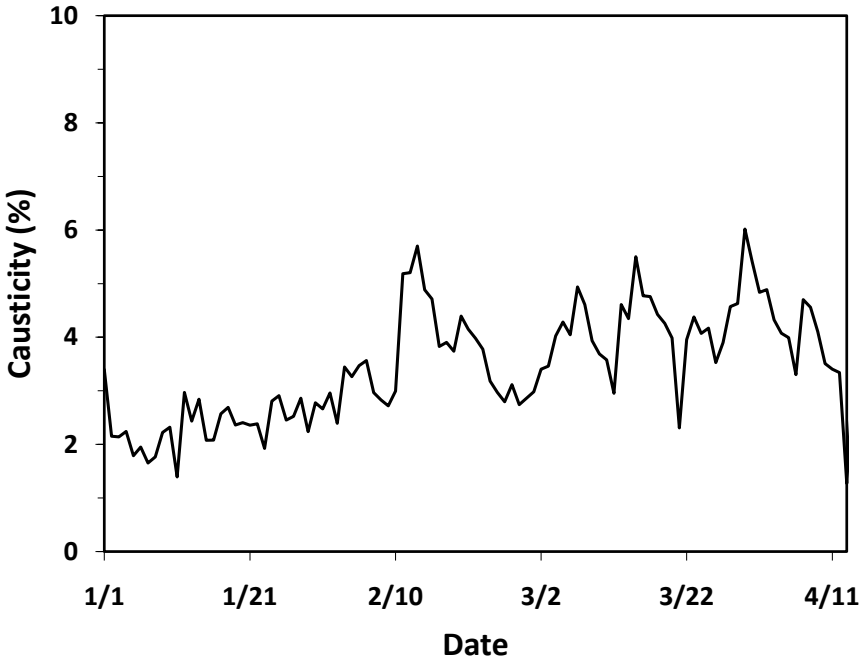

Figure 5-15: *Clarified green liquor causticity data for mill I*

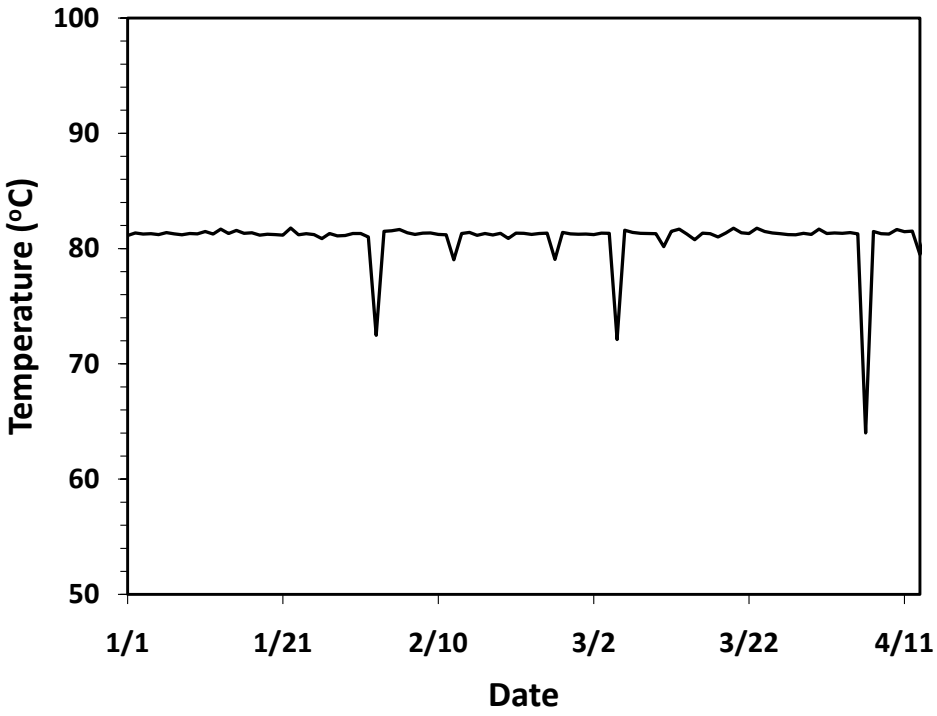

Figure 5-16: *Clarified green liquor temperature data for mill I*

It was observed that the temperature of clarified green liquor was on average 81°C. The average values of TTA, sulfidity and causticity were about 126.5 g/L of Na_2O, 28.7% and 3.4% respectively. Figure 5-9 and 5-10 were used to determine the TTA_{sat} point at 81°C, 28.7% sulfidity and 3.4% causticity which has a value of 108 g/L of Na_2O (See Appendix D for sample calculation). This TTA_{sat} value is below their operating TTA, as a result of this, pirssonite will precipitate from their clarified green liquor as observed in this mill. The TTA_{sat} point at 95°C, under the same sulfidity and causticity conditions, is about 139 g/L of Na_2O. Therefore, to prevent pirssonite deposition problem using the same green liquor, the mill must control their liquor temperature at about 95°C. The other solution is to decrease their green liquor TTA below the saturation point at 81°C.

It is also interesting to note that this mill did not encounter deposition problems in their raw green liquor handling systems, such as the dissolving tank, the storage tank or the pipeline that carries raw green liquor. Figure C-1 to C-4 in Appendix C present the raw green liquor data obtained from mill I. The average values of temperature, TTA, sulfidity and causticity of raw green liquor were 94°C, 129.3 g/L of Na_2O, 26.6% and 3.3% respectively. Under these

conditions, the TTA_{sat} point, as determined from Figure 5-9 and 5-10, is about 140 g/L of Na_2O. Since the raw green liquor TTA is below the TTA_{sat} point, there was no driving force in the raw green liquor system to initiate pirssonite precipitation. Figure 5-17 shows a comparison plot of the driving forces that led to pirssonite precipitation in the clarified green liquor system but not in the raw green liquor equipment.

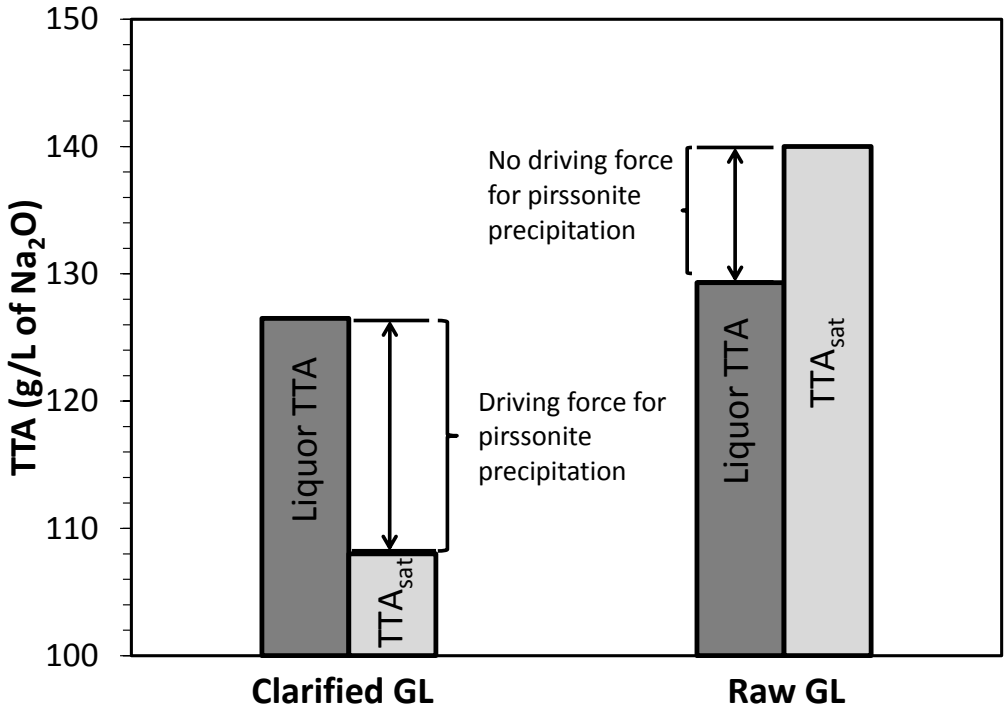

Figure 5-17: *Comparison of the driving forces for pirssonite precipitation in clarified and raw green liquor systems*

5.5 Summary

A database for pirssonite was created in OLI in order to simulate its solubility behavior. The validity of the database was tested against the experimental data generated in this work. The validated database was subsequently used to create a series of pirssonite solubility curves under various kraft mill operating conditions. These curves can be easily used by the kraft mills as guidelines to prevent pirssonite deposition by detecting the saturation point under their operating conditions. The effects of temperature and chloride on pirssonite solubility were also investigated. It was observed that pirssonite solubility increases with temperature and decreases with an increasing concentration of Cl^- in green liquor solutions. Finally, a case study was

discussed in order to show the applicability of the solubility curves to determine the TTA saturation point using the actual mill data obtained from a kraft mill that experienced pirssonite deposition problems. Based on the solubility curves, recommendations were provided to prevent pirssonite deposition at this kraft mill.

Chapter 6

6 Conclusions

Scaling in green liquor system was investigated in this work. Specific attention was given to understand the formation of pirssonite in green liquor processing equipment. The major conclusions that can be extracted from this work are summarized below:

1. Green liquor scale samples were characterized by analyzing 12 scale samples collected from various mills. It was found that only one-third of the samples consisted of pirssonite, the rest were composed of calcium carbonate. Further experiments were conducted to explain the occurrence of calcium carbonate in green liquor scale. It was evident from experimental results that pirssonite will incongruently dissolve in weak wash solutions very quickly leaving only $CaCO_3$ behind. Six of the eight scale samples identified as $CaCO_3$ were collected from the pipelines after the dissolving tank. Since green liquor and weak wash flows are switched in these pipelines, it is consistent with the observed experimental behavior of selective dissolution of pirssonite. On the other hand, none of the scale samples characterized as pirssonite in this study were collected from these pipelines where green liquor and weak wash flows are switched. This means pirssonite scale samples found in this study were formed in locations where the operating conditions do not permit selective dissolution of it after its formation. Therefore, it is safe to conclude that $CaCO_3$ scales found in this study were a combined effect of pirssonite precipitation under supersaturated green liquor conditions followed by incongruent dissolution during weak wash flows in the pipelines that run between the dissolving tank and the clarifier.

2. The solubility behavior of pirssonite was also experimentally investigated in this work. It was observed that the solubility of pirssonite increases with temperature and decreases with the presence of other sodium salts in the solution. The solubility of pirssonite was also extended in this work from Frederick et al. [6] by conducting experiments in low concentration regions of sodium sulfide and sodium hydroxide. Finally, attempts were made to explain the mechanism for pirssonite formation. It was speculated that pirssonite

might form through a continuous dissolution-re-precipitation mechanism where $CaCO_3$ continuously dissolves to provide free Ca^{2+} ions in the solution which then reacts with Na^+, CO_3^{2-}, and H_2O in the aqueous phase to precipitate pirssonite as a new crystalline phase.

3. The solubility of pirssonite was also simulated in this work using OLI software. A database for pirssonite was created in OLI that can be used to predict the solubility behavior of pirssonite. This database was used to generate pirssonite solubility curves that can be used by the kraft mills to prevent pirssonite deposition problems. It was also found that the presence of NaCl in green liquor decreases pirssonite solubility significantly. Therefore, solubility curves were also created for green liquors that contain NaCl. These curves are useful for those mills that have high chloride contents in their systems.

4. Scale sample # I was characterized as pirssonite in Chapter 3. Green liquor data, during the time frame of scale deposition, was obtained from mill I and analyzed in Chapter 5. It was shown that the green liquor TTA of mill I during the scaling period was below the solubility limit of pirssonite. Recommendations were provided based on the pirssonite solubility curves to prevent pirssonite deposition problems in the future.

Chapter 7

7 Recommendations for Future Work

Calcium carbonate was found in the majority of the green liquor scale samples analyzed in this work. Although the presence of $CaCO_3$ in green liquor scale samples was determined to be the result of incongruent dissolution of pirssonite scale, more work is still required to explain the hardness of calcium carbonate scale observed in the mill samples, as the calcium carbonate resulting from pirssonite dissolution in this work was found to be in soft powder form. It is recommended to further extend this work to investigate $CaCO_3$ scaling potential in green liquor system by studying $CaCO_3$ deposition possibilities from its suspended particles that are present in green liquor.

The mechanism of pirssonite formation from calcium carbonate particles was investigated in this work. It was shown that pirssonite might have been formed from a slurry of $CaCO_3$, Na_2CO_3 and water through a continuous dissolution-re-precipitation mechanism. More work is needed to confirm this mechanism and/or discover any other underlying mechanism that leads to the formation of pirssonite from such systems.

References

1. Biermann, C. J., *Essentials of pulping and papermaking*. San Diego: Academic Press, Inc., 1993
2. Tran, H., and Vakkiainnen, E. K., "Advantages in the kraft chemical recovery process", *The 3rd International Colloquium. on Eucalyptus Pulp,* Belo Horizonte, Brazil, 2007
3. Sanchez, D.R., "Recausticizing principles and practice", *TAPPI Kraft Recovery Course Notes,* 2009
4. Cornell, C.F.,"Cooking liquor preparation", *Chemical Recovery in Alkaline Pulping Processes*, TAPPI Pr., 1987
5. Kosonen, J., and Salmenoja, K. "Solving deposit problems in the smelt dissolving tank", *Proceedings of the TAPPI Engineering Conf*erence, 793-797, 1996
6. Frederick, W.J., Krishnan, R., and Ayers, R.J. "Pirssonite deposits in green liquor processing", *Tappi Journal*, 73(2): 135-140, 1990.
7. DeMartini, N., and Frederick, W. J., "Review of sodium salt scaling in the liquid streams of the chemical recovery cycle of kraft pulp mills", in *TAPPI Engineering, Pulping & Environmental Conference*, Oregon, 2008
8. Zakir, T., Tran, H., and Papangelakis, V.G., " Characterization of hard scale formed in the kraft mill green liquor processing equipment", *TAPPI Peers Conference,* Portland, Ore, 2011
9. York, J.L., and Schorle, B.J, *Principles of desalination,* New York: Academic Press, Inc., 1966
10. Cowan, J.C., and Weintritt, D. J., "Scale deposition mechanisms", *Water-Formed Scale Deposits,* Houston: Gulf Publishing Company, 204-249, 1976
11. Dirksen, J.A., and Ring, T.A., "Fundamentals of crystallization: kinetic effects on particle size distributions and morphology", *Chemical Engineering Science, 46(10): 2389-2427, 1991*
12. Dorris, G. M., Allen, L.H., "Operating variables affecting the causticizing of green liquors with reburned limes", *Journal of Pulp and Paper Science,* 13(3), 1987
13. Grace, T. M., "Preparation of white liquor", *Pulp and Paper Manufacture,* 5: 563-589, 1989
14. "Pirssonite", *Handbook of mineralogy,* Mineralogical Society of America, 5, 2003

15. Corazza, E., and Sabelli, C. The crystal structure of pirssonite, $CaNa_2(CO_3)\cdot 2H_2O$. *Acta Cryst.*, 23: 763-766, 1967
16. "Pirssonite Mineral Data", *Mineralogy Database*, http://webmineral.com/data/Pirssonite.shtml, accessed June 23, 2011
17. Bury, C.R., and Redd, R. "The system sodium carbonate-calcium carbonate-water", *Journal of Chemical Society*, 1160-2, 1933
18. Allen, E.M., "Purification of calcium carbonate", *U.S. Patent 2 292 503*, 1939
19. Dickens, B., and Brown, W., "The crystal ctructures of $CaNa_2(CO_3)_2\cdot 5H_2O$, synthetic gaylussite, and $CaNa_2(CO_3)_2\cdot 2H_2O$, synthetic pirssonite", *Inorganic Chemistry*, 8(10): 2093-2103, 1969
20. Dheilly, R.M., and Tudo, J. "Contribution à létude de la gaylussite: $Na_2Ca(CO_3)_2\cdot 5H_2O$", *Solid state chemistry and crystal chemistry*, 325: 407-414, 1998
21. "Gaylussite Mineral Data", *Mineralogy Database*, http://webmineral.com/data/Gaylussite.shtml, June 23, 2011
22. "Nyerereite Mineral Data", *Mineralogy Database*, http://webmineral.com/data/Nyerereite.shtml , June 23, 2011
23. Ulmgren, P., Rådeström, R., Edblad, M., and Wennerström, M. "On the chemistry of non-process elements in systems with a pressurized black liquor gasifier", *Proceedings of the 1998 International Chemical Recovery Conference*, Tampa, FL, TAPPI/CIPPA, 721-731, 1998
24. Smith, J.W., Johnson, D.R., and Robb, W.A., "Thermal synthesis of sodium calcium carbonate-a potential thermal analysis standard", *Thermochimica Acta*, Elsevier Publishing Company, Amsterdam, 305-312, 1970
25. Johnson, D.R., and William, A.R., "Gaylussite: thermal properties by simultaneous thermal analysis", *American Mineralogist*, 58:778-784, 1973
26. Littman, F. E., and Gaspari, H. J. "Causticization of carbonate solutions", *Industrial and Engineering Chemistry*, 48(3): 408-410, 1956
27. Taylor, K., and McGuffie, B., "Investigation of non-process element chemistry at Elk Falls mill-green liquor clarifier and lime cycle", *Pulp and Paper Canada*, 108: 27-32, 2007

28. Martins, F.M., Martins, J.M., Ferracin, L.C., and Cunha, C.J., "Mineral phases of green liquor dregs, slaker grits, lime mud and wood ash of a Kraft pulp and paper mill", *Journal of Hazardous Materials,* 147: 610-617, 2007
29. Bialik, M., Wadsborn, R., Karlholm, I., and Berglin, N. "Assessment of scaling risk in a pressurized black liquor gasification pilot plant", *Proceedings of the 2010 International Chemical Recovery Conference*, 1:279-286, 2010
30. Email from Donald, M.F., Senior Process Engineer, Irving Pulp and Paper Limited, Saint John, NB, 20 June, 2011
31. TAPPI Standard, T624os-68: Analysis of soda and sulfate, white liquor and green liquors
32. Saeidi, A.S., "Prediction of the causticizing equilibrium in the kraft chemical recovery process", *M.A.Sc thesis*, Department of Chemical Engineering and Applied Chemistry, University of Toronto, 2007
33. OLI Systems, Inc., "A guide to using the OLI engine-version 6.7", Morris Plains, NJ, 2004
34. Wang, P., Anderko, A., Young, R.D., and Springer, R.D., "A comprehensive model for calculating phase equilibria and thermophysical properties of electrolyte systems", OLI Systems, Inc., Morris Plains, NJ
35. OLI Systems, Inc., "MSE regression course", Morris Plains, NJ, 2011
36. Königsberger, E., Königsberger, L.C., and Gamsjager, H., "Low-temperature thermodynamic model for the system Na_2CO_3-$MgCO_3$- $CaCO_3$-H_2O", *Geochimica et Cosmochimica Acta,* 63(19/20): 3105-3119, 1999
37. OLI Systems, Inc., "A brief guide to using OLI/MSE data regression", Morris Plains, NJ, 2009
38. Tran, H.N., Burnham, D., Reeve, D.W., "Chloride and potassium in the kraft chemical recovery cycle", *Pulp and Paper Canada*, 91:5 (1990)

Appendices

Appendix A1: TGA/DSC Profiles for Mill Samples

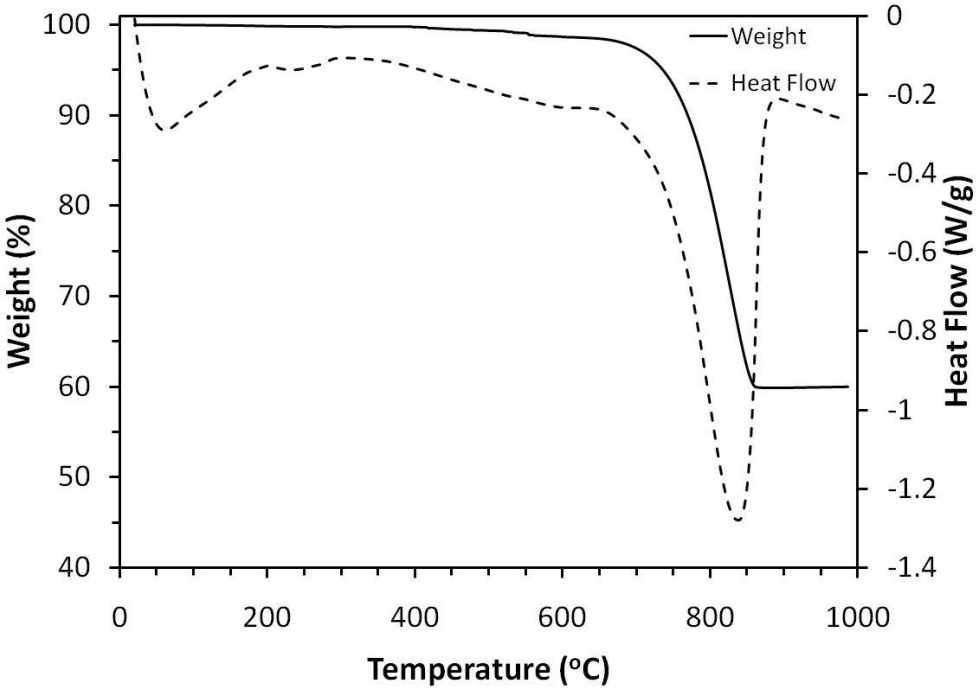

Figure A1-1: *Thermal profile for sample B*

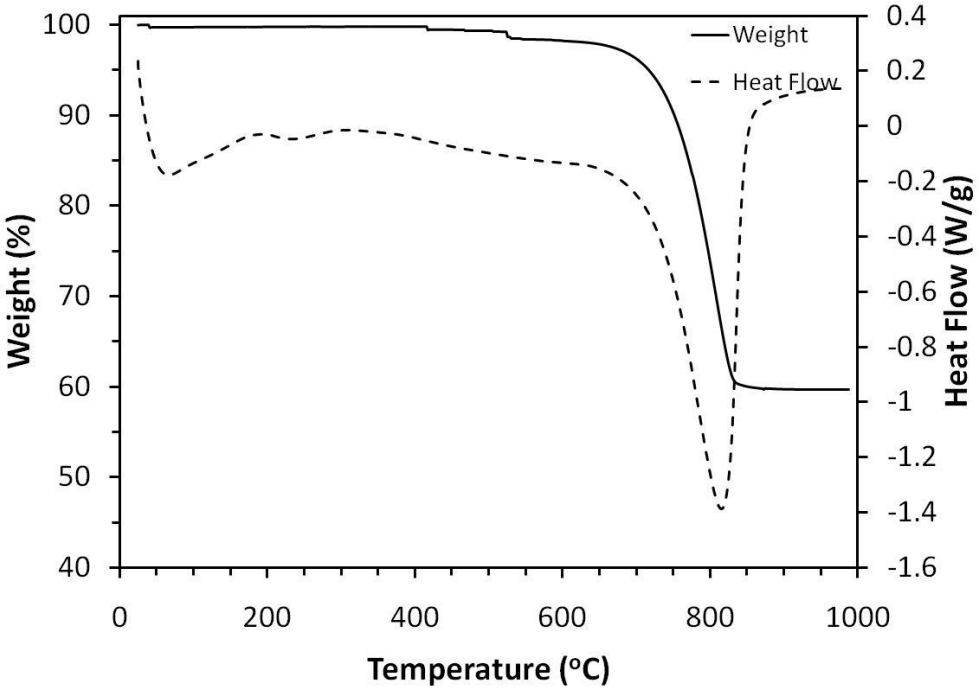

Figure A1-2: *Thermal profile for sample C-i*

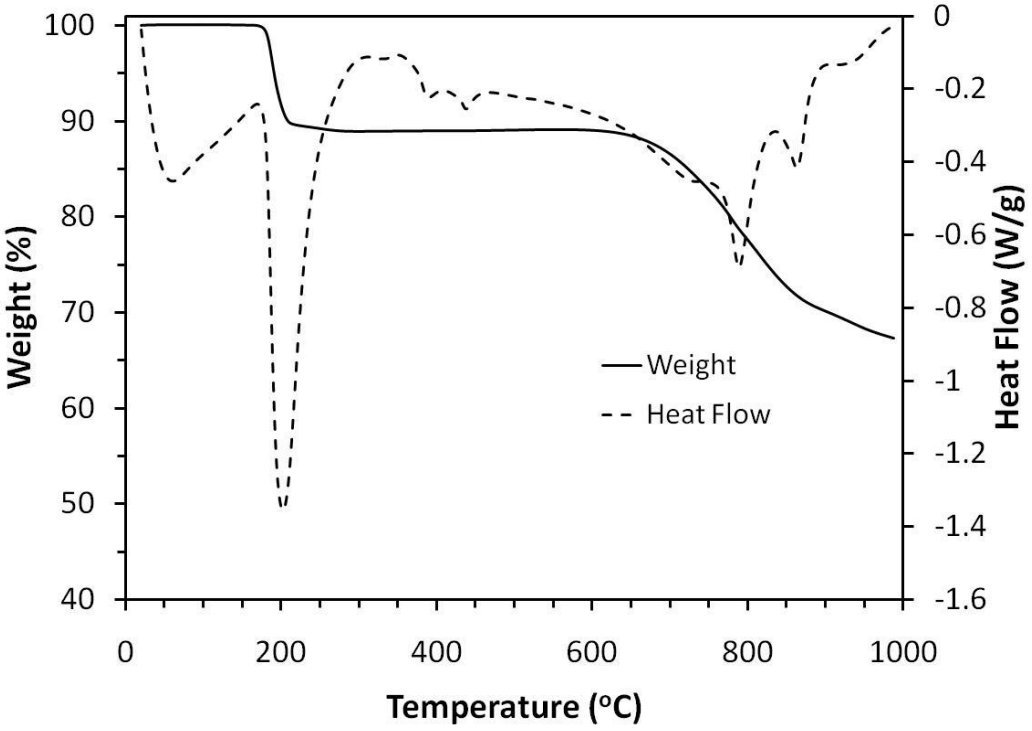

Figure A1-3: *Thermal profile for sample C-ii*

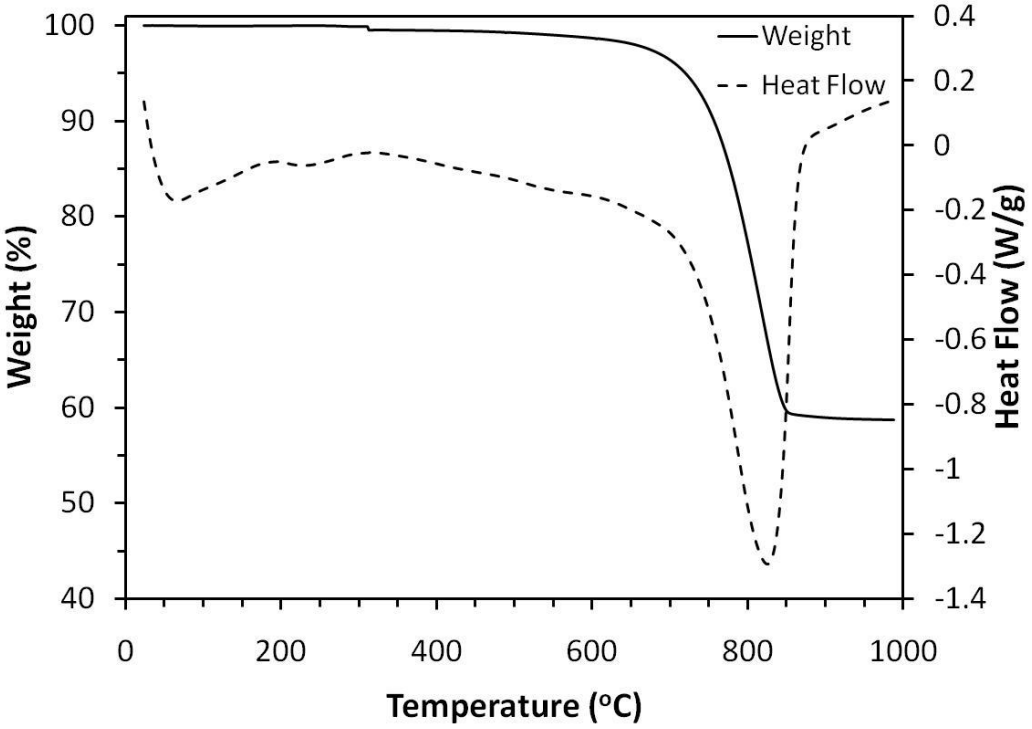

Figure A1-4: *Thermal profile for sample D*

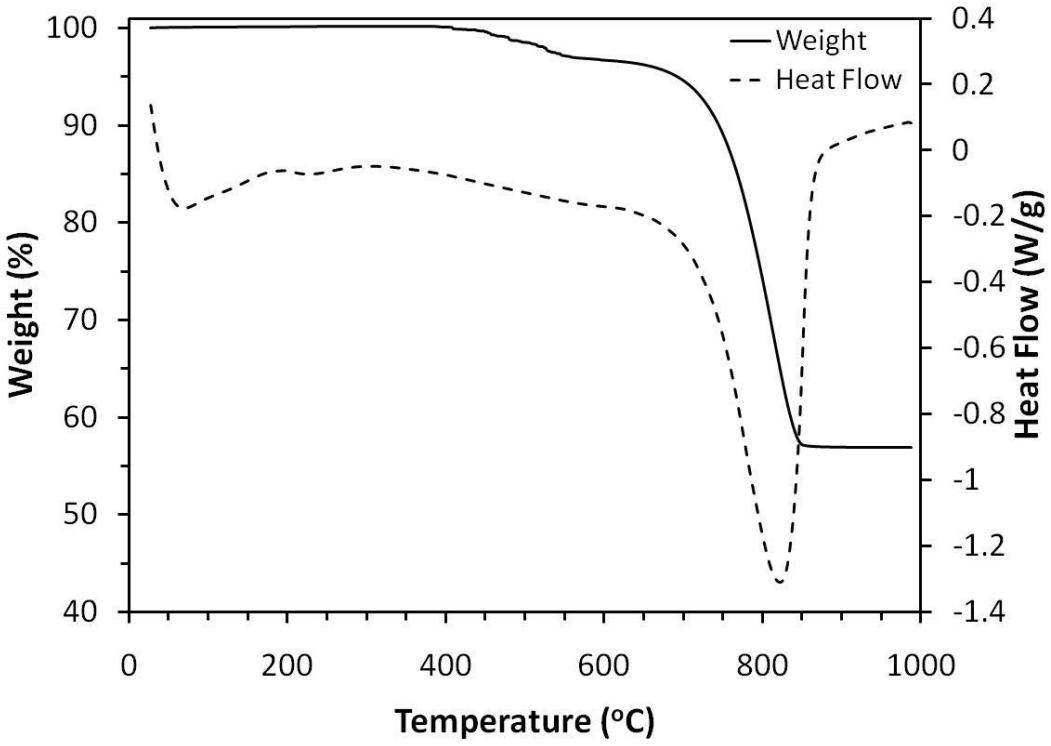

Figure A1-5: *Thermal profile for sample E*

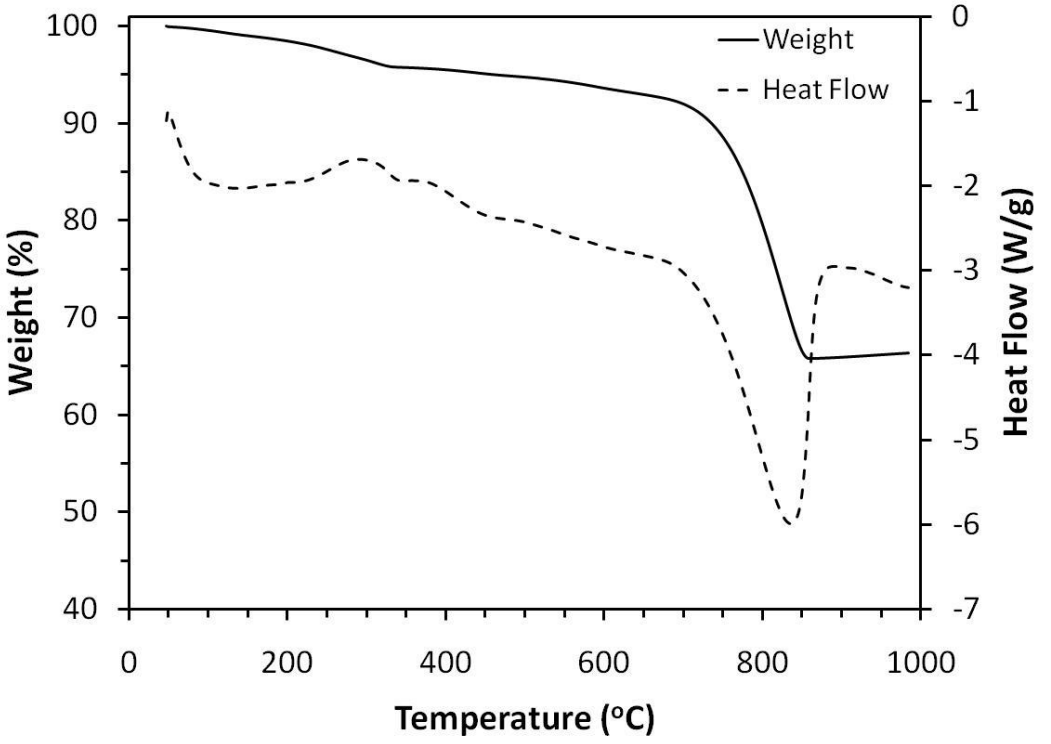

Figure A1-6: *Thermal profile for sample F*

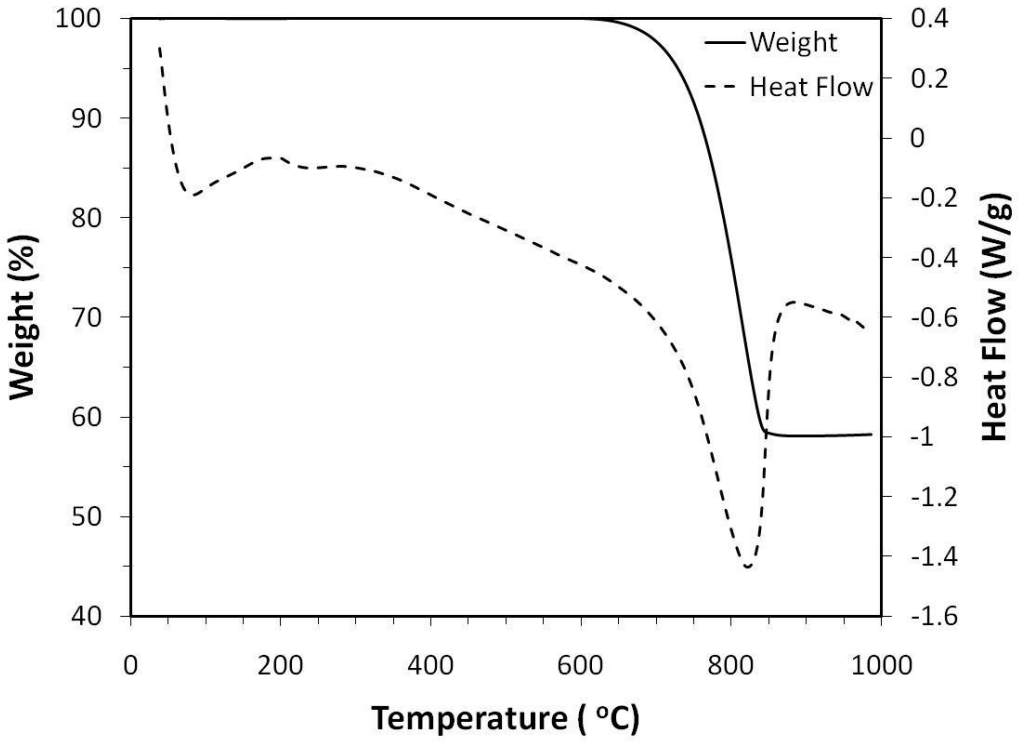

Figure A1-7: *Thermal profile for sample G*

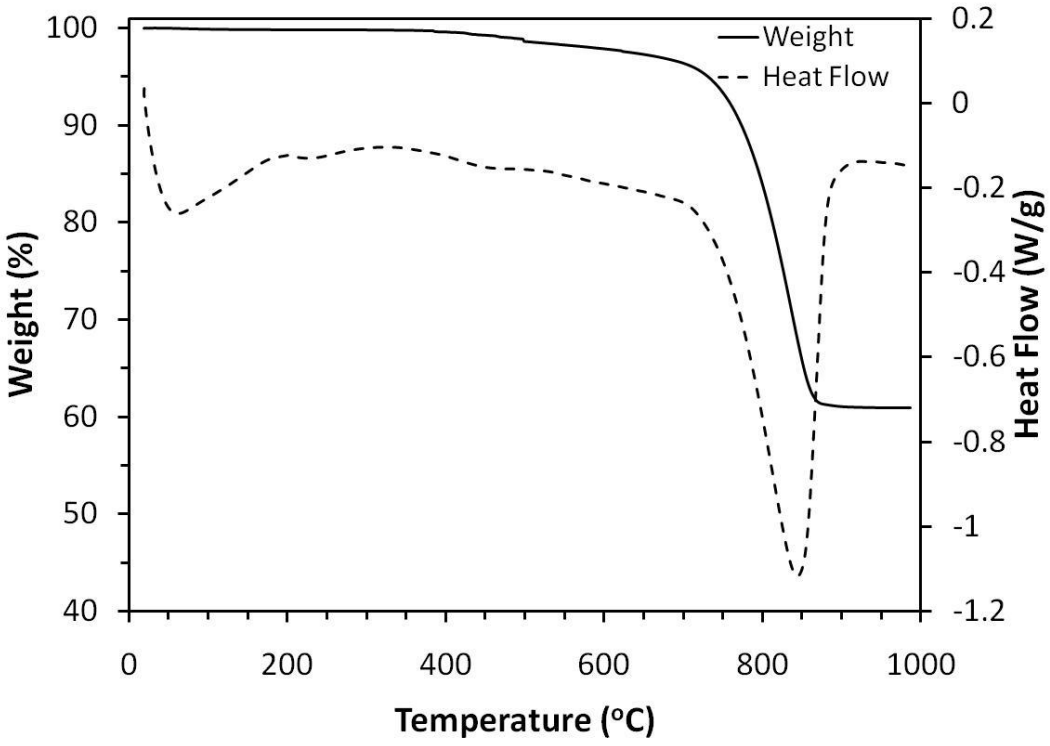

Figure A1-8: *Thermal profile for sample H-i*

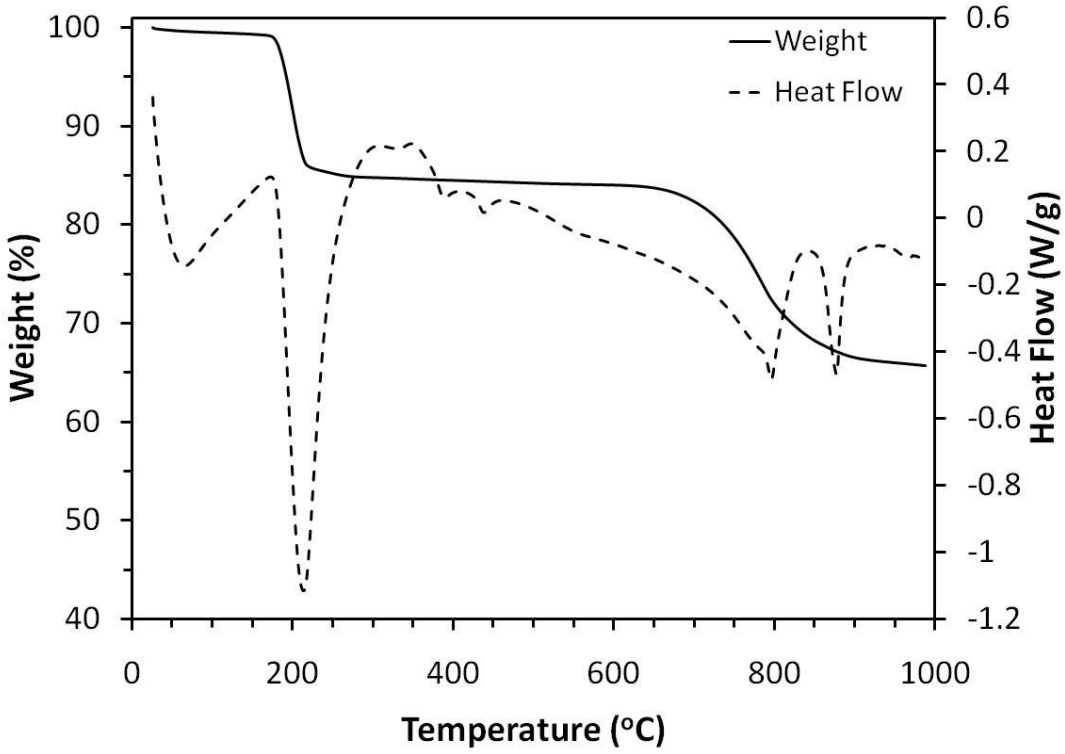

Figure A1-9: *Thermal profile for sample H-ii*

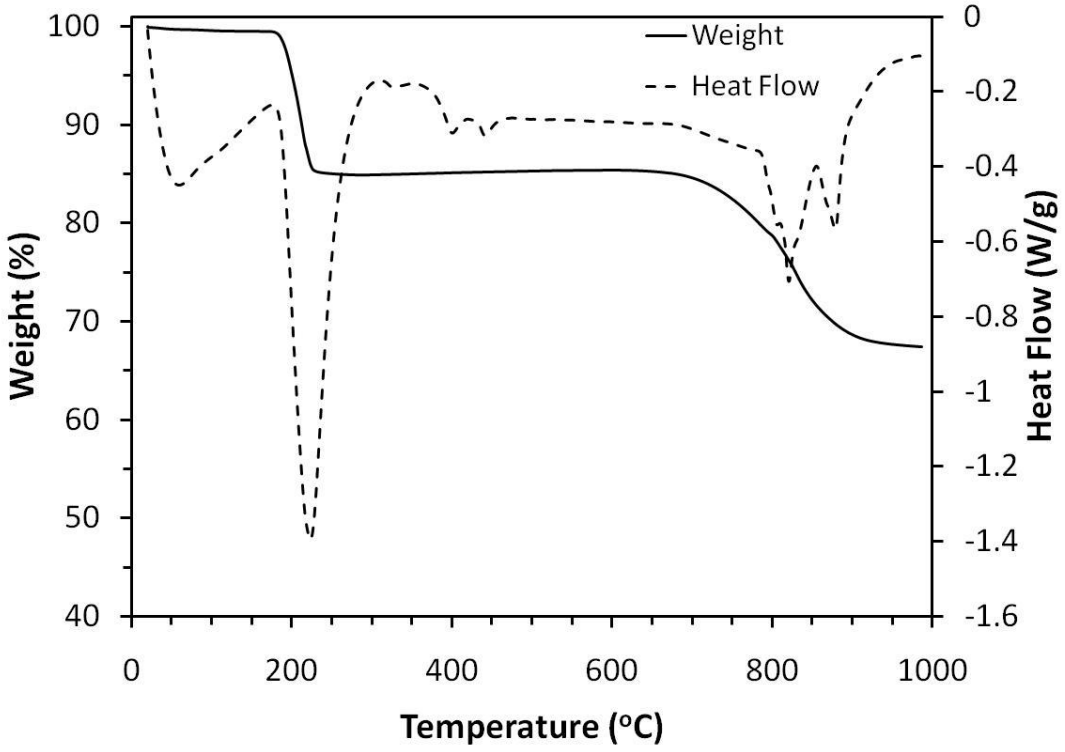

Figure A1-10: *Thermal profile for sample J*

Appendix A2: TGA/DSC Profiles for Experimental Solid Samples

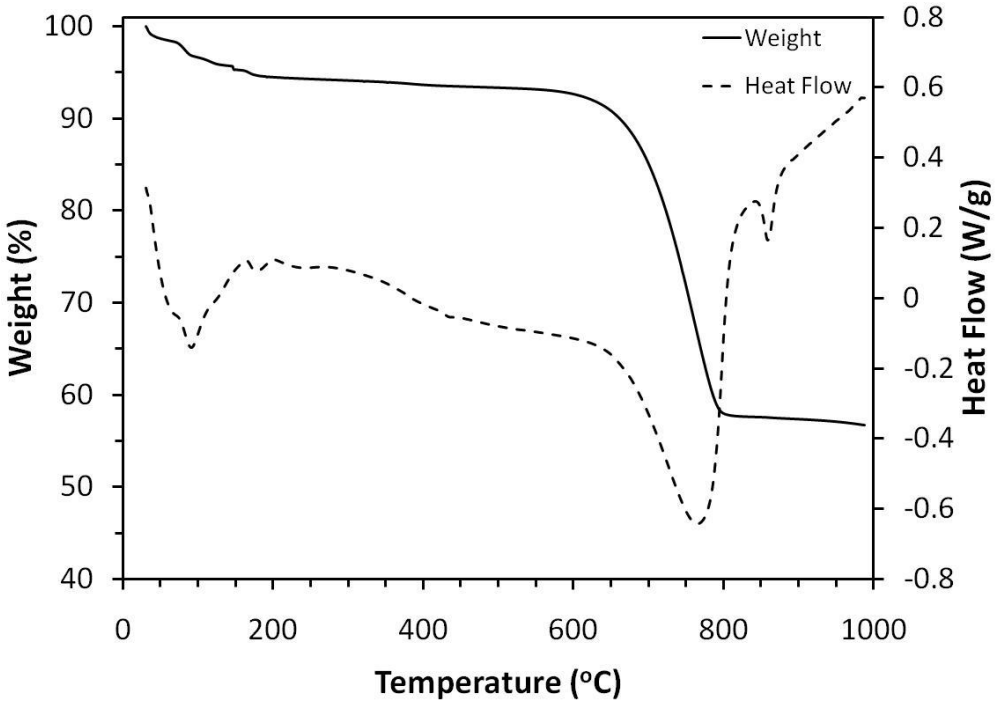

Figure A2-1: *Solid sample collected at t=3 h from Na_2CO_3-NaOH-$CaCO_3$-H_2O system at 95^oC*

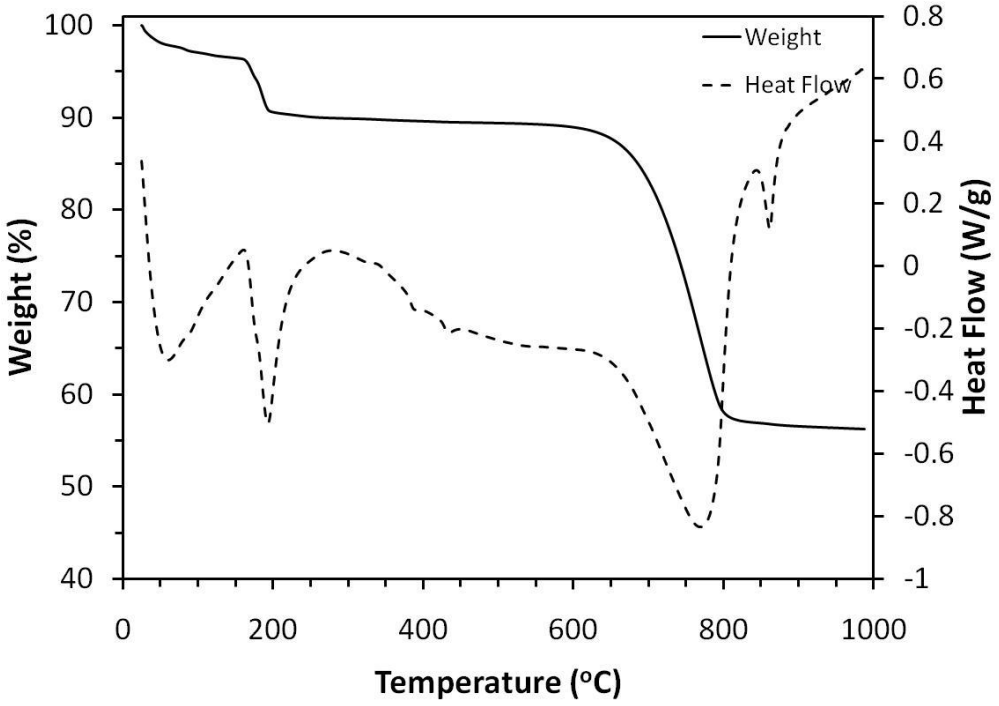

Figure A2-2: *Solid sample collected at t=6 h from Na_2CO_3-NaOH-$CaCO_3$-H_2O system at 95^oC*

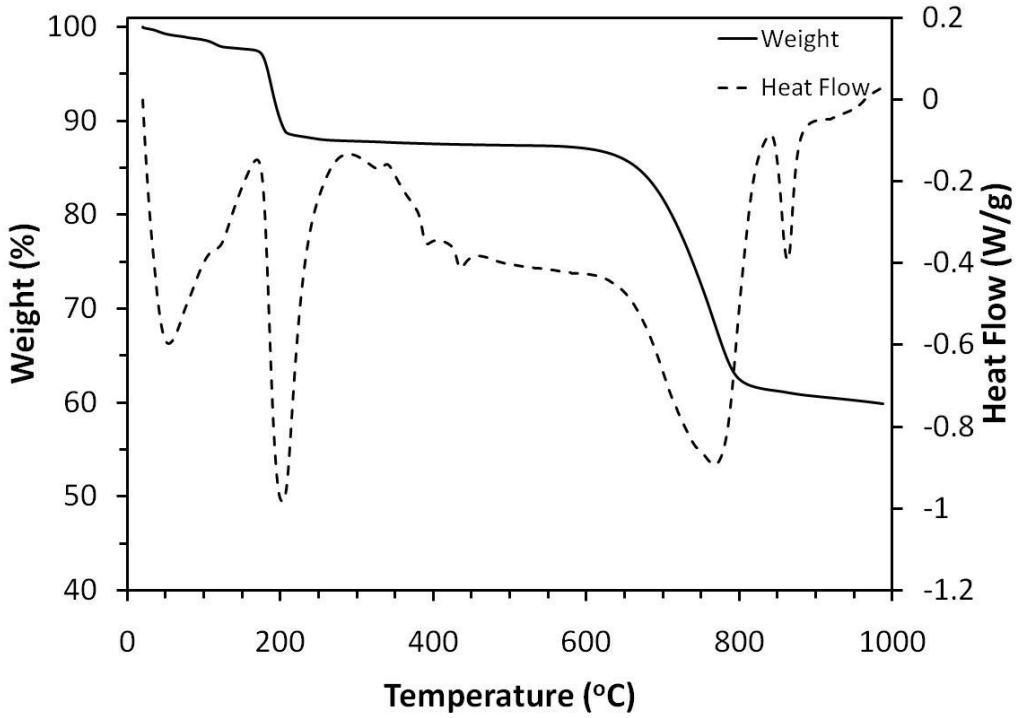

Figure A2-3: *Solid sample collected at t=9 h from Na_2CO_3-NaOH-$CaCO_3$-H_2O system at 95°C*

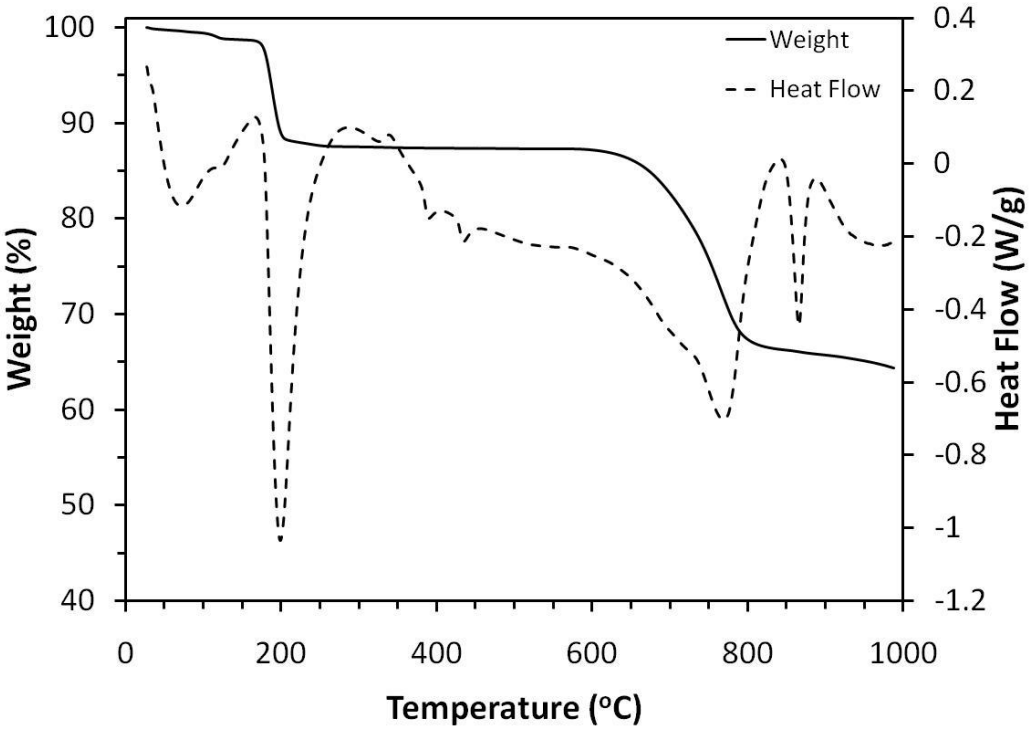

Figure A2-4: *Solid sample collected at t=12 h from Na_2CO_3-NaOH-$CaCO_3$-H_2O system at 95°C*

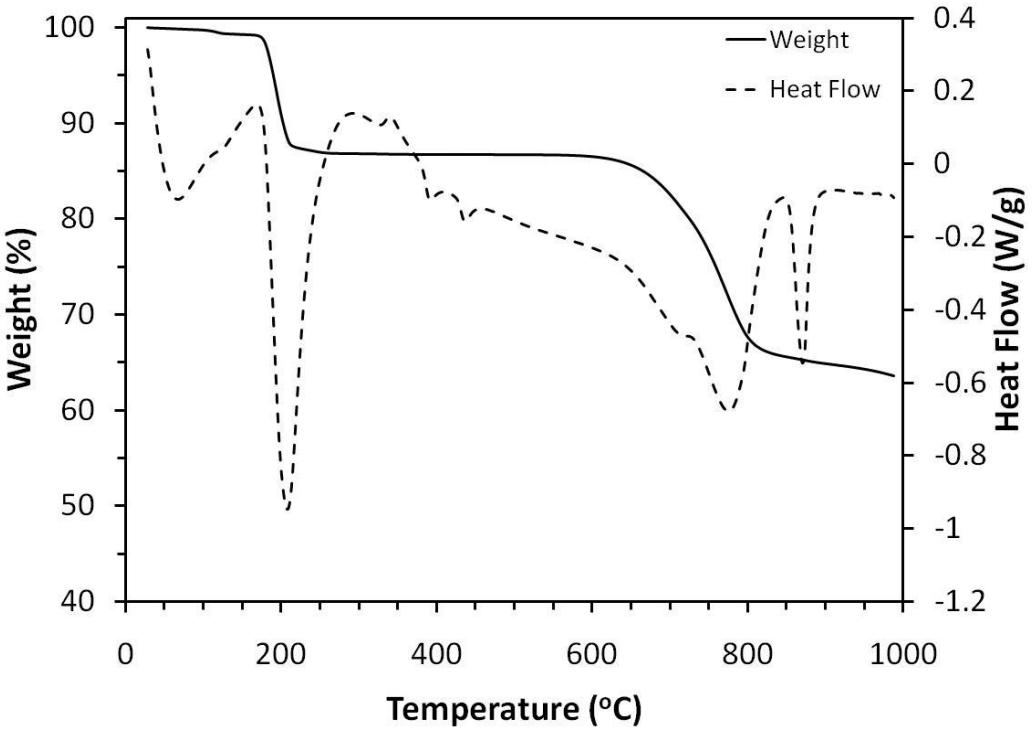

Figure A2-5: *Solid sample collected at t=14 h from Na_2CO_3-NaOH-$CaCO_3$-H_2O system at 95°C*

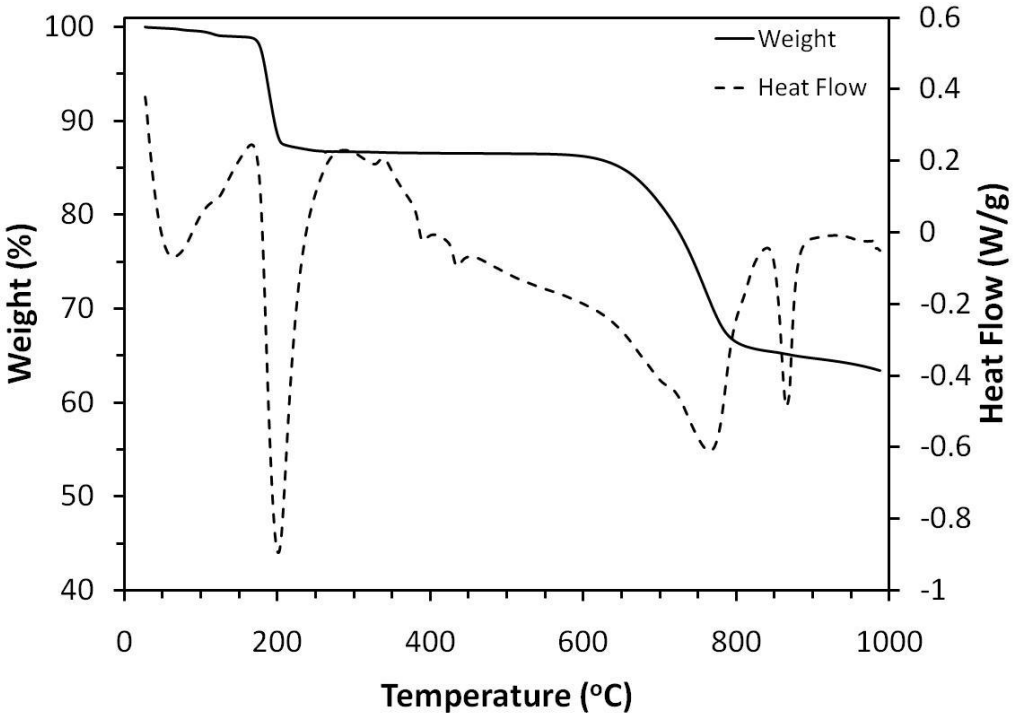

Figure A2-6: *Solid sample collected at t=16 h from Na_2CO_3-NaOH-$CaCO_3$-H_2O system at 95°C*

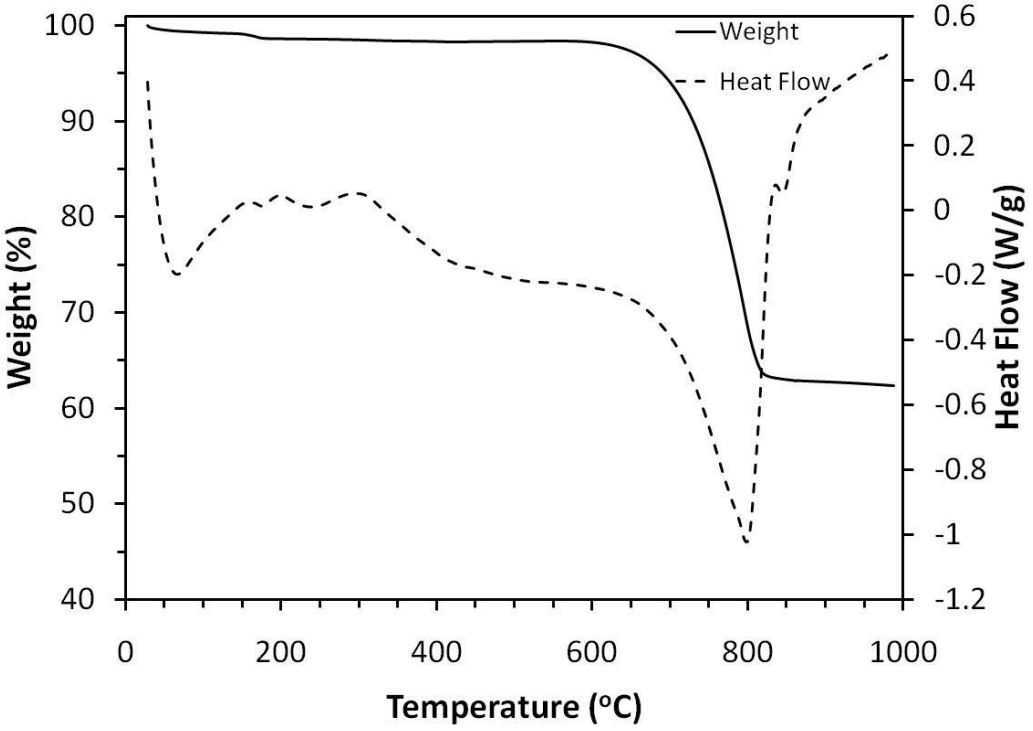

Figure A2-7: *Solid sample collected at t=24 h from Na_2CO_3-Na_2S-$CaCO_3$-H_2O system at 95°C*

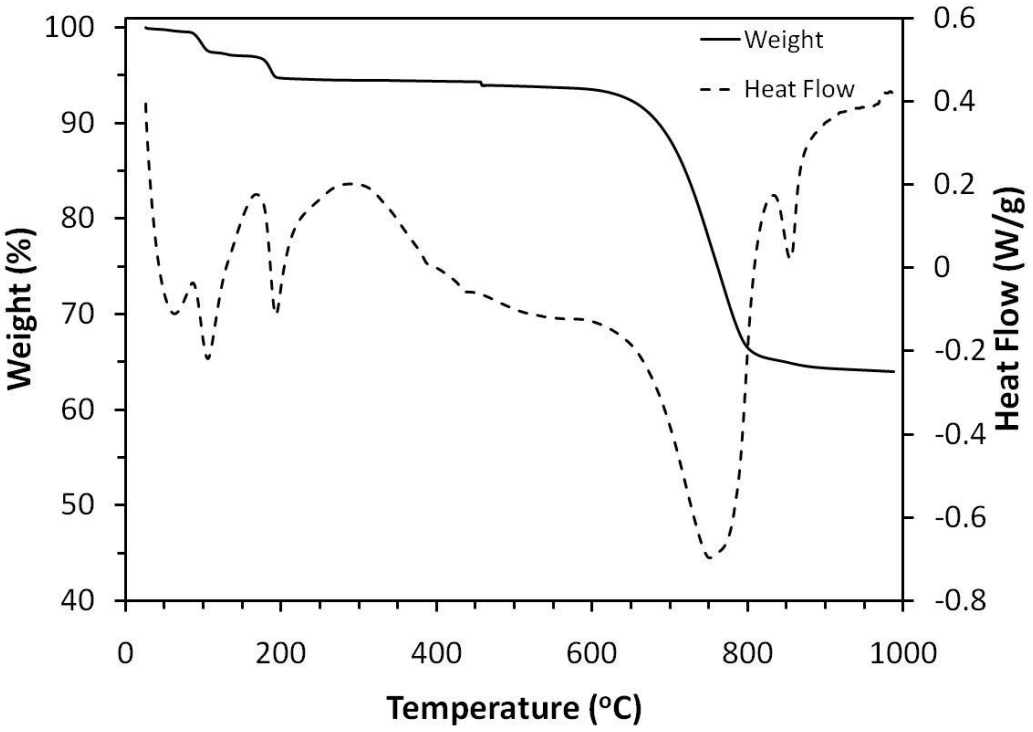

Figure A2-8: *Solid sample collected at t=36 h from Na_2CO_3-Na_2S-$CaCO_3$-H_2O system at 95°C*

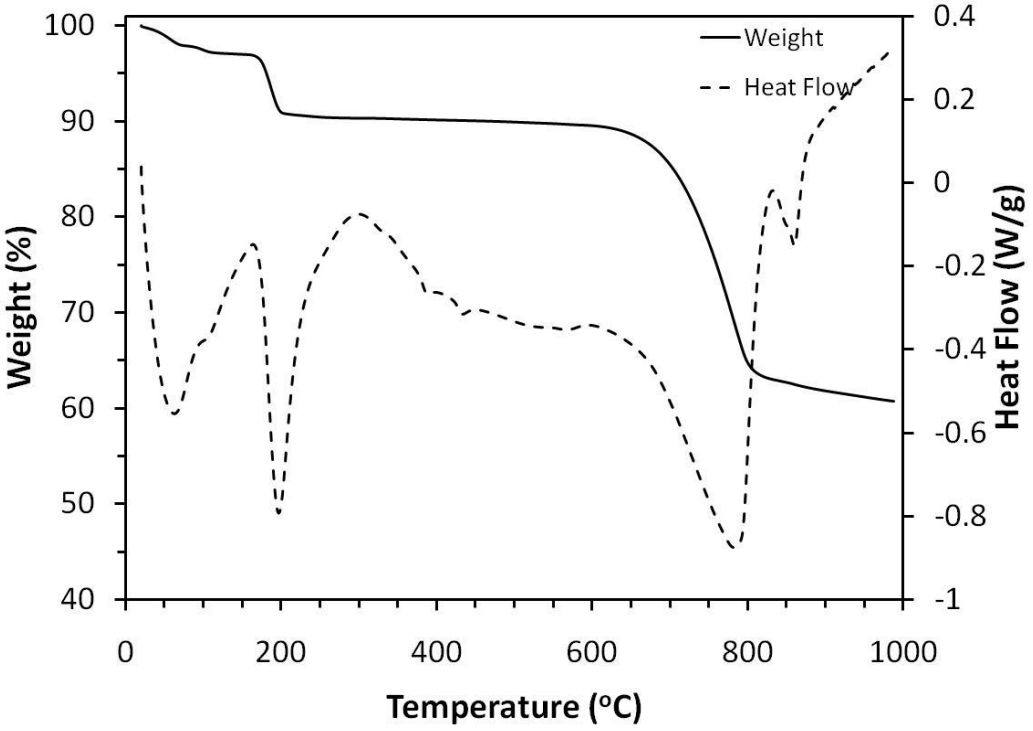

Figure A2-9: *Solid sample collected at t=48 h from Na_2CO_3-Na_2S-$CaCO_3$-H_2O system at 95°C*

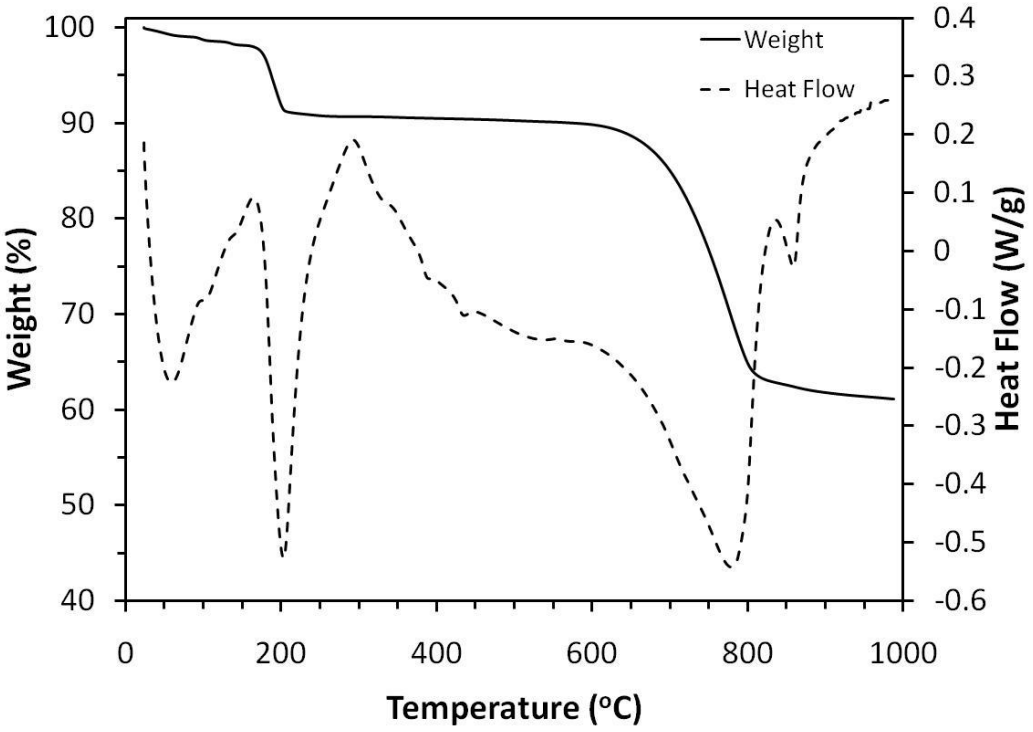

Figure A2-10: *Solid sample collected at t=54 h from Na_2CO_3-Na_2S-$CaCO_3$-H_2O system at 95°C*

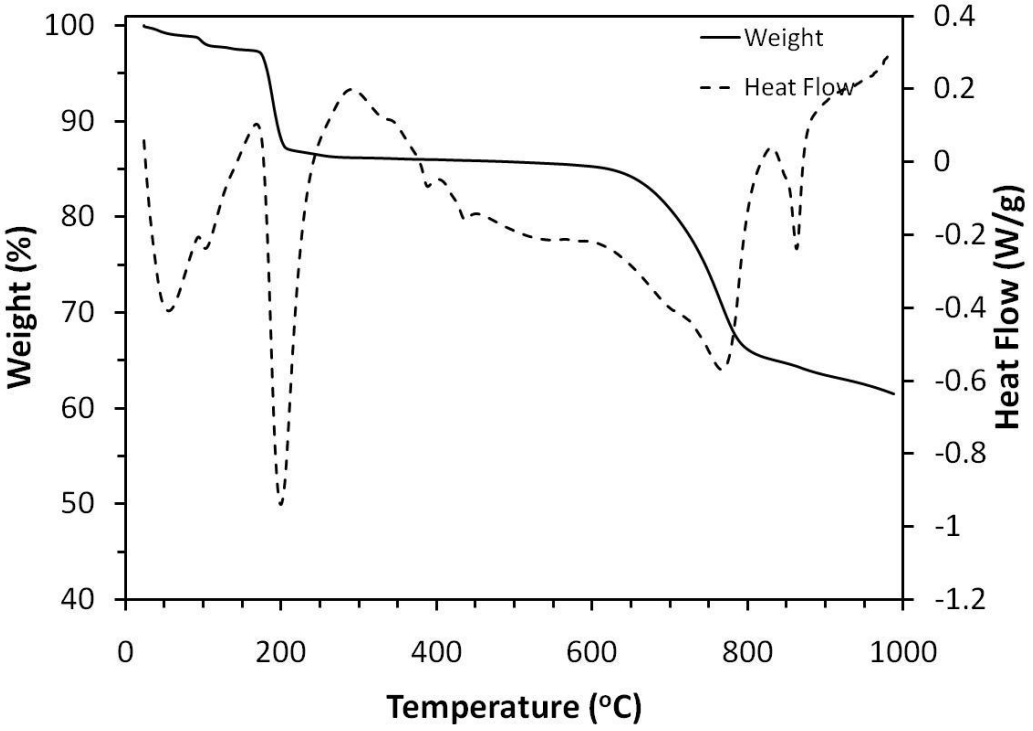

Figure A2-11: *Solid sample collected at t=67 h from Na_2CO_3-Na_2S-$CaCO_3$-H_2O system at 95°C*

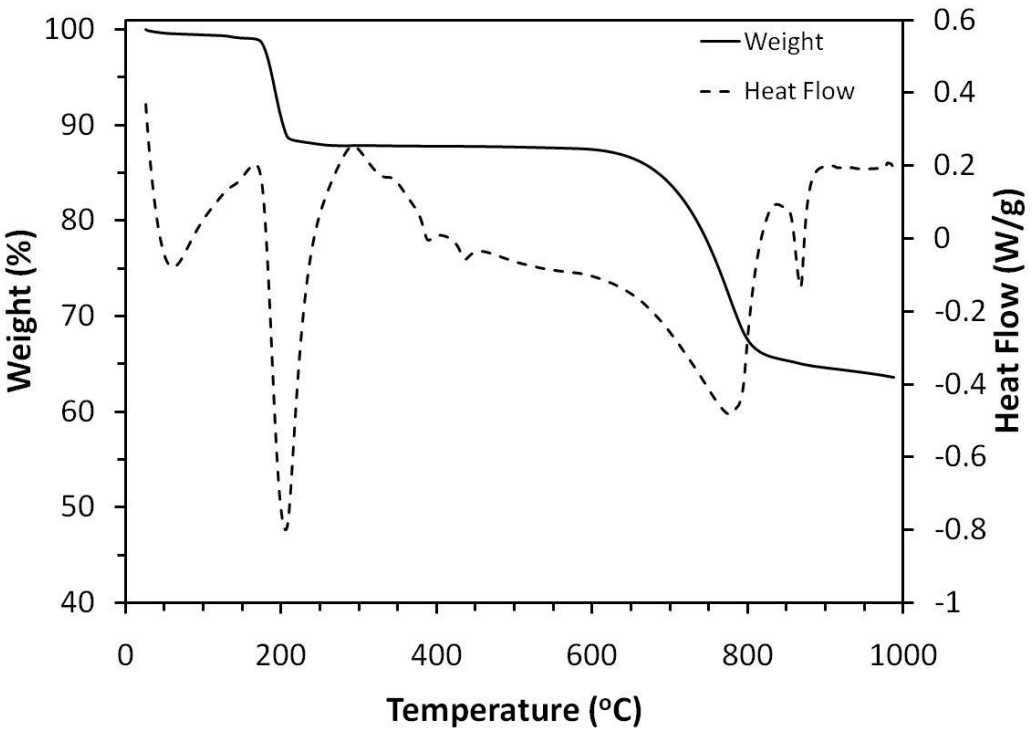

Figure A2-12: *Solid sample collected at t=75 h from Na_2CO_3-Na_2S-$CaCO_3$-H_2O system at 95°C*

Appendix B: SEM Images

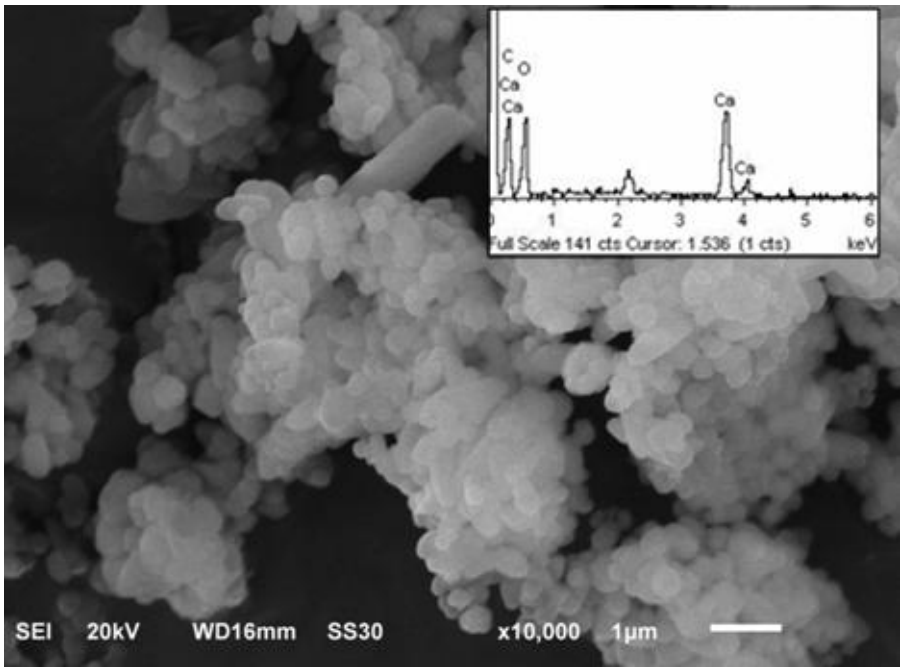

Figure B-1: *SEM image for solid sample taken at t=2 h from Na_2CO_3-$CaCO_3$-H_2O system at 95^oC, inset: EDS*

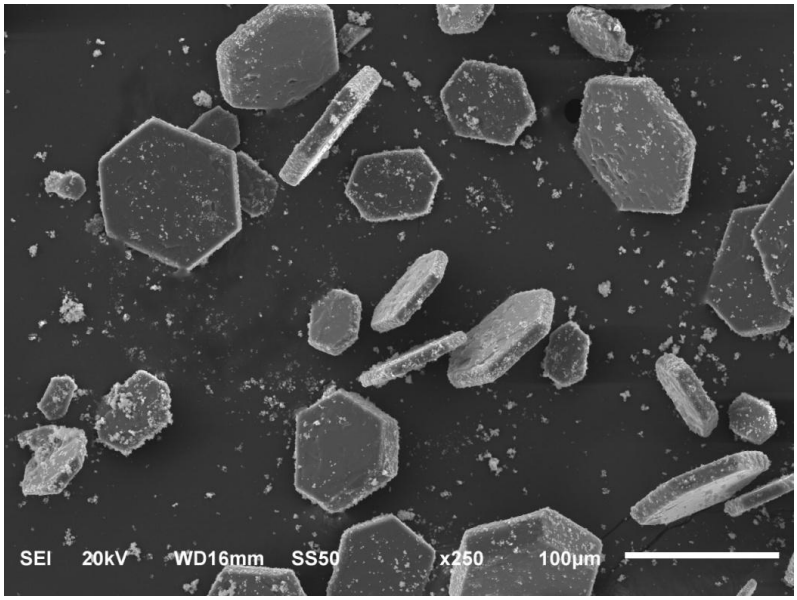

t = 9 hours

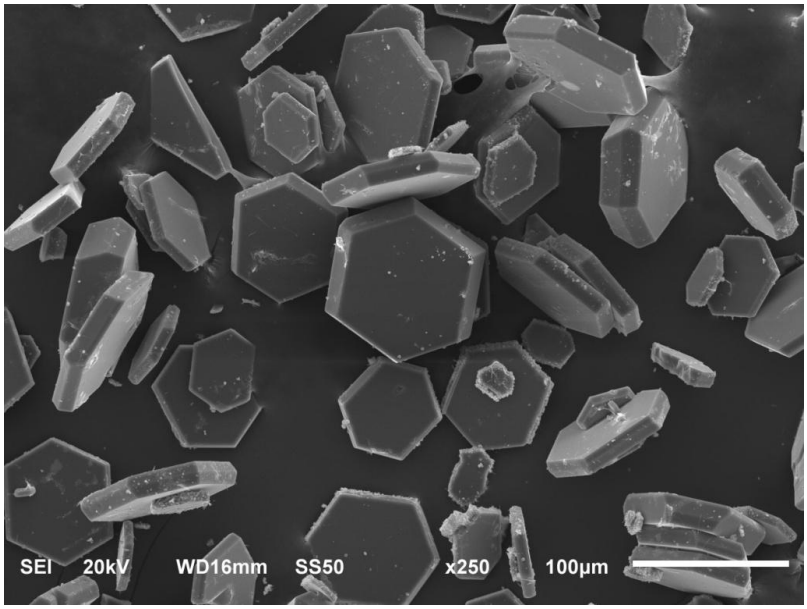

t = 15 hours

Figure B-2: *SEM image of solid samples taken at t=9 and 15 h from Na_2CO_3-$CaCO_3$-H_2O system at 95^o*

Appendix C: Raw Green Liquor Data for Mill I

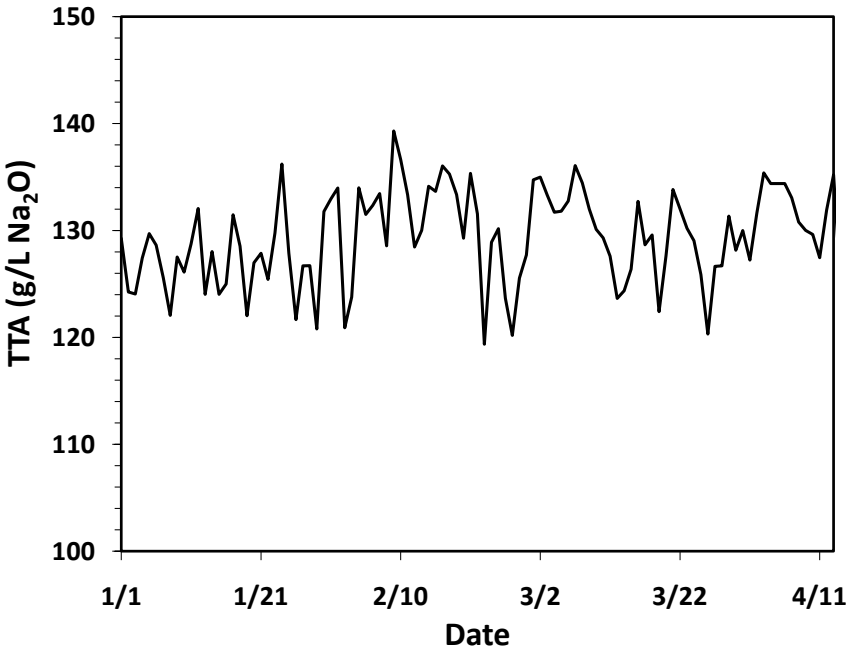

Figure C-1: *Raw green liquor TTA data for mill I*

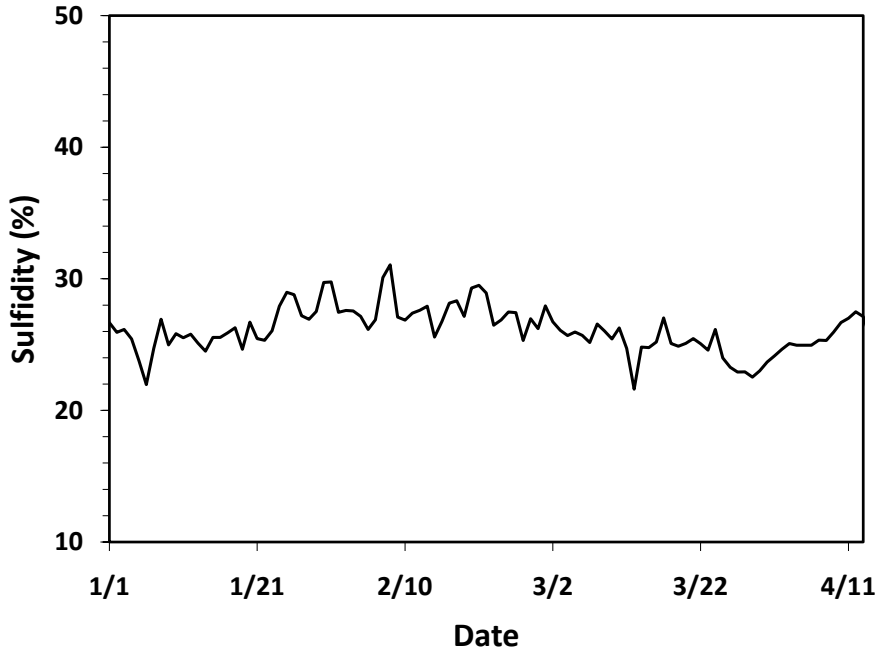

Figure C-2: *Raw green liquor sulfidity data for mill I*

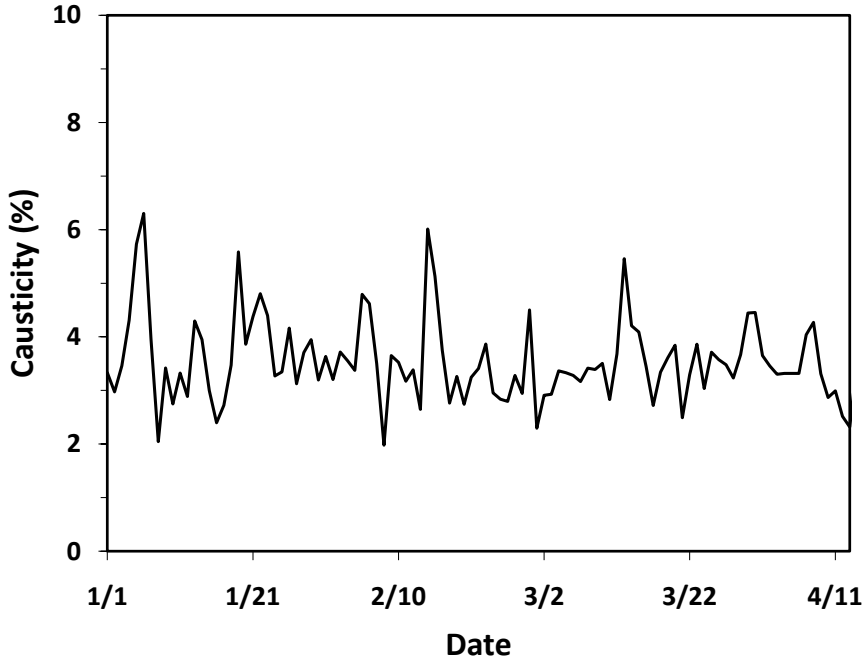

Figure C-3: *Raw green liquor causticity data for mill I*

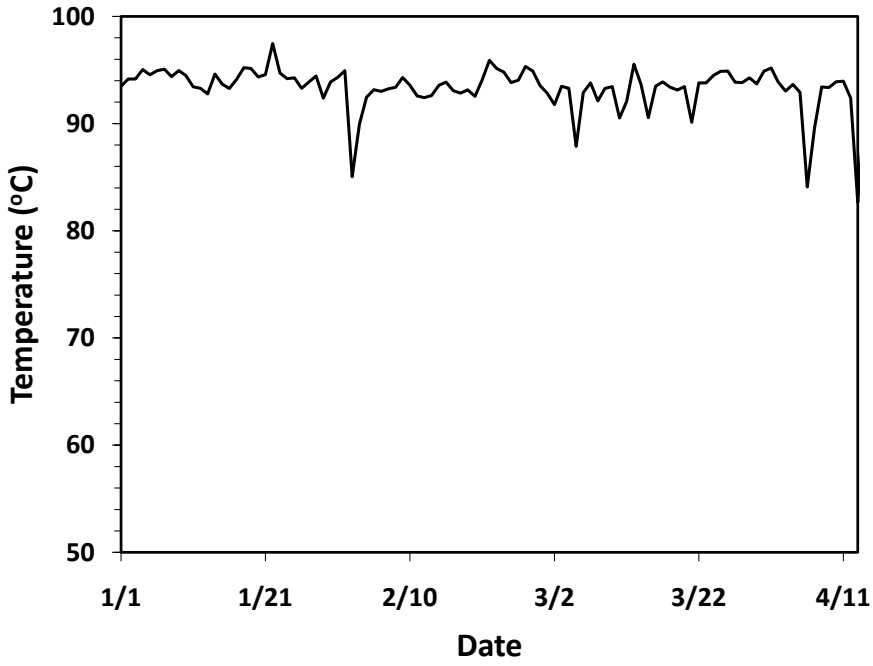

Figure C-4: *Raw green liquor temperature data for mill I*

Appendix D: Sample Calculation

Determination of TTA_{sat} Using the Solubility Curves Presented in Chapter 5:

Clarified green liquor properties:

Temperature = 81^{o}C

Sulfidity = 28.7%

Causticity = 3.4%

The following sulfidities and their corresponding TTA_{sat} points (as g/L Na_2O) are retrieved from Figure 5-10 (for 0% causticity) and 5-11(for 5% causticity) at 75^{o}C and 85^{o}C and are listed in the following table:

T = 75^{o}C, Causticity = 0%		***T = 75^{o}C, Causticity = 5%***	
S = 25%	*S = 30%*	*S = 25%*	*S = 30%*
TTA_{sat} = 102 g/L	*TTA_{sat} = 98 g/L*	*TTA_{sat} = 98.5 g/L*	*TTA_{sat} = 95.5 g/L*
T = 85^{o}C, Causticity = 0%		***T = 85^{o}C, Causticity = 5%***	
S = 25%	*S = 30%*	*S = 25%*	*S = 30%*
TTA_{sat} = 118.5 g/L	*TTA_{sat} = 115.8 g/L*	*TTA_{sat} = 115.4 g/L*	*TTA_{sat} = 113.8 g/L*

Linear interpolation was used in the above dataset to determine the TTA_{sat} points at *28.7 % sulfidity*:

TTA_{sat} (75^{o}C, 0% causticity, 28.7% sulfidity) = 99.04 g/L

TTA_{sat} (75^{o}C, 5% causticity, 28.7% sulfidity) = 96.28 g/L

TTA_{sat} (85^{o}C, 0% causticity, 28.7% sulfidity) = 116.50 g/L

TTA_{sat} (85^{o}C, 5% causticity, 28.7% sulfidity) = 114.22 g/L

The above dataset were linearly interpolated again to obtain the following TTA_{sat} values at *81^{o}C*:

TTA_{sat}(81^{o}C, 0% causticity, 28.7% sulfidity) = 109.52 g/L

TTA_{sat}(81^{o}C, 5% causticity, 28.7% sulfidity) = 107.04 g/L

Finally, linear interpolation was used one more time to obtain the TTA_{sat} point at *81^{o}C, 3.4% causticity and 28.7% sulfidity*, which has a value of 108 g/L of Na_2O.